UNIVERSITEIT VAN PRETORIA
UNIVERSITY OF PRETORIA
YUNIBESITHI YA PRETORIA

Department of Materials Science and Metallurgical Engineering

STRENGTHENING OF A COLD WORKED 17% CHROMIUM FERRITIC STAINLESS STEEL BY HEAT TREATMENT

by **Michelle Sephton**

A thesis submitted in partial fulfillment of the requirements for the

Masters in Engineering

degree in the Faculty of Engineering, University of Pretoria, Pretoria

Supervisor: Professor P.C. Pistorius

February 1997

Acknowledgements

I would like to thank Professor P.C. Pistorius for his invaluable help and contributions, Mintek for their financial support, Dr. M.B. Cortie for new ideas and directions, my mother and father for their support and encouragement, and my Father without whom I would not have been able to do anything.

Abstract

Slat-band chains are used as conveyors by the food industry, breweries and bottling plants. The operating conditions require abrasion resistance and strength which are at the limit of the capabilities of the current material of choice, cold worked type 430. In an unconventional way of strengthening this material, Mintek developed a process in which the cold worked material is aged between 450°C and 500°C. The present work aims to elucidate the strengthening mechanism, using type 430 stainless steel containing 16.42% Cr and 0.036% C, in the cold-rolled condition (38% reduction in area), with and without prior solution heat treatment.

The Cr-rich precipitate α" may form in the 450°C to 500°C range (due to the miscibility gap in the Fe-Cr system), resulting in the increased hardness and lowered ductility. Mössbauer studies confirmed that the α", at this composition and temperature, forms through the process of nucleation and growth. Hardening due to α" precipitation was only observed after aging for 64 hours or more, however. After increasing the dissolved interstitial content by solution heat treatments (in the vicinity of 900°C), increases in Vickers hardness of 30-50 kg/mm^2 could be obtained after only 8 minutes at 475°C. This hardness increase corresponds to an increase in tensile strength of more than 100 MPa. The increased hardness does not appear to be caused by strain aging, and presumably results from fine carbide or nitride precipitation. Solution treatment at 930°C also introduced some martensite (α') into the microstructure, which raised the hardness of the unaged cold worked material.

Overaging of the carbide and nitride precipitates was observed at 475°C, but not at 450°C, probably due to the lower diffusion rates at the lower temperature. No overaging of the α" precipitates occurred, for aging times up to 2072 hours.

Samples aged for selected periods of time at 475°C had low impact strengths – even well before the formation of α" – and revealed predominantly cleavage fracture with some ductile fracture areas, mostly at grain boundaries. Both impact strength and lateral expansion

indicated that embrittlement accompanies the increased hardness obtained by aging. Calculation of critical crack lengths from the impact data, however, revealed that a maximum flaw length of 0.8 mm, for specimens solution treated at 880°C, could be tolerated before catastrophic failure. Since it is not expected that flaws of that size would exist in the as-manufactured links, fatigue will probably determine the lifetime of the chains, although the lower K_{Ic} values indicate that less crack propagation will be tolerated before brittle fracture.

During the aging treatment, the strength may be lowered by recrystallisation of the cold-worked material. Transmission electron microscopy (TEM) revealed the start of recovery, but no recrystallisation. Some large precipitates (around 1μm in diameter) were present. These were identified, through their diffraction patterns, as $M_{23}C_6$; these carbides were present in both aged and unaged material and hence represent precipitates which had not dissolved during the initial solution treatments. The α" precipitates – and the presumed newly formed nitride and carbide precipitates – were too fine for detection by TEM.

Potentiodynamic testing of the treated material in a 0.5M H_2SO_4 solution indicated that, although the probable hardening mechanisms imply localised Cr depletion of the matrix, the general corrosion resistance and passivation behaviour were not affected.

It is concluded that the strength of the chain may be increased markedly by short-term heat treatments at 475°C, with lowered toughness, but with no decrease in corrosion resistance. Martensite, work hardening, and precipitation of carbides and nitrides all contribute to the final strength, with α" formation only becoming significant after longer aging times.

Keywords

slat-band chain

Type 430 ferritic stainless steel

475°C embrittlement

carbide and nitride precipitation

cold work

martensite

strengthening through heat treatment

corrosion resistance

alpha (double) prime

Opsomming

Vervoerbandkettings word veral in die voedselbedryf, brouerye en bottelarye gebruik. Die gebruikstoestande vereis slytasieweerstand, sterkte en korrosiebestandheid. Tipe 430 ferritiese roesvrye staal word tans tot by sy sterktelimiet gebruik. 'n Onkonvensionele versterkingsproses is deur Mintek ontwikkel waarin die bestaande materiaal tussen 450°C en 500°C verouder word. Die doel van hierdie studie is om die moontlike versterkingsmeganismes wat betrokke is, te identifiseer deur van 'n 430 roesvrye staal, met 16.42% Cr en 0.036% C, gebruik te maak. Die materiaal is in die koudverwerkte toestand (38% reduksie in area) getoets, met en sonder voorafgaande oploshittebehandelings.

Die Cr-ryke presipitaat (α") vorm in die 450°C tot 500°C gebied (a.g.v. 'n onmengbaarheidsarea in die Fe-Cr fasediagram) en veroorsaak 'n toename in hardheid en afname in taaiheid. Dit is deur middel van Mössbauer-studies bevestig dat die α", by hierdie samestelling en temperatuur, vorm deur 'n proses van kernvorming en groei van partikels. Verharding deur die α"-presipitate is egter eers waargeneem na veroudering vir meer as 64 uur by 475°C. Nadat die opgeloste interstisiële inhoud verhoog is deur addisionele oploshittebehandelings (in die omgewing van 900°C), is gevind dat 'n toename in Vickershardheid van 30-50 kg/mm^2 verkry kan word binne 'n verouderingstyd van 8 minute. Dié toename stem ooreen met 'n verhoging in treksterkte van meer as 100 MPa. Dit blyk dat die verhoging nie die gevolg van rekveroudering is nie, maar wel waarskynlik toegeskryf kan word aan die presipitasie van fyn karbiede en nitriede. Oplosbehandeling by 930°C het ook die vorming van martensiet tot gevolg, wat die hardheid van die onverouderde materiaal verhoog.

Oorveroudering van die karbied- en nitriedpresipitate is by 475°C waargeneem, maar nie by 450°C nie, moontlik as gevolg van die laer diffusietempo's by die laer temperatuur. Geen oorveroudering van die α"-presipitate is waargeneem nie, selfs vir verouderingstye van tot 2072 uur.

Veroudering by 475°C het lae slagsterktes tot gevolg, selfs voor die vorming van α". Breukvlakke het hoofsaaklik uit splytingsvlakke bestaan, met smeebare breukareas meestal op korrelgrense. Beide die slagsterkte en die laterale uitsetting het getoon dat verbrossing gepaardgaan met die verhoging in hardheid wat verkry word deur veroudering. Die berekening van kritieke kraaklengtes uit die impakdata het egter getoon dat, vir oplosbehandelings by 880°C, die maksimum defekgrootte - voor katastrofiese faling - 0.8 mm is. Dit word nie verwag dat defekte van hierdie grootte in die soos-vervaardigde skakels teenwoordig sal wees nie, en daarom sal die leeftyd van die kettings waarskynlik deur vermoeidheid bepaal word. Die laer K_{1c} waardes toon egter dat minder kraakvoortplanting plaas sal kan vind voor bros faling.

Tydens veroudering kan die sterkte van die materiaal moontlik weens herkristallisasie verlaag. Deur transmissie-elektronmikroskopie (TEM) is dit wel waargeneem dat herstel, maar geen herkristallisasie nie, plaasvind. Presipitate (van ongeveer 1 μm in diameter) is deur middel van hul diffraksiepatrone as $M_{23}C_6$ geëien, en aangesien die presipitate teenwoordig was in beide die verouderde en onverouderde materiaal, is dit waarskynlik dat die presipitate nie opgelos het tydens die oorspronklike oplosbehandelings nie. Die α" en nuutgevormde karbied- en nitriedpresipitate was te fyn om deur middel van TEM waargeneem te word.

Potensiodinamiese toetse in 'n 0.5M H_2SO_4 oplossing het getoon dat, alhoewel die waarskynlike versterkingsmeganismes gelokaliseerde chroomverarming tot gevolg het, die algemene korrosieweerstand en passiveringsgedrag nie deur die hittebehandelings beïnvloed word nie.

Dit kan gevolglik afgelei word dat die sterkte van die materiaal noemenswaardig verhoog kan word deur koue verwerking, en hittebehandeling by 475°C. Dit gaan gepaard met ‘n afname in taaiheid, maar algemene korrosiebestandheid word nie beïnvloed nie. Martensiet, werksverharding en die presipitasie van fyn karbiede en nitriede dra by tot die finale sterkte, terwyl α" eers 'n invloed na langer verouderingsperiodes het.

Sleutelwoorde

vervoerbandkettings

Tipe 430 ferritiese roesvrye staal

475°C verbrossing

karbied- en nitriedpresipitasie

koue verwerking

martensiet

versterking deur hittebehandeling

korrosie weerstand

alfa (dubbel) aksent

Table of Contents

List of Tables

List of Figures

Chapter 1

Introduction

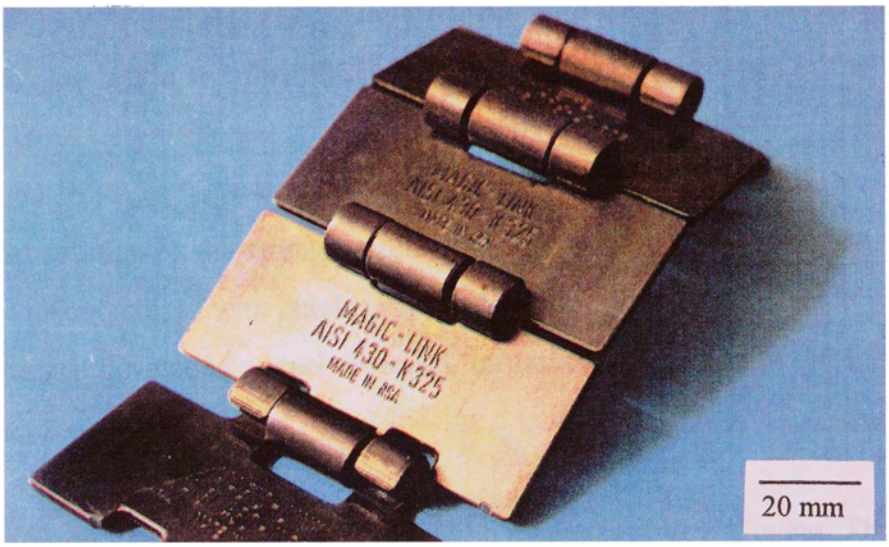

Figure 1.1: *Slat band chain used as conveyor belt*

In places such as breweries and bottling plants conveyors are used to transport bottles between various stages in the operation. One type of conveyor is slat-band chains, which consist of flat links connected by pins through interlinking holes (figure 1.1). The chains are manufactured by hot rolling a sheet of the material, followed by annealing and then cold rolling it to its final thickness. The links are then formed through a blanking process.

Usually stainless steels are utilised for this application, and in 1990 some 5000 tons of stainless steel, including 2500 tons of the ferritic grade AISI 430, was used in Europe for the manufacture of these transporting lines (Charenton and Baltenneck 1992).

The properties required of a material used as a conveyor are a high tensile strength (ultimate tensile strength 850 to 950 MPa) for abrasion resistance, a high yield strength (0.2% yield strength 750 to 850 MPa) to withstand high tensile loads (for maximum possible conveyor length), good formability (as required for cutting and forming of 3mm thick sheet), together

with intergranular and uniform corrosion resistance. These properties coupled with affordability are therefore key issues.

Thus far the steels employed were annealed and cold worked 430 (which is used to the limit of its mechanical properties), and cold worked 201 and 304, which perform satisfactorily, but are expensive. Martensitic stainless steels would be the most economical choice (Thielsch 1951, 1955), but they are brittle and their low formability would be a problem in the manufacturing process.

The traditional solution to the strength problem would be to replace the material from which the chains are manufactured with one having the desired properties. Charenton and Baltenneck (1992) for instance developed a steel especially for conveyors, with a 50-50 ferrite-martensite structure.

As another solution, the existing material could be strengthened by alloying. Though these are sure ways of obtaining the desired effect, they are not always practical, inasmuch as the material is manufactured as a process alloy through mass production, and it may not be economically feasible to produce special batches.

What would be acceptable then, is to find some way to strengthen the material already in use.

Mintek (Council for Minerals Technology) developed the unconventional way of strengthening the 430 by isothermally heating it between 450°C and 500°C after cold working. This temperature range is commonly known as the "475°C Embrittlement Temperature Range", as the effects occur most readily at 475°C. By carefully heat treating the cold worked 430 in this range, it was found that the hardness, yield strength and breaking load could be improved. This made the strength of the locally manufactured chain equal to or even better than any of the imported ones that are available.

The purpose of this study is to elucidate the strengthening mechanism, using type 430 stainless steel containing 16.42% Cr and 0.036% C.

In the manufacturing and treatment process there are several microstructural processes which affect the material properties. Some would cause hardening (or strengthening), while others would have just the opposite effect.

Therefore the following hypothesis was proposed: the mechanisms that could increase the strength of the material are deformation by cold work, strain aging, precipitation of carbides and/or nitrides, precipitation of the Cr-rich phase α" and the presence of martensite in the structure. The mechanisms that could cause a decrease in strength include recovery and grain growth.

In this study, experiments were designed to establish whether these mechanisms are present and whether their effect can be quantified.

Chapter 2

Literature Survey

2.1. Material

2.1.1. Ferritic stainless steels

Background

Since the second decade of this century the use of stainless steels has been extensive. Austenitic stainless steels especially received much attention because of their excellent mechanical and corrosion properties. However, usage of ferritic stainless steels have been limited because of the comparatively poor toughness demonstrated by the conventional ferritic stainless steels such as Types 430 and 446. A major breakthrough for these steels occurred when it was discovered that by keeping the carbon and nitrogen contents sufficiently low, the toughness and ductility of the ferritic grades could be greatly improved (Sheppard and Richards 1987).

Since the ferritic stainless steels can now be more economically produced, because of improved steel refining practices such as AOD (argon-oxygen decarburisation) and VIM (vacuum induction melting) (Nichol *et al.* 1980), their use has increased considerably. Thus a major advantage of the ferritic stainless steels is their relative low cost.

Ferritic stainless steels are generally straight-chromium types containing from 11 to 30% chromium, with no other major alloying elements, having essentially a single phase bcc (body centred cubic) structure. Some of the grades can be more highly alloyed though.

Chromium is of course the basic alloying element and is added to improve the corrosion resistance of the material. Chromium has the additional effect of leading to either a ferritic or martensitic structure in the steel (Thielsch 1951). The minimum chromium content of stainless

steel is about 12.7% while the upper limit of the composition is dictated by the possibility of the formation of the sigma phase. In general the common ferritic stainless steels contain less than 27% Cr (Brooks 1979).

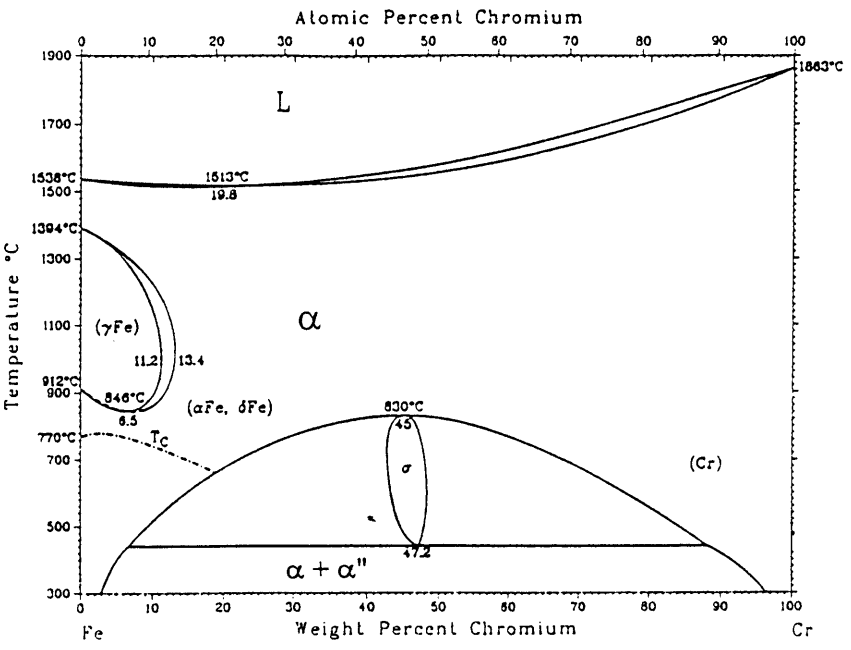

***Figure 2.1**: Iron - chromium phase diagram (Baker 1992)*

In a relatively pure binary solution of iron and chromium the material would be ferritic at most compositions and temperatures (figure 2.1). Because of the alloying elements present in stainless steels a much more complex structure results. With the addition of alloying elements such as C, N and Ni (austenite stabilisers) it is possible to enlarge the austenitic-loop to such an extent that austenite is formed at the customary annealing temperatures. The alloying elements can further retard the ferrite formation sufficiently for the austenite to transform to martensite on cooling (i.e. not having to quench). With alloying it is also possible to stabilise the austenite to such a degree that it is present at room temperature and that the M_s temperature (start of martensite) is below room temperature.

Carbon is the principal element which affects the amount of martensite which may be present. In the absence of other carbide formers (such as Ti and Nb), carbon tends to combine with chromium and iron to form the mixed iron-chromium-carbides M_7C_3 and $M_{23}C_6$. At elevated temperatures (up to 540°C), carbon somewhat improves the short time tensile properties and

the creep resistance. Above 540°C, however, the carbides tend to coalesce (Thielsch 1951). The carbon content is restricted both to maintain high toughness and ductility and to prevent austenite formation related to the expansion of the gamma loop by carbon (Krauss 1989).

In its tendency to form austenite, nitrogen is almost as effective as carbon. Thus N widens the extent of the gamma loop considerably, particularly the two phase ($\alpha + \gamma$) region (Thielsch 1951). The nitrogen is detrimental to the corrosion resistance and the toughness as it does not stay in solution, but combines with other elements such as Cr. The nitrogen is therefore not added deliberately, but is picked up from the atmosphere during tapping and teeming processes.

Molybdenum is sometimes introduced for improved pitting and crevice corrosion resistance (Redmond and Miska 1982)

Of the standard ferritic steels typically only those with over 18% Cr are truly ferritic, that is, have a bcc delta ferrite structure at all temperatures below the solidus, and thus are not hardenable by a quench-and-temper heat treatment. The remainder form varying amounts of austenite on heating to elevated temperatures; the austenite transforms to martensite on cooling (Truman 1992).

In the absence of carbon and other austenite forming elements, the (austenite + ferrite)-region is very narrow (figure 2.1). With increasing carbon content the fully austenite region widens somewhat and is extended at 0.1%C to about 12.5% Cr. The two phase region is widened considerably more to about 18% Cr. Effects similar to those produced by carbon are produced by other austenite forming elements such as N, Ni and Mn. The ferrite formers, on the other hand, tend to reduce the extent of the gamma loop. These include elements such as Al, Si and Mo (Thielsch 1951).

A pseudo-binary phase diagram was constructed which takes into account the effect of carbon (at a fixed chromium content) on the austenite-loop - figure 2.2. It is indicated by this diagram for instance, that solution treatment at 930°C (for a steel containing 16.4% Cr and 0.05% C,

i.e. the one investigated) would result in a three phase structure, namely ferrite, austenite and (Fe,Cr)-carbides (see also section 6.1.1).

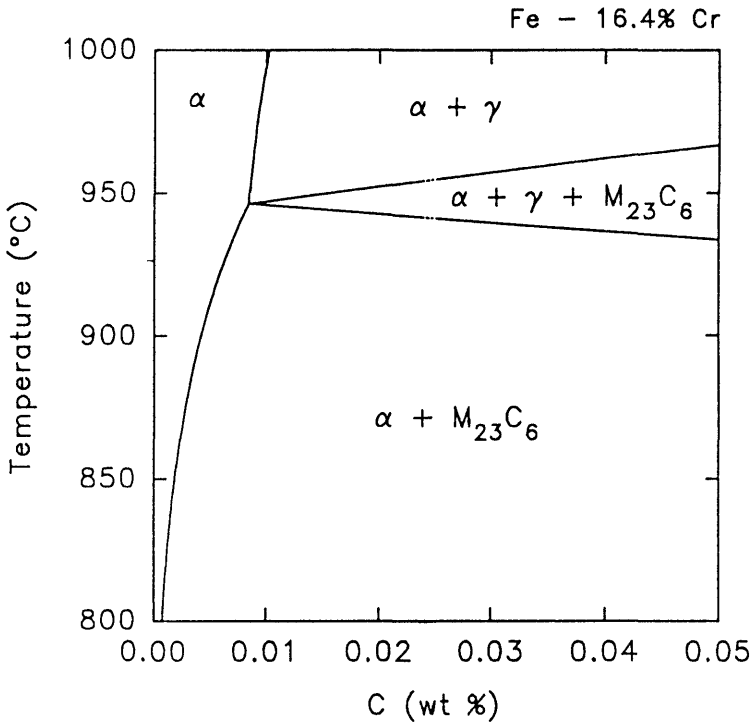

***Figure 2.2**: Pseudo Binary phase diagram at 16,4% Cr (Pistorius and Coetzee 1996)*

In these steels the microstructure-property relationships are important, but by no means simple, because (Truman 1992):

(a) the ferrite commonly contains polygonised sub-grains which influence the yield stress but not the ductile-brittle transition temperature,

(b) the structures often include martensite regions, or tempered martensite, originating from austenite present at the solution treatment temperature. Increasing amounts of austenite cause a progressive grain refinement of the ferrite, due to a second phase pinning effect,

(c) substitutional-interstitial interactions can occur which markedly influence solid solution strengthening,

(d) many interstitial and substitutional solutes have pronounced embrittling effects, increasing the ductile-brittle transition temperature, and

(e) pronounced embrittling effects, produced by precipitation of α" and sigma phase, can occur in certain heat treatment conditions.

In general the mechanical properties of the ferritic grades do not match those of the austenitic steels, but they are being increasingly utilised where the combination of cost and corrosion resistance is the prime selection criterion (Sheppard and Richards 1986).

Ferritic stainless steels are magnetic and can be cold-worked or hot-worked, but they develop their maximum softness, ductility and corrosion resistance in the annealed condition. In this condition the strength of these steels is approximately 50% higher than that of carbon steels, and they are superior to the martensitic stainless steels in corrosion resistance and machinability (M.B. Cortie, personal communication).

In comparison with low-carbon steels, the conventional ferritic stainless steels, such as type 430, exhibit higher yield and tensile strengths, as mentioned, but low elongations; thus they are not as formable as the low-carbon steels. Low levels of sulphur and silicon promote good formability of the ferritic types, because inclusions can act as initiation sites for cracks during forming (Redmond and Miska 1982).

A notable problem with this type of stainless steel is that its impact properties are sensitive to the ferrite grain size. This is a problem in body-centred cubic alloys, and in the ferritic stainless steels the grain size can be controlled only by cold working and annealing. Thus prolonged heating at high temperature will cause grain growth, and hence lower the impact resistance. This can be a problem particularly in welding, where the cast structure or the heat-affected zone may contain large grains which cannot be altered if the fabricated part cannot be cold worked and annealed. To minimise this problem a second phase (e.g. carbides or austenite) may be required at high temperatures to retard grain growth (Brooks 1979).

Generally, toughness in the annealed condition decreases as the chromium content increases. The grain growth and relatively low toughness at low temperatures have limited the use of ferritic stainless steels in structural applications. As a result, ferritics are used for nonstructural applications that require good resistance to corrosion and bright, highly polished finishes.

As a class the ferritics are highly resistant to chloride-induced stress-corrosion-cracking (Redmond and Miska 1982).

An advantage of these steels is that the solubility of carbon and nitrogen at the normal annealing temperature of 800 to 850°C is very low (figure 2.1) so that precipitation and homogenisation are largely completed by such a treatment, and there is no detrimental effect on the corrosion resistance should the steels subsequently be heated for moderate periods at lower temperatures. However, heating to temperatures above 925°C reduces the corrosion resistance and the corrosion is usually intergranular (Truman 1992). At these temperatures the solubility of the carbon is sufficiently high for chromium carbides to be precipitated, on cooling, at the ferrite grain boundaries. Intergranular corrosion results from this precipitation, as it produces local Cr impoverishment (sensitisation) and thus preferential corrosive attack. This problem can be overcome by annealing at 650 to 850°C, which allows Cr diffusion into the depleted regions, or stabilising the steel by additions of Nb or Ti to prevent the precipitation of Chromium carbides (Pickering 1979).

It is commonly believed that these steels cannot be hardened by heat treating, and only moderately so by cold working. This, however, is not invariably true, and carefully controlled heat treatment can give higher hardness and sometimes higher toughness (M.B. Cortie, personal communication).

Embrittlement

Ferritic stainless steels are prone to the following types of embrittlement:

475°C embrittlement

This type of embrittlement will be discussed in detail in section 2.2.4.

Sigma-phase precipitation

Sigma phase is an intermetallic compound of Fe and Cr, with approximately equi-atomic composition. It appears as a hard, highly brittle, nonmagnetic phase exhibiting a tetragonal unit cell in certain chromium steels (Rajkay 1967). The maximum temperature at which this form of

embrittlement can occur depends on Cr content; and is approximately 620°C for a 17% Cr steel (Lena and Hawkes 1954), it is also indicated by the Fe-Cr phase diagram (figure 2.1).

In most alloys the rate of sigma formation is very slow (10^3-10^4 hours for a 18% Cr steel (Folkhard 1984, p.130)), but cold work has been shown to enhance the formation. It deteriorates both notch toughness and corrosion resistance (Rajkay1967, Mashimo *et al.* 1985).

High temperature embrittlement

This phenomenon seems to be structure-dependent, as it appears in the completely ferritic matrix (usually at temperatures higher than 1150°C) as soon as the carbides are in solution; and is apparently caused by the failure or inability of the carbides to reprecipitate during the cooling process (Rajkay1967).

It is accompanied by severe grain growth, although a large grain size alone will not account for the embrittlement: it appears that the severity of the high temperature embrittlement depends on carbide solution and not on grain growth (Thielsh 1951). The solution of carbides not only promotes subsequent grain growth, but the carbon in the matrix that is obtained in this way is not uniformly distributed in the ferrite lattice. The carbon is grouped in atomic clusters, as suggested by the segregation or coherent state theory. These carbon clusters cause the embrittlement (Demo 1971).

The embrittlement is especially pronounced with high cooling rates but the detrimental effects can be removed by annealing between 730°C and 790°C. This will, however, not reduce the excessive grain size. The detrimental effects can be prevented by retention of some austenite at carbon-solution temperatures, or by stabilisation of the carbides (Thielsch 1951 and 1955, Rajkay 1967, Demo 1971).

2.1.2. Type 430 Ferritic Stainless Steel

Type 430 has about 17% Cr and is a general-purpose grade. It has good drawing properties due to its low rate of work hardening, as well as good ductility and corrosion resistance to atmospheric conditions. It is used frequently for automotive trim, nitric acid tanks, annealing baskets and other such applications in which weldability is not a requirement. It is also used increasingly for domestic sinks, kitchen utensils and cutlery.
The composition range of 430 ferritic stainless steel is given in Table 1 (Redmond and Miska 1982):

Table 2.1: Composition of type 430

Element	C	Mn	Si	Cr	P	S
Weight%	0.1*	1*	1*	16 - 18	0.04*	0.03*

* maximum values

The specific composition of the material studied in this investigation will be given in Chapter 3.

2.2. Strengthening Mechanisms

The two main ways to strengthen ferritic stainless steels are cold work, and solution treatment and aging. These are discussed in more detail.

2.2.1. Cold Work

When a metal is plastically deformed at temperatures that are low relative to its melting point, it is said to be cold worked. The temperature defining the upper limit cannot be expressed exactly, for it varies with composition as well as the rate and amount of deformation (Reed-Hill 1992).

Cold work distorts the grains and causes a persisting deformation of the crystalline structure of the metal (increase in dislocation density), as recrystallisation does not occur simultaneously with the plastic deformation (unlike hot working). The stress needed to continue the process of

cold working increases with increasing degree of deformation (work hardening), as is illustrated in the true stress - true strain curve (figure 2.3).

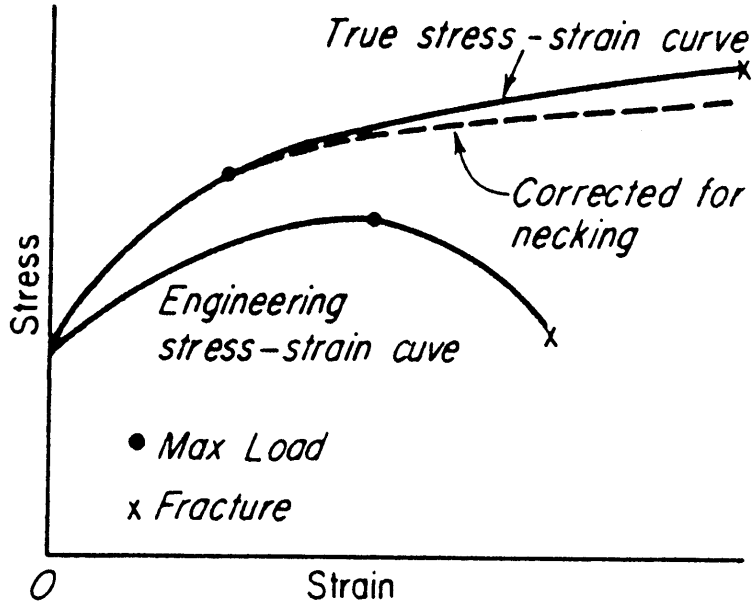

***Figure 2.3**: True stress-true strain curve (Dieter 1988, p.285)*

All the properties of the metal that are dependent on the lattice structure are affected by this plastic deformation. Tensile strength, yield strength and hardness, as well as electrical resistance, increase after cold work. Ductility is lowered by the increase in the number of dislocations. Certain planes in the crystal structure become severely distorted (Dieter 1988, pp. 229-231).

Every metal shows a certain amount of elongation before it breaks. During cold work some of this elongation is consumed, reducing the available ductility. In general, heat treatment after cold work produces recovery or recrystallisation and a subsequent lowering in hardness, with restoration of ductility.

Most of the energy expended in cold work is converted to heat, but a finite fraction is stored in the metal as strain energy associated with the various lattice defects created by the deformation. The amount of energy retained depends on the deformation process and a number of other variables, such as composition of the metal and rate and temperature of deformation.

The fraction of the energy that remains in the metal can be up to as much as 10% (Reed-Hill 1992, pp. 227-228).

It had been shown that the stored energy increases with increasing deformation, but at a decreasing rate, so that the fraction of the total energy stored decreases with increasing deformation. The amount of stored energy can be greatly increased by increasing the severity of the deformation (as mentioned), lowering the deformation temperature and by changing the pure metal to an alloy.

The increase in internal energy, particularly at the grain boundaries, renders the material more susceptible to intergranular corrosion; stress corrosion cracking can occur due to residual stresses.

Cold working, as said before, greatly increases the number of dislocations in a metal. Since each dislocation represents a crystal defect with an associated lattice strain, increasing the dislocation density increases the strain energy of the metal.

2.2.2. Solution Treatment and Aging

Solution treatment and aging can be used as a strengthening procedure in an alloy where the solubility of the alloying element increases significantly with increasing temperature. The solubility of carbon in 430 is a case in point - figure 2.2.

In the most simplistic approach, if an alloy is solution treated, i.e. reheated to the single phase region, all excess of the second phase will be dissolved and the structure will be a homogeneous solid solution. If the alloy is then rapidly cooled (quenched) to room temperature, a supersaturated solution results with the excess elemants which form the second phase trapped in solution. This is an unstable state and the excess solute will tend to come out of solution.

The rate of precipitation, when a solution treated alloy is aged, varies with temperature (figure 2.4).

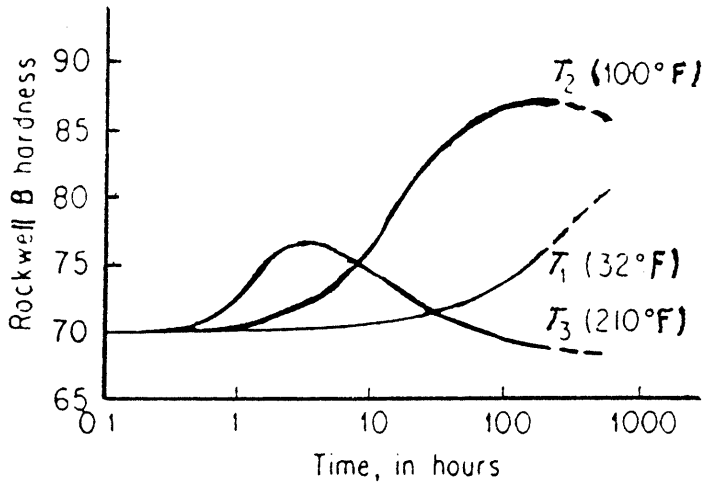

***Figure 2.4**: The influence of temperature on precipitation (Avner 1992)*

At low temperatures (represented by T_1) the diffusion rate is so low that no appreciable precipitation occurs. At high temperatures (T_3) hardening occurs quickly, due to rapid diffusion, but softening effects are also accelerated, resulting in a lower maximum hardness. The optimum temperature is where maximum hardening occurs within a reasonable length of time.

In the early theory of the aging process, it was thought that the excess phase comes out of solution as fine submicroscopic particles, many of which form on the slip planes. These particles were thought to have a keying action, thereby interfering with movement along planes of ready slip, thus increasing strength and hardness. Subsequent studies showed that the strengthening of a heat treatable alloy by aging is not due merely to the presence of the observable precipitate, but also to both the uniform distribution of a finely dispersed submicroscopic precipitate and the distortion of the lattice structure by those particles before they reach a visible size.

The coherent lattice theory is widely accepted as one mechanism by which these second phase particles harden the matrix: after solution treatment and quenching the alloy is, as mentioned before, in a supersaturated condition, with the solute atoms distributed at random in the lattice structure (figure 2.5a).

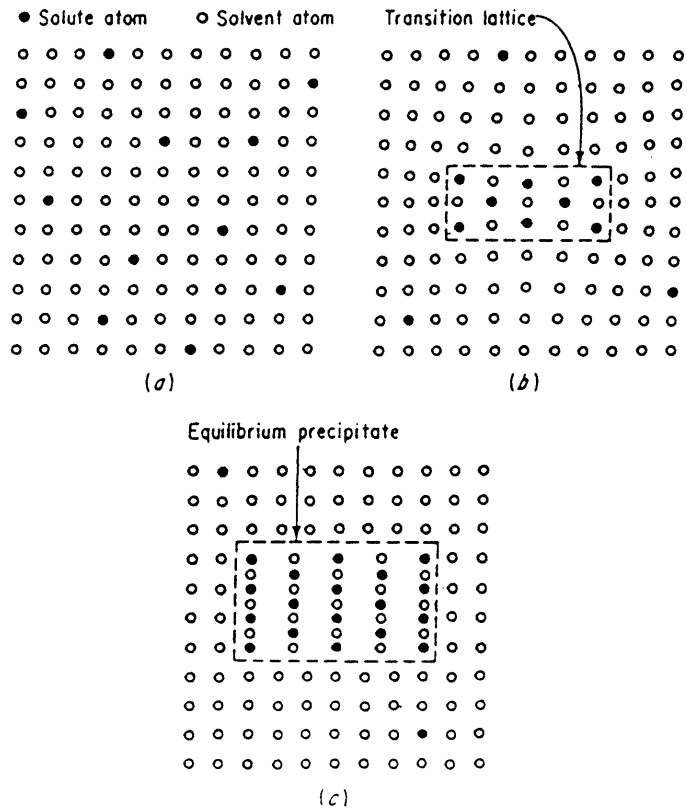

***Figure 2.5**: Schematic diagram of a lattice structure consisting of two elements (Avner 1992) (a) solution treated, (b) aged to form coherent precipitate and (c) overaged to form equilibrium precipitate*

During an incubation period, the excess solute atoms tend to migrate to certain crystallographic panes, forming clusters or embryos of the precipitate. With aging, these clusters form an intermediate crystal structure or transitional lattice, maintaining coherency with the lattice structure of the matrix.

In most cases the excess phase will have different lattice parameters from those of the solvent, and as a result of the atom matching (coherency), there will be considerable distortion of the matrix (figure 2.5b). This distortion extends over a larger volume than would be the case if the excess phase were a discrete particle. It is this distortion that interferes with the movement of dislocations and accounts for the rapid increase in hardness and strength during the aging process.

Eventually, the equilibrium excess phase is formed with its own lattice structure (figure 2.5c). This causes a loss in coherency with the matrix and accordingly less long distance distortion.

The material properties are not only affected by the aging temperature, but also by the time held at temperature. Figure 2.6 gives a schematic illustration of the effect that aging time has on the most important mechanical properties.

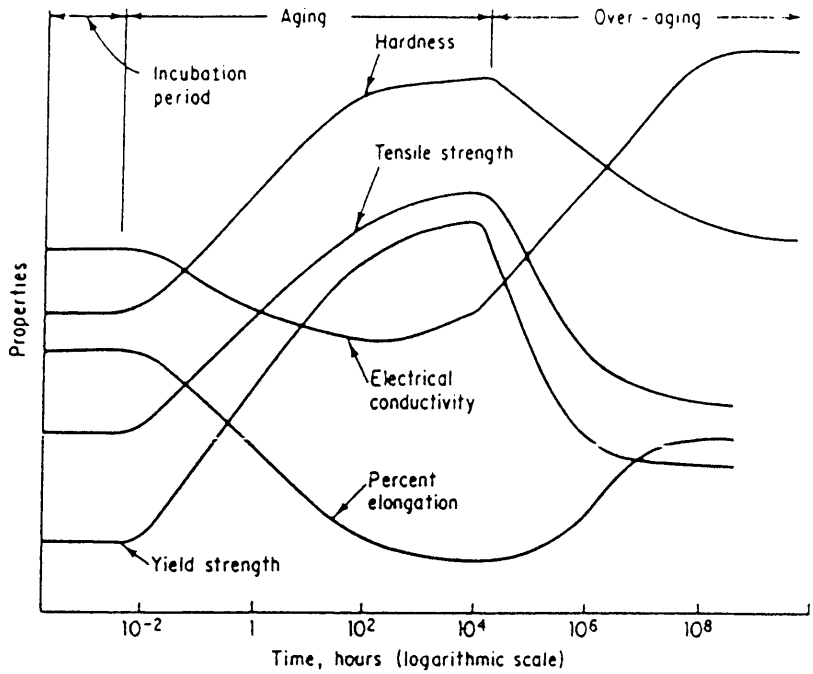

***Figure 2.6.**: Effect of aging time on mechanical properties (Avner 1992)*

2.2.3. Fine Particles

It was mentioned in the previous section that fine coherent particles can cause strengthening by producing local strain fields in the matrix and their influence on dislocation movement. Coherent and noncoherent particles can further induce strengthening through *their* effect on dislocation motion.

Coherent precipitates can act as particles through which dislocations can pass, but only at stress levels much above that required to move dislocations through the matrix phase. The dislocation-particle interactions cause an increase in strength.

Noncoherent precipitates can also be strong impenetrable particles where an increase in strength is obtained by the shear stress required to bow a dislocation line between two particles - the Orowan mechanism. As dislocations pass around the particles, dislocation loops are left

around each particle, leaving the original dislocations free to move on. The dislocation loops exert a back stress on dislocation sources which must be overcome for additional slip to take place. This results in an increase in shear stress (Dieter 1988, pp 215-219).

This strengthening mechanism is typical of hard particles, such as carbides, and the strengthening effect of these particles becomes greater as the size of the particles decreases.

2.2.4. 475°C Embrittlement

Another, unconventional way to strengthen a material is to embrittle it. In most cases embrittlement operates on the same principle as the classic precipitation hardening where dislocation motion is impeded or arrested - causing an increase in strength. As mentioned before, ferritic stainless steels are prone to four main types of embrittlement, one of which - 475°C embrittlement - was used in the strengthening treatment applied to the original chains.

Background

Early work showed that when Fe-Cr alloys containing between 13 and 90% Cr are held in or slowly cooled through the temperature range 800-400°C hardening accompanied by embrittling occurs. In this, two distinct reactions are involved: the formation of the hard and brittle sigma phase (at high temperatures) and the Cr-rich precipitate known as α" in the lower temperature regions (Newell 1946, Blackburn and Nutting 1964).

This latter type of embrittlement was noted after the steels have been exposed to temperatures between 371°C and 550°C. The embrittlement can occur during manufacturing of the steels, with handling of primary or intermediate product forms such as ingots, slabs and hot-rolled coils, or during fabrication of finished products where welding is necessary (Plumtree and Gullberg 1976, Nichol *et al.* 1980).

As this embrittlement affects the mechanical properties, it is usually thought of as detrimental and thus worthwhile avoiding.

Proposed Theories

At first several theories were advanced to account for the embrittlement observed with aging at the lower temperatures. These include the precipitation of minor phases such as carbides, nitrides, oxides (Blackburn and Nutting 1964) and phosphates (Lena and Hawkes 1954) and the formation of a series of super-lattices (ordering) based on Fe_3Cr and FeCr (Williams and Paxton 1957; Marcinkowski *et al.* 1964).

Theories of this kind, however, have difficulties accounting for the influence of alloying elements on the embrittlement, for the fact that a minimum Cr content is necessary for embrittlement, as well as that the intensity of embrittlement increases with Cr content. Grobner (1973) demonstrated through the construction of a free energy diagram of the iron-chromium system at 482°C that ordering processes cannot be responsible for this phenomenon; the free energy diagram contains the local maximum which is typical of alloys which exhibit immiscibility.

The formation of a transition phase prior to the formation of equilibrium sigma phase was also suggested as a possible explanation for the embrittlement (Williams and Paxton 1957). Several factors have, however prevented the complete acceptance of this theory. Foremost is that the embrittlement can be removed by reheating for short periods above 600°C, which in the higher Cr steels, is well within the stable sigma region. No sigma has ever been observed after one of these curing treatments, nor has any sigma been found as a result of embrittlement at 475°C. In addition, the simple precipitation of the sigma phase cannot explain the time-temperature relationship for reactions between 350°C and 750°C. Lena and Hawkes (1954) proposed a schematic time-temperature dependence diagram for the formation of σ and 475°C embrittlement (figure 2.7), which indicate these to be quite separate processes.

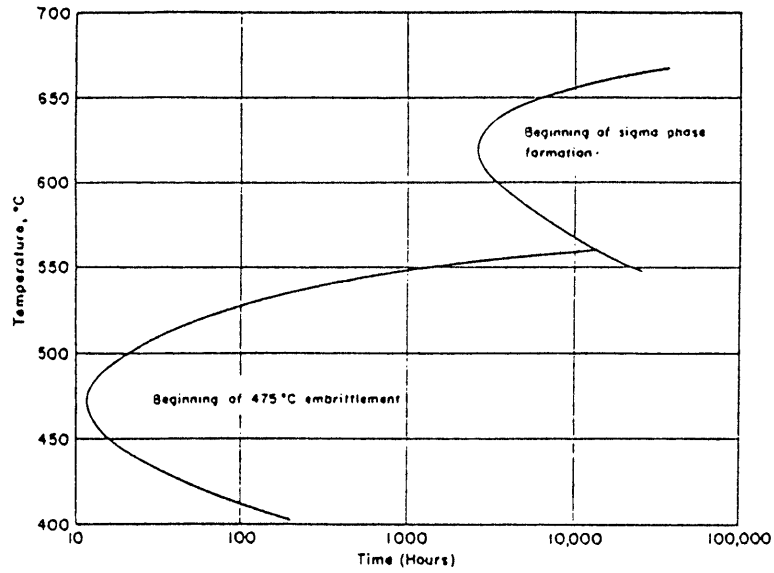

***Figure 2.7**: Schematic time-temperature dependence diagram for the formation of sigma phase and 475 ℃ embrittlement (arbitrary alloy) (Lena and Hawkes 1954)*

The most widely accepted theory for the 475°C embrittlement is the one first proposed by Williams and Paxton (1957), namely the precipitation of a coherent Cr-rich phase, α". It is an aging or precipitation hardening phenomenon, where precipitation occurs because of a miscibility gap in the Fe-Cr system.

Stages in the embrittlement process

It was found that the 475°C embrittlement was actually a two stage process. Hardness and strength increase rapidly in the early stages of aging was observed, followed by a plateau region and then a relatively large increment after long periods of aging (Plumtree and Gullberg 1976, Nichol *et al.* 1980, Golovin *et al.* 1992).

The initial increase (at short aging times) is ascribed to the precipitation of Cr-rich carbides and nitrides at and near grain boundaries and at inclusions and dislocations. The precipitates were identified as $M_{23}C_6$ and Cr_2N (Blackburn and Nutting 1964, Marcinkowski *et al.* 1964, Lagneborg 1967).

The influence of α" precipitation seems to come into effect only after longer periods of aging (several hours, even days), and it is believed that the rate of α" formation is much lower than the precipitation of carbides and nitrides, because the interstitial atoms have relatively high diffusivities (Chun and Polonis 1992, Golovin *et al.* 1992). This argument assumes that the formation of α" is governed by the growth rate of the particles, whereas it may well be that the nucleation rate is the determining factor.

Interstitial elements

The two most important interstitial elements are carbon and nitrogen. Both form interstitial solid solutions in ferrite and the atomic radii and weights of the two are nearly the same (Binder and Spendelow 1950).

Carbon solubility is considerably lower than that of nitrogen at temperatures below 982°C and is approximately 0.004% at 900°C, where the kinetics of carbide formation are so rapid that it is impossible to prevent completely carbon precipitation, even by water quenching (Pollard 1974).

Carbon has three hardening effects: a straining effect in solid solution, dispersion hardening by precipitation of carbides (Orowan mechanism) and an increase in nucleation of α" because of the mechanical straining effects of the precipitated carbides (Tisinai and Samans 1957).

It was demonstrated that for good room temperature toughness, ductility and impact strength, as well as resistance to intergranular corrosion, the interstitial content must be reduced with increasing Cr content - for an 18% Cr steel of high toughness the maximum interstitial content, which still allows acceptable toughness, is approximately 0.055% (Binder and Spendelow 1951, Grobner 1973, Aggen *et. al.* 1978, Chun and Polonis 1992).

The interstitials have a two-fold effect on 475°C embrittlement: as precipitates they cause strengthening, and they influence the precipitation of the α". Precipitates of carbon and nitrogen below 500°C appear to consist of little more than clusters of C and N on the {100} planes of the ferrite (Cortie 1995). These precipitates or clusters are surrounded by intense

strain fields, and exert a hardening and embrittling effect on the microstructure. There are some controversy as to the precise effect the interstitials have on α" formation. Some investigators reported an enhancement in precipitation, because of the local strain fields surrounding the carbide and nitride precipitates; while others reported significant retardment in the development of α" formation (Cortie 1995).

α" precipitate

Precipitation

Convincing proof was found for the existence of a region in the Fe-Cr system where the iron and chromium atoms are not randomly distributed on the bcc crystal lattice, but separate and cluster (Krause 1989). This necessitated a modification to the central portion of the FeCr phase diagram - figure 2.8 - to include the miscibility gap.

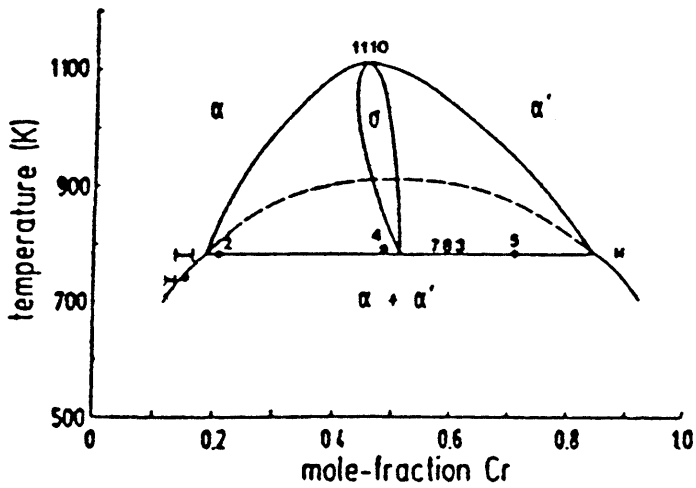

***Figure 2.8**: Thermodynamic assessment of the Fe-Cr system (Dubiel and Inden 1987)*

This region is formed due to the thermodynamic qualities of the Fe-Cr system rather than to basic structural distinctions. Consideration of the thermodynamic properties of regular solutions with positive heats of mixing leads to the conclusion that in such a system a critical temperature must exist above which the components are completely miscible, and below which the system consists of a mixture of two solutions, one rich in component A and the other in component B - in this case Fe and Cr (Grobner 1973, Trindade and Vilar 1991).

The phase diagram proposed by Williams indicates that in alloys with 14 to 18% Cr, formation of the α" phase can be expected at temperatures up to about 516°C and that it can be completely redissolved at temperatures higher than this. The lower temperature limit of this embrittlement is evidently determined by the kinetics of the α" formation. The kinetics are those of two partially parallel processes: that of nucleation, and growth of the nuclei. That is to say the nucleation process of new α" centres continues while growth of the initial nuclei occurs.

Chemical and/or magnetic energies are considered to be responsible for this miscibility gap rather than strain energy or valency effects. The miscibility gap is connected by an eutectoid reaction to the region where sigma phase is stable and the eutectoid temperature for the decomposition of α into the Fe- and Cr-rich regions lies within the interval 500°C to 532°C (Williams and Paxton 1957, Dubiel and Inden 1987).

The miscibility gap contains what is known as a spinodal. The spinodal is the locus of points for which the second derivative of free energy (G) with composition (c) equals zero. In the region where the mechanism of nucleation and growth prevails, $d^2G/dc^2 > 0$ and the resultant activation energy restricts decomposition to nuclei of a critical size and a composition very near the equilibrium values given by the miscibility gap solubility boundaries. Below the spinodal $d^2G/dc^2 < 0$ (i.e. no internal stability) and no activation energy for growth exists, so the decomposition is governed by diffusion alone and can start spontaneously without any nucleation event (Miller 1961, Lagneborg 1967, Chandra and Schwartz 1971, Porter and Easterling 1992).

In this way two mechanisms, depending on alloy composition and aging temperature, exist by which α" is formed: nucleation and growth and spinodal decomposition.

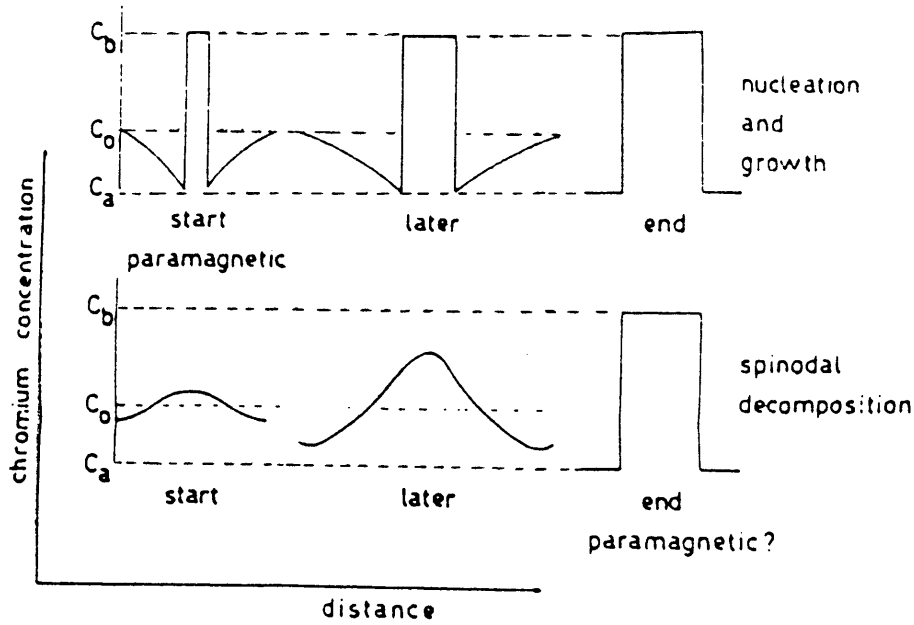

***Figure 2.9**: Schematic evaluation of concentration profiles to illustrate the difference between the spinodal mechanism and nucleation and growth (De Nys and Gielen 1971)*

In the nucleation and growth process, the solid solution separates into two phases, one of which, the chromium-rich, must be paramagnetic from the very beginning of the process, since it has the final composition right from the start - see figure 2.9.

Spinodal decomposition, on the other hand, produces fine clusters of iron and chromium without well defined interfaces and with fine-scale concentration gradient. It is proposed that in this decomposition mechanism, the Cr-rich region should become paramagnetic only at the end of the decomposition, because the chromium regions form slowly and the Cr concentration in these regions increases slowly with time - figure 2.9 (De Nys and Gielen 1971).

Spinodal decomposition is favoured by high Cr contents and low aging temperatures (Nichol *et al.* 1980). An alloy with less than 24% Cr - as the one investigated in this study - is expected to lie outside the spinodal and hence decompose via nucleation and growth processes (Chandra and Schwartz 1971, De Nys and Gielen 1971, Grobner 1973).

Size and detection of the α" precipitate

No apparent changes in microstructure (as revealed by optical microscopy and X-ray diffraction analysis) accompany the embrittlement, except for an initial widening of the grain boundaries, which may indicate an increased rate of attack by etchants (Fisher *et al.* 1953, Blackburn and Nutting 1964, Grobner 1973, Aggen *et al.* 1978, Nichol *et al.* 1980).

The precipitates have been detected through transmission electron microscopy and though the orientation of the foils is critical - primarily because of the similarity in scattering factors and atomic volumes of the Fe and Cr atoms (Lagneborg 1967) - the precipitates could be detected because they were mostly defined by regions of contrast adjacent to them. These regions have been interpreted as regions of coherency strain induced in the matrix lattice by differences in atomic size of the zone constituents or differences in lattice parameter of the precipitate phases.

The α" precipitates were revealed to consist of a simple bcc phase of approximately 200Å in size (after 10 000 to 34 000 hours at 475°C), with a lattice parameter of 2.878Å - only 0.2% larger than the matrix. This corresponds to an Fe-Cr alloy with 70 - 90% Cr. This phase is not ferromagnetic (Fisher *et al.* 1953, Grobner 1973).

As the volume fraction of the precipitates increases their morphology changes from isolated, roughly spherical to a continuous interconnected network as predicted from percolation theory. The volume fraction might be increased either by increasing the solute content or by changes in the aging temperature and shape of the miscibility gap at a constant solute content (Miller 1961). It has also been shown that in the iron-chromium system, a plate-like morphology (as opposed to spherical) would be expected to lead to a somewhat lower strain energy (Blackburn and Nutting 1964, Lagneborg 1967). A decrease in the coherency strains will lower the activation energy for nucleation and will consequently enhance the rate of nucleation. Hence, it seems likely that discs, which produce a minimum coherency strain, will form outside the spinodal where the decomposition must be initiated by nucleation.

It is thought that a slow process like coalescence may determine the growth rate, also at fairly short times, which offers an explanation for the lack of significant changes in the particle sizes during the first 1000 hours of aging. The reasons for the very slow coalescence is the low surface energy between the precipitate and the matrix, and the low diffusion rate at 475°C (Lagneborg 1967).

Rate at which embrittlement occurs

It was found that the time of most rapid embrittlement coincided with the beginning of the formation of zones enriched in Cr and also that the rate and intensity of the embrittlement increase with increasing Cr and interstitial content. This may be related to carbide and nitride precipitation acting as competing or supplementary reactions to that of the α" precipitation (Lena and Hawkes 1954, Tisinai and Samans 1957, Grobner 1973, Aggen *et al.* 1978, Nichol *et al.* 1980, Golovin *et al.* 1992).

There is evidence that lattice straining increases the rate of nucleation of α" (Tisinai and Samans 1957) and that the rate of *growth* of the α" precipitate during extended periods of aging at 475°C is very low, as the sizes stay virtually the same between 10 000 and 34 000 hours of aging (Fisher *et al.* 1953).

Mechanical properties

It was found that the formation of α" phase causes significant changes in the mechanical properties of the steels.

Hardness increases markedly when aged at 475°C, but stays virtually constant with aging at 550°C. For the first few hundred hours at 475°C the increase in hardness is rapid. After that the hardness still increases, but at a much lower rate. Eventually (at 10 000 to 34 000 hours of aging) no further changes are apparent (Lagneborg 1967, Fisher *et al.* 1953). Also, higher hardness (and yield strength) can be obtained for samples quenched from 850°C in water, rather than cooled in the furnace, before aging; in the former, a uniform distribution of α" is responsible for the hardness increase whereas on furnace cooling, the hardening is mainly due

to the heterogeneous precipitation of relatively large chromium nitrides (or carbonitrides) at the grain boundaries (Plumtree and Gullberg 1976).

Thus the changes in the physical and mechanical properties can be summarised as follows: the hardness, yield stress and Curie temperature increase while the electrical resistiwity, impact resistance and corrosion resistance decrease.

Mechanism by which strengthening is obtained

The fact that iron and chromium have almost the same diffusion coefficient and because their lattice parameters, both bcc, are almost identical (iron = 2.86005Å and Cr = 2.8786Å), make the determination of the way by which strengthening is obtained difficult (De Nys and Gielen 1971).

Both the matrix and precipitate (α") are under essentially isotropic stresses and are strained to a common lattice parameter, that of the unaged material. Strengthening is caused by the interaction of the particles and matrix with the hydrostatic stresses around edge dislocations. It is proposed that both the matrix and the particles are hydrostatically stressed and that the particles are unable to withstand great shearing forces in that they are continuous with the matrix and the slip planes are undistorted. The coherency also increases the hardness due to internal strains (Fisher *et al.* 1953, Williams and Paxton 1957).

Through an increase in the Peierls friction stress the presence of the small spherical α" precipitates could strengthen Fe-Cr alloys. A large friction stress arises as dislocations move through high-chromium ferrite. It was found that, for a 47.8% Cr alloy, in the case of slip, lattice friction within the Cr-rich α" phase and the chemical energy associated with the interface between the two phases contribute about 60% of the total strength. The contributions of coherency strains and modulus differences are thought to contribute the remaining 40%, but are difficult to evaluate because of the uncertainties regarding the flexibility of the dislocation line (Marcinkowski *et al.* 1964).

Chemical strengthening arises as a dislocation cuts through the Cr-rich precipitates, creating an interface between the particle and the matrix which consist of unlike Fe-Cr bonds. The creation of these bonds requires an expenditure of energy and thus impedes the motion of the dislocation.

The effects of differences in lattice parameter and elastic modulus (of the Cr-rich zones and the matrix) are thought to be greater for slip than for twinning, and because of this the shear stress for slip increases rapidly with aging time until it surpasses that for twin propagation. As embrittlement proceeds, twinning becomes an increasingly important mode of deformation at room temperature (Blackburn and Nutting 1964; Marcinkowski *et al.* 1964; Aggen *et al.* 1978).

It seems that the embrittlement of pure Fe-Cr alloys requires the presence of lattice strains, which increases the energy level of the homogeneous α and provides energy for the decomposition to α and α". Although stresses are necessary for extensive embrittlement in short times, the amount of stress required does not have to be large. The straining necessary for embrittlement can be achieved by external deformation or by the precipitation of a second phase such as carbides and nitrides (Lena and Hawkes 1954).

The presence of antiferromagnetism is believed to result in an additional strengthening mechanism very similar to that for ordered precipitates (atomic ordering) (Williams 1958).

Overaging

As the embrittlement is an age-hardening phenomenon it should exhibit overaging, but this is not observed experimentally, even after thousands of hours of exposure (Fisher *et al.* 1953, Marcinkowski *et al.* 1964).

This unique feature of Fe-Cr alloys not to produce overaging is thought to be due mainly to slow coalescence. The coalescence is slow because of low surface energy between the precipitates and matrix, and the low diffusion rate at 475°C (Lagneborg 1967).

Recovery

The embrittlement can be removed by re-annealing. With heating above 550°C complete resolution of the particles and reversion to the unaged condition can be attained.

Considerable growth of the carbide and nitride phases might however occur at this temperature (Blackburn and Nutting 1964, Marcinkowski *et al.* 1964, Brooks 1979).

Effect of alloying elements on embrittlement

It was found that the rate of the embrittlement increases with increasing Cr content and appears to decrease with increasing purity (i.e. decrease in mainly C and N content). Although the phase diagram predicts that 475°C embrittlement could occur in steels with as low as 10% Cr, effects are rarely noted unless the Cr content exceeds 13% (Heger 1951; Nichol *et al.* 1980).

The extent of changes in physical characteristics during embrittlement depends on Cr concentration and time at temperature, higher alloy content and longer time both promoting more rapid and extensive changes. The temperature of most pronounced embrittlement decreases with declining Cr content (Binder and Spendelow 1950, Fisher *et al.* 1953, Rajkay 1967).

Carbon increases the effects of the embrittlement as hardness was seen to increase and elongation decrease with increasing C.

Titanium accelerates the embrittlement phenomenon, as it forms carbides and thus prevents the forming of chromium-carbides. In this way more Cr is left to take part in the embrittling process (Heger 1951; Grobner 1973; Nichol *et al.* 1980).

Niobium accelerates the embrittling in the same way as titanium (Heger 1951; Nichol *et al.* 1980).

Molybdenum has a negligible effect at low Cr contents, but significantly increases embrittlement as the amount of Cr is increased (Heger 1951; Grobner 1973; Nichol *et al.* 1980).

Manganese (up to 3%) lowers the effect of the 475°C embrittlement, perhaps by promoting the formation of austenite, while the embrittling is confined to ferrite (Heger 1951).

Si, P, Al and N also intensify the embrittlement (Heger 1951, Trindade and Vilar 1991).

Addition of nickel enhances the spinodal decomposition kinetics and hence the rate of embrittlement (Nichol *et al.* 1980, Trindade and Vilar 1991) at low amounts, while at higher concentrations austenite begins to form and hence embrittlement is decreased (Heger 1951).

Vanadium decreases rather than increases the 475°C embrittlement, as it slightly lowers the rate of embrittlement, although it increases the hardness if added in amounts up to approximately 1%. Because the atomic diameter of the vanadium atom is larger than that of iron or chromium, the dissolution of V would cause higher coherency stresses and thus a greater increase in hardness during aging (Koutaniemi *et al.* 1974).

Effect of cold work on embrittlement

Although it had been reported that deformation before aging does not have an effect (Williams and Paxton 1957, Lagneborg 1967), it was demonstrated that a small degree of deformation can cause a decided increase in the amount of hardening produced by subsequent heat treatment at 475°C. This effect is usually attributed to increased nucleation because of strain (Lena and Hawks 1954, Tisinai and Samans 1957). Severely cold worked alloys seem to be more susceptible to 475°C embrittlement than annealed or tempered grades (Thielsh 1951).

It was also found that cold work before aging promotes the formation of sigma phase (Fisher *et. al.* 1953).

Effect of aging at 475℃ and cooling rate from annealing temperature on corrosion properties

It seems that no deterioration in corrosion resistance with the aging at 475°C, is to be expected, and that effects on corrosion resistance appear to occur more slowly and have less significance than the effects on mechanical properties (Aggen *et al.* 1978).

Sensitisation might be a problem, though it can be largely reduced by low interstitial contents (Grobner 1973, Plumtree and Gullberg 1976, Aggen *et al.* 1978). The interstitial content would have to be less than 0.002% to be effective, however, and this is not commercially viable yet.

2.3. Microstructure

Two further aspects may have an influence on the properties of the material, they are grain size and the presence of martensite in the microstructure.

2.3.1. Grain size

Rates of grain growth in ferritic stainless steels become appreciable only when temperatures are reached at which the structure is fully ferritic (i.e. contains no austenite or martensite) (Rajkay 1967). Hence it is not expected that grain size and growth would have an effect in the present study.

2.3.2. Martensitic-ferritic stainless steels

Ning *et al.* (1991) found that the strengthening of 17% Cr - 2%Ni steels is mainly caused by the presence of martensite in the microstructure (after austenitising at temperature in the range 950-1150°C, oil quench and tempering at 300 - 650°C. These steels are also susceptible to 475°C embrittlement where the ferrite (but not the martensite) is affected (Anzai *et al.* 1988)

Chapter 3

Material and Experimental Procedure

In the previous two chapters the practical and theoretical background of this work was outlined. This chapter provides a description of the experimental procedures which were followed to investigate the possible strengthening mechanisms.

3.1. Material

The material examined in the investigation - Type 430 ferritic stainless steel - was tested in the form of links of the actual slat-band chain as well as 8mm hot-rolled sheet. The sheet material was used to investigate the effects of cold rolling and aging such as may be used during the chain manufacturing process.

3.1.1. Slat band chain

The chain links are manufactured from continuously annealed and cold rolled 430 stainless steel. The composition of the material (as determined through Spark spectroscopy analysis) is as follows:

Table 3.1: *Composition of the slat band chain*

Element	Cr	C	N	Ni	P	S	Mn	Si	Mo
Weight%	16.0	0.05	0.012	0.15	0.024	0.003	0.61	0.77	0.032

3.1.2. Sheet material

The 430 sheet in the received form was 8mm thick, hot-rolled, batch annealed and pickled. The composition of this sheet is given in table 3.2.

Table 3.2: Composition of sheet material (provided by Columbus Stainless)

Element	Cr	C	N	Ni	P	S	Mn	Si	Mo	Co
Weight%	16.42	0.036	0.033	0.13	0.025	0.004	0.57	0.63	0.02	0.02

3.2. General Experimental Procedure

The following is a simplified flow chart of the steps followed in the preparation of samples and the investigation itself.

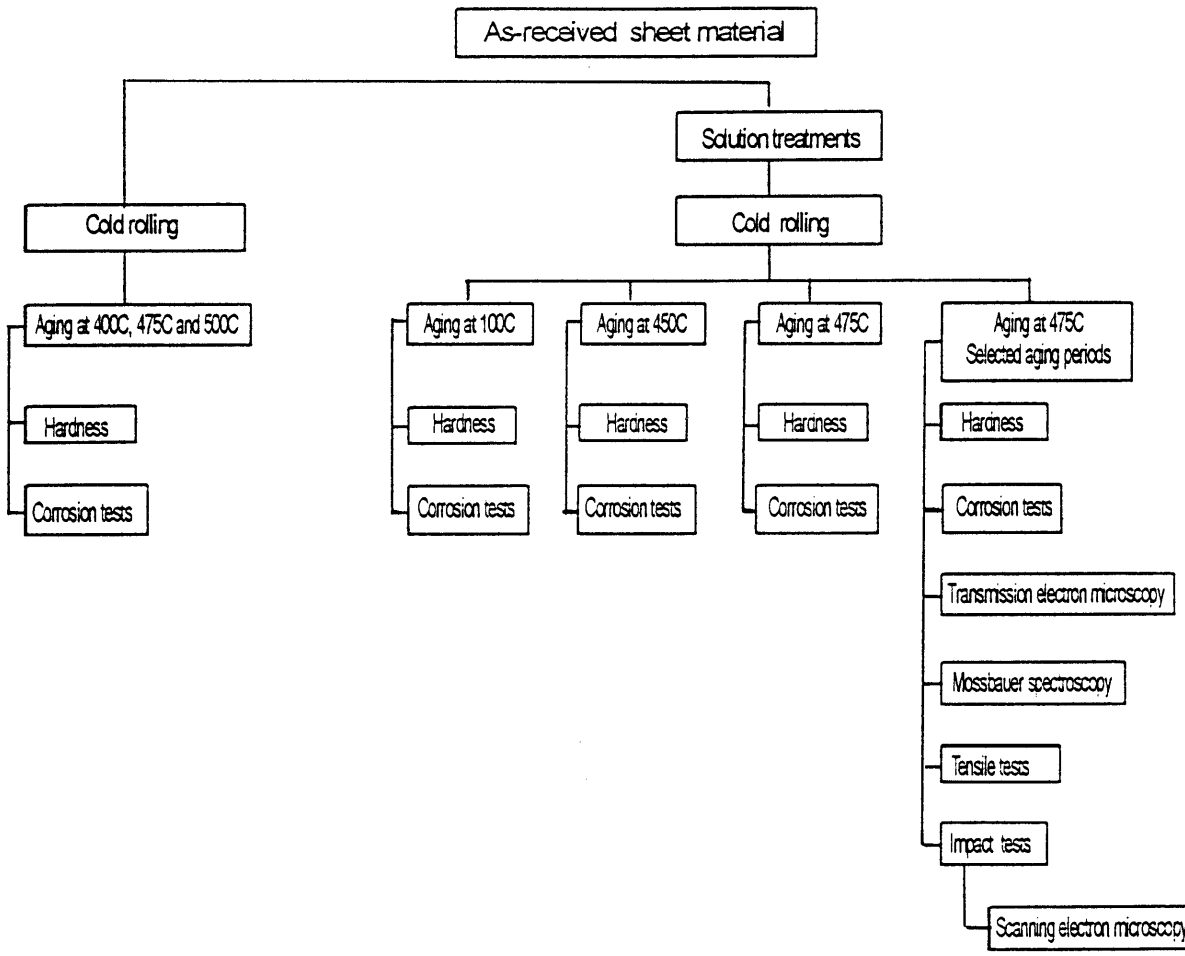

Figure 3.1: Flowsheet of experimental procedure

The investigation was performed along two parallel paths. In the first the as-received sheet material was cold rolled before aging, while in the second, solution heat treatments were performed prior to cold rolling and aging. Table 3.3 describes the experimental procedure in detail:

Table 3.3: Aging treatments and testing procedures on the 8mm hot-rolled sheet.

Solution treatment (°C) before cold rolling	920		930	none			800-1200	930	990	880 and 930	880 and 930
Reduction in area during cold rolling	0	38%	38%	38%			0	38%	38%	38%	38%
Aging temperature (°C) after cold rolling	475	475	100	400	475	500		475	475	475	450
Aging times (h)	0-260	0-260	0-14	0-48	0-260	0-260		0-260	0-260	0-2072	0-520
Vickers hardness tests (20 kg load) performed on	all	all	all	all	all	all	all	all	all	all	all
Potensiodynamic corrosion tests in 0.5M H_2SO_4 performed on	all	all	all	all	all	all	all	all	all	all	
Potensiostatic corrosion tests at 0V in 0.5M H_2SO_4 performed on									0h and 16h		
Pitting corrosion tests in 3.56% NaCl performed on				0h and 260h							
TEM (100 keV) performed on										0;0.13;32; 260h	
Mössbauer spectroscopy performed on										0;0.13;32; 260;2072h	
Impact tests performed on										0;0.13;32h	
Tensile tests performed on										0;0.13;32; 277h	
SEM performed on										0;0.13;32h	
Described in section	4.1.2	4.1.2	4.3.2	5.1	5.1	5.1	6.1.1	6.2.2	6.2.2	6.3.1;6.4.1 6.4.2;7.1; 7.2	6.3.2

Cold rolling was done at ambient temperature, in the original rolling direction. In all instances the area was reduced by 38% (8mm down to 5mm), since it was found that for type 430 ferritic stainless steel, 40% cold work produces a yield and tensile strength corresponding to the minimum levels required for conveyor applications (Charenton and Baltenneck 1992).

Aging treatments were mostly performed in a lead bath because of its good thermal stability, but some samples were solution treated and aged with the aid of a weld simulator. The simulator works on the principle of a current passing through the sample, which will cause it to heat up because of internal resistance. By using a controller at a certain EMF setting (which corresponds to the desired temperature) the sample could be held at temperature for any length time, after which it rapidly cools to room temperature. For temperature control a Pt -

Pt13%Rh thermocouple was spot welded onto the sample. The welding simulator was used for short-term heat treatments where changes in the lead bath temperature could have affected the aging behaviour.

Hardness values were determined by using a Vickers diamond pyramid indentor, each value being the mean of twenty measurements. The specimens were ground to a 1200 grit finish before hardness testing, which used a load of 20 kg.

The corrosion resistance was established by potentiodynamic testing in a 0.5M H_2SO_4 solution at room temperature. A scanning rate of 2 mV/s was used and a 123mm^2 area was exposed to the solution. Pitting corrosion tests were performed according to ASTM standard G61-78 (1979) in a 3.56% NaCl solution.

The dimensions of the samples used to determine tensile and impact strengths are shown in figure 3.2:

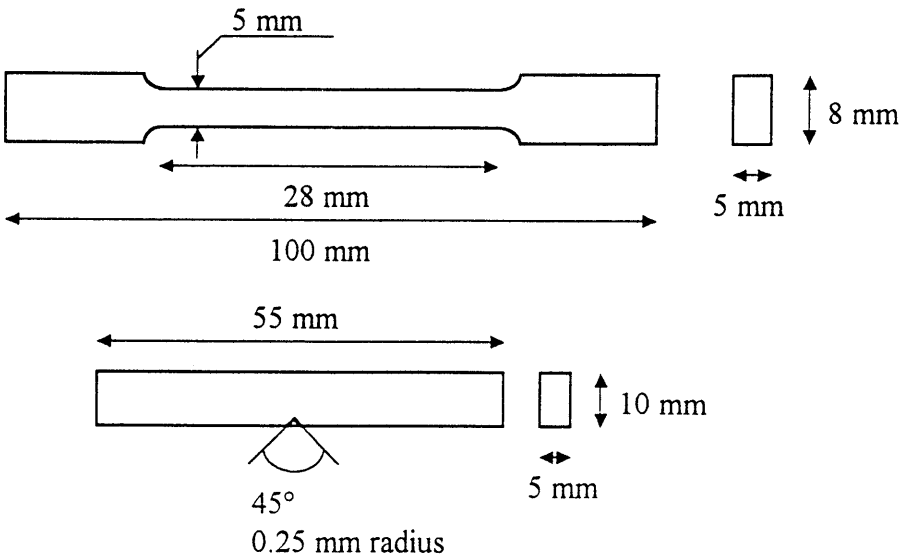

***Figure 3.2**: Dimensions of tensile and impact samples*

The impact fracture surfaces were analysed with the aid of a scanning electron microscope.

Transmission electron microscopy studies were performed in a 100 keV microscope. The foils were prepared longitudinal to the rolling direction.

Mössbauer studies (using a cobalt source) were performed. Tests ran for two days.

All the mechanical tests were performed at room temperature.

3.3. Handling of material and sample selection

The sheet material was received as a 8mm thick sheet of 1×2m in size. Solidification effects such as segregation are probably present in the sheet. To minimise bias from such inhomogeneity, the sheet was cut into 140 smaller pieces (170×70×8 mm) and allocated randomly to three groups. Specimens were then procured as needed, sampling from one group until it is depleted. Thus it was assured that samples would be extracted randomly and from different positions in the sheet.

Chapter 4

The Effects of Cold Work, Recovery and Strain Aging on the Hardness of Aged Cold-worked 430

This chapter is the first of five which report the results of the experimental measurements which were outlined in chapter 3. It is aimed at elucidating the effects of cold work, recovery and strain aging. Cold work increases the strength of the material by work hardening; recovery during aging would tend to decrease this strengthening effect, while strain aging is expected to enhance it.

4.1. Effect of Cold Work on the hardness and aging behaviour of as-received sheet material (8mm thick)

4.1.1. Hardness and Microstructure

It was found that a 38% reduction in area through cold rolling (in the original rolling direction) raised the Vickers hardness of the material by 100 kg/mm^2 from an original hardness of 167 kg/mm^2.

Cold rolling also caused changes in the microstructure; these changes were less apparent under the optical microscope (figure 4.1) than during examination in a transmission electron microscope (figure 4.2). The steel consists at room temperature (and in the equilibrium state) of ferrite and carbides (visible as black dots in figure 4.1).

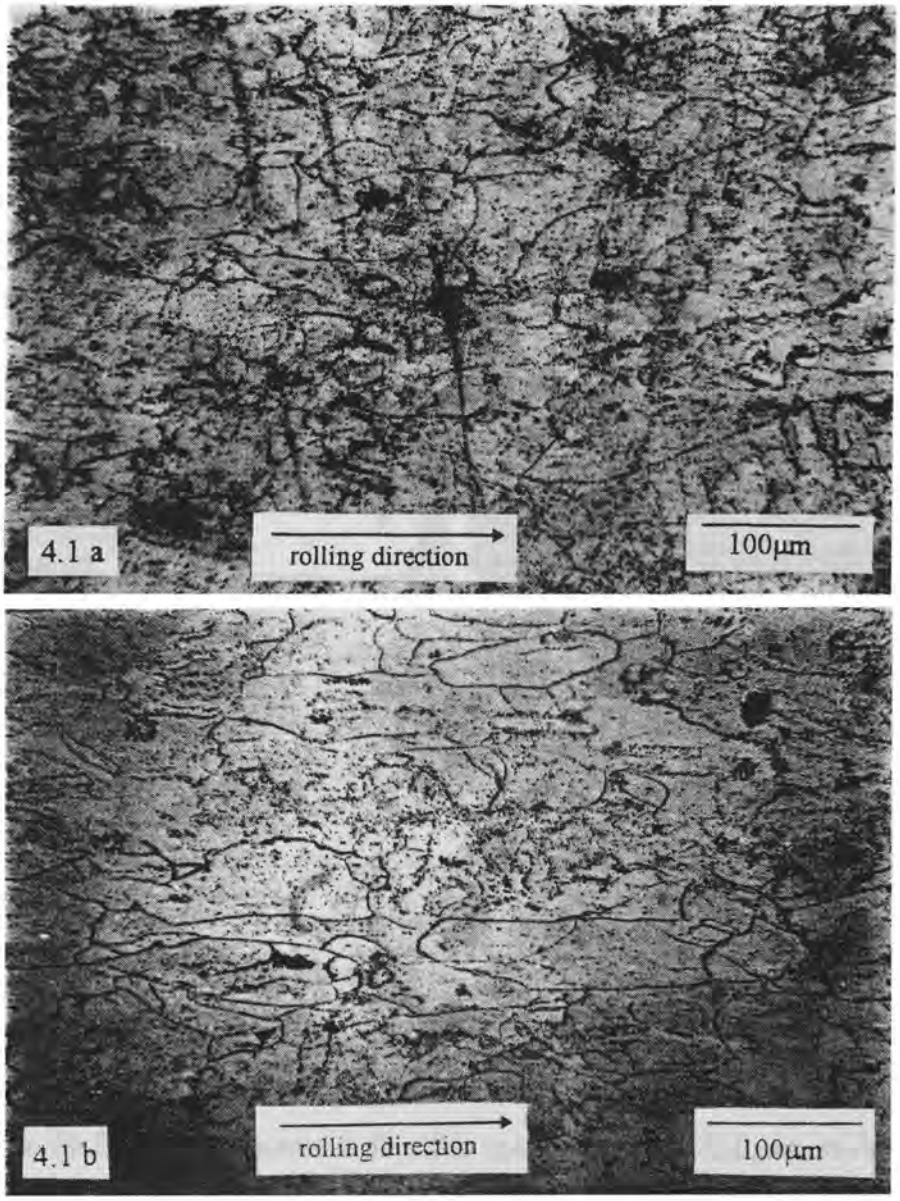

***Figure 4.1**: Microstructure of (a) as-received sheet material - 8mm thick, and (b) sheet material after cold rolling - 38% reduction in area (5mm thick)*

Cold work increases the number of dislocations and distorts the structure, and the pronounced elongated structure in the rolling direction is clearly visible (figure 4.1(b)).

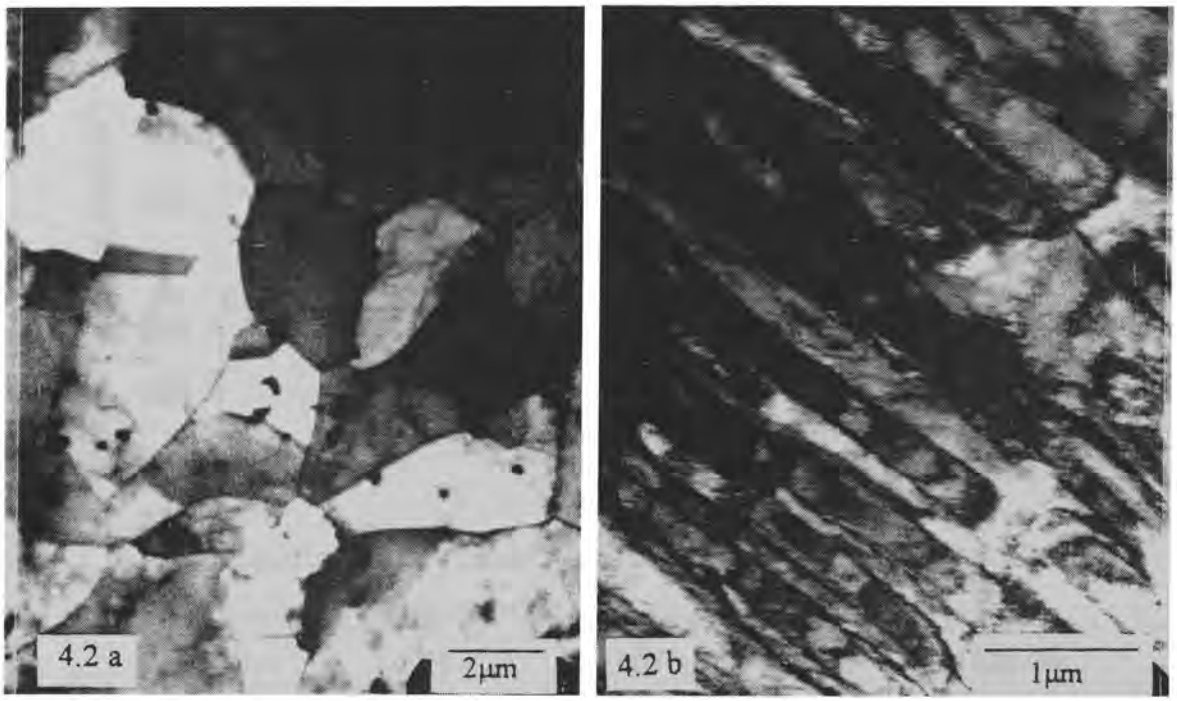

***Figure 4.2**: TEM micrographs (bright field) of as-received material (a) before cold work and (b) after cold work (38% reduction in area), indicating dislocation-rich layers after cold rolling*

In some regions of the as-received material smaller grains could clearly be seen, but overall the material consisted of large grains with a low dislocation density. This type of structure is that expected for an annealed ferritic stainless steel (Krauss 1989). Precipitates were also visible e.g. as black dots in figure 4.2(a). After cold rolling, the dislocation-rich layers running in one direction became very prominent (figure 4.2(b)).

4.1.2. Aging Behaviour

Figure 4.3 shows the hardness after aging at 475°C for different periods, with and without prior cold work. It is revealed by the curves that for the material that was cold worked the initial increase in hardness (at t = 0.5 h) is more pronounced than for the material that did not receive any cold rolling. The aging behaviour at longer periods of aging is similar with and without cold working - a hardness increase occurs for aging beyond 100 hours in both cases. That is to say, the stage where α" is the prime strengthening mechanism (refer to section 6.5.2) does not seem to be affected by deformation.

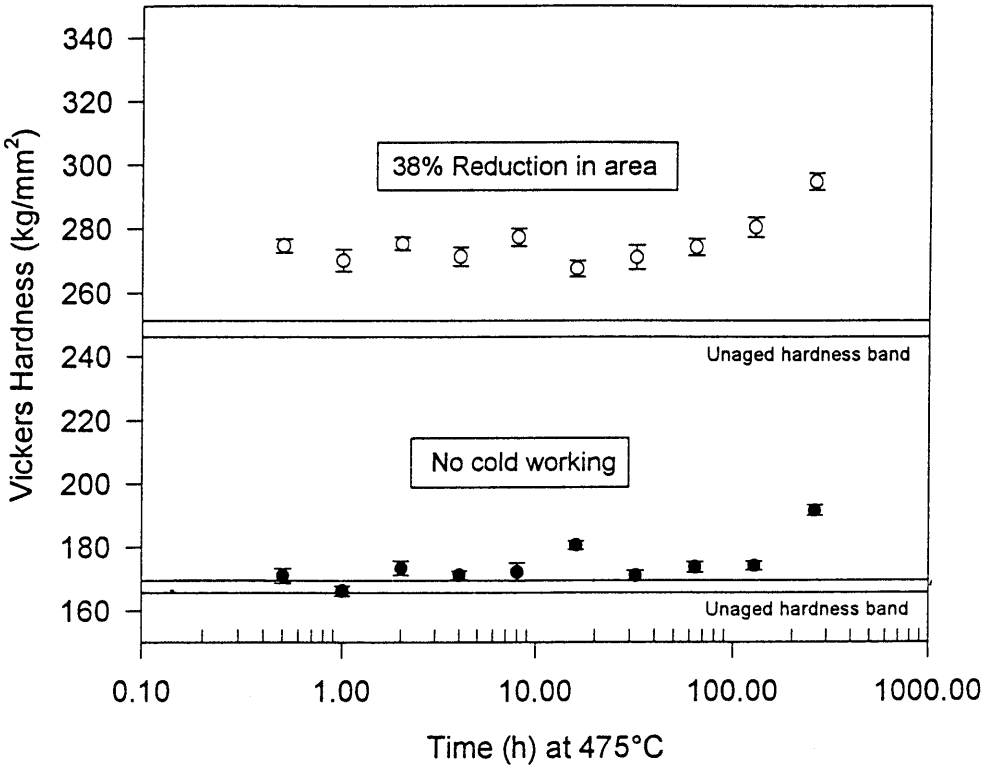

***Figure 4.3**: Comparison of aging behaviour (at 475 ℃) of sheet material, solution treated at 920 ℃ for 15 minutes, before and after cold rolling (38% reductiuon in area). 95% confidence intervals are shown. Hardening behaviour is similar for long periods of aging*

It is known that cold working, because it increases the internal energy or strain of a material, causes an increased nucleation of second phase particles (Tisinai and Samans 1957). This probably accounts for the more pronounced initial increase in hardness (at t = 0.5 h) of the cold worked material, as it is energetically more favourable for the carbides and nitrides to precipitate.

When the general corrosion resistance of the treated material was examined, the samples that were not cold rolled and aged for intermediate periods at 475°C, formed second anodic current peaks (associated with sensitisation (Mao and Zhao 1993)) at 0V. These peaks disappeared again with longer aging. The cold worked material did not exhibit the same behaviour.

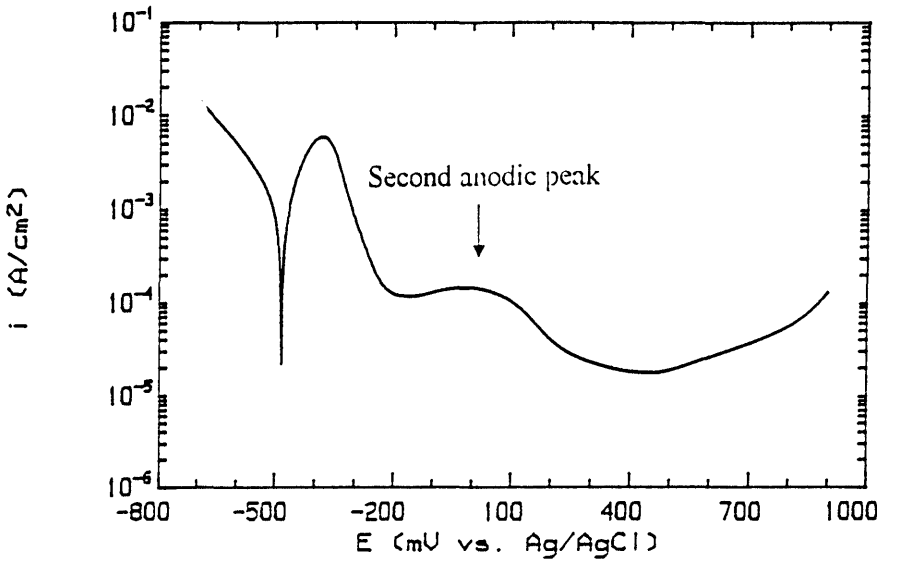

***Figure 4.4**: Polarisation diagram showing second anodic current peak of sheet material solution treated at 920 ℃, water quenched and aged at 475 ℃ for 64 hours (0.5 M H_2SO_4 test solution)*

For the material that was not cold rolled prior to aging, the precipitation of Cr-rich carbides and nitrides (causing localised chromium depletion of the matrix) and reduction of this depletion at the longer aging times (as Cr diffuses to the impoverished areas), are thought to explain the appearance and subsequent disappearance of the anodic peak.

In the cold rolled material, cold working, in addition to increasing the dislocation density and internal (strain) energy, also has an influence on the nucleation of carbides. This might offer the reason for the absence of second anodic current peaks in the heavily deformed material. In an annealed material carbides form essentially on the grain boundaries during aging. In this way a continuous area, depleted in chromium, is formed. This area is very sensitive to corrosion. With increasing amounts of cold work prior to aging, heating at the aging temperature results in progressively more widespread precipitation of carbides within the grains. This presumably shortens the diffusion paths for chromium, and along with the expected faster Cr diffusion rate in cold worked metal, can result in the total absence of sensitisation in highly cold worked material (Pednekar and Smialowska 1980).

4.2. Recovery

4.2.1. Background

A cold worked material, being in a state of higher energy, is thermodynamically unstable. With thermal activation, such as provided by annealing, the material tends to transform to states of lower energies through a sequence of microstructural changes. The first stage is known as recovery. As recovery proceeds, the following emerge: the annealing out of point defects and their clusters, the annihilation and rearrangement of dislocations, polygonisation and the forming of recrystallisation nuclei energetically capable of further growth. These structural changes do not involve high-angle boundary migration (ASM Metals Handbook vol 9, 1985, p. 692,693). The principal effect of recovery seems to be the relief of internal stresses caused by cold working, while the mechanical properties are essentially unchanged (Dieter 1988, p. 233).

4.3.2. Aging at 475°C

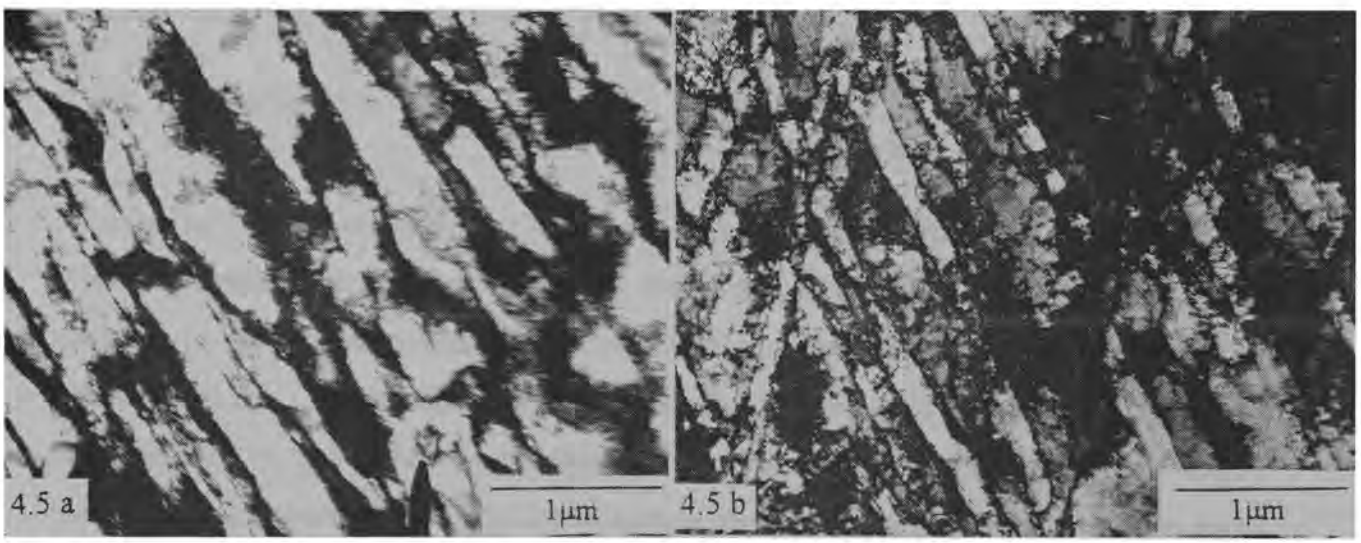

***Figure 4.5**: TEM micrograph (bright field) of the matrix after cold working with (a) no aging and (b) aging at 475 ℃ for 260 hours, indicating that recovery occurs with aging*

The thin ribbon-like structure, characteristic of cold worked material, is clearly visible in the unaged material (figure 4.5(a)). The structure is formed by dislocation-rich layers running in the same direction. As deformation by cold work proceeds, cross slip takes place, and the cold-worked structure forms high dislocation density regions or tangles, which develope into tangled networks. Thus the characteristic structure of the cold worked state is a cellular substructure in which high-density-dislocation tangles form the cell walls (Dieter 1988, p. 230).

With aging, the cell boundaries became more definite in appearence. This parallelogram structure is formed by dislocation double walls running in two directions. The double walls are two thin dislocation walls parallel to a crystallographic slip plane (Dymek and Blicharski 1985). The cells are bound by low angle grain boundaries which form as dislocations group together in low energy arrangements. This results in the formation of a subgrain structure in which the centre of each grain is relatively dislocation-free.

The TEM micrographs indicate that recovery does occur during aging, but no recrystallisation is observed.

4.3. Strain Aging

4.3.1. Background

Strain aging is the phenomenon by which a cold-worked steel hardens by the formation of interstitial solute atom atmospheres around dislocations. The dislocation sources that were active in the deformation process just before cessation of the deformation operation, are thus pinned down as a result of the aging process. Because solute atoms must diffuse through the lattice in order to accumulate around dislocations, strain aging is a function of time; and of temperature, inasmuch as diffusion is temperature dependent (Reed-Hill 1992). Strain aging of steel causes a loss of ductility and a corresponding increase in hardness, yield strength and tensile strength. Strain aging may occur at ambient temperature, but the rate can be considerably enhanced by aging at higher temperatures; for instance, strain aging may occur within a few minutes at 200°C (ASM Metals Handbook vol. 8, 1985, p. 12).

To acertain whether strain aging contributes to the total strengthening effect, aging heat treatments were performed at 100°C on chain links and sheet material.

4.3.2. Aging at 100°C

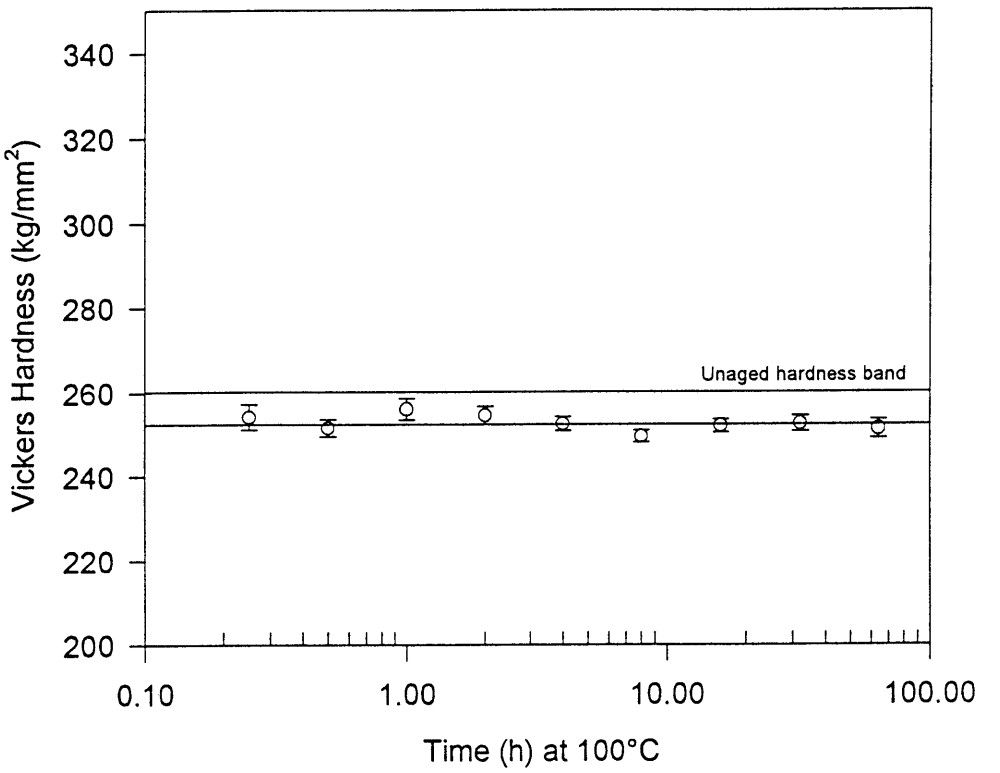

***Figure 4.6**: Hardness of Chain links aged at 100℃, indicating that no strain aging occurs. 95% confidence intervals are shown*

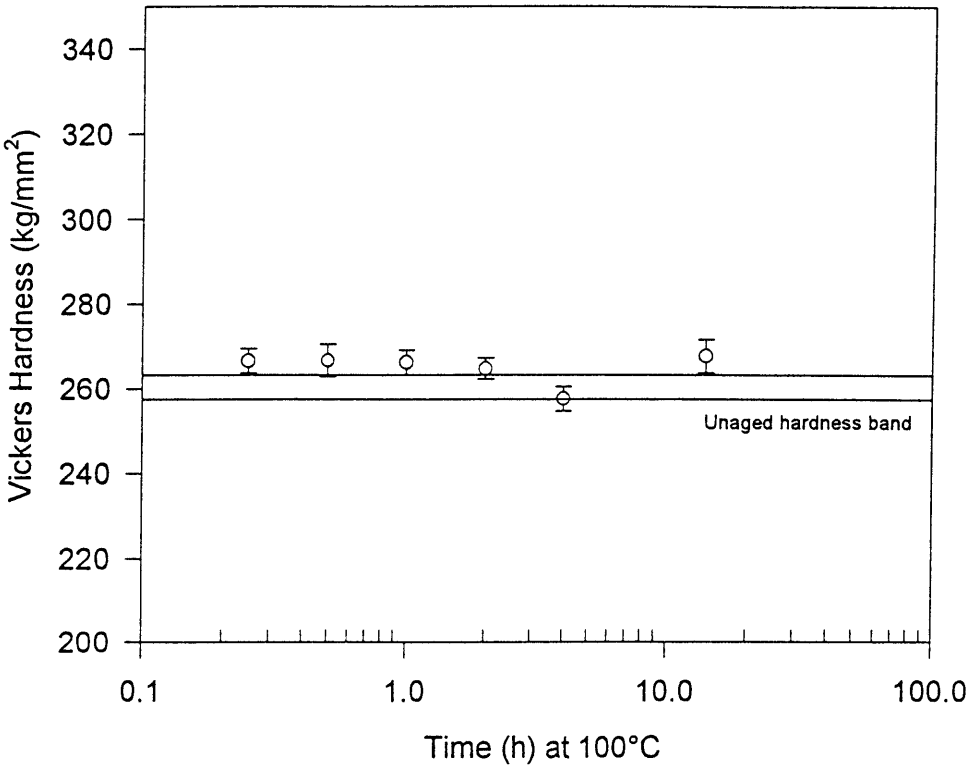

***Figure 4.7**: Hardness of sheet material solution treated at 930℃ (45 minutes), water quenched, cold rolled (38% reduction in area) and aged at 100℃, indicating that no strain aging occurs. 95% confidence intervals are shown*

If strain aging has an effect, it is to be expected that some hardness increase would be evident within the first 12 hours at 100°C. It can clearly be seen that no sign of any significant hardness increase is present even after aging for 64 hours (figures 4.6 and 4.7). It can therefore be concluded that strain aging doen not have a significant effect on the observed aging behaviour. This is consistent with results obtained by others, which reported only a slight increase in hardness after one month at room temperature (Lagneborg 1967).

4.4. Conclusions

Cold working increases the initial hardness of the material substantially. This is probably due to two effects: an increase in hardness directly related to the increased dislocation density; and an increase in hardness because of precipitation processes being promoted by the cold work.

For the present case cold work does not seem to enhance the formation of α", in contrast to previous results (Thielsh 1951, Lena and Hawkes 1954, Tisinai and Samans 1957), as it does not seem to have any other influence on the aging behaviour at longer periods of aging

Strain aging does not play a significant role in the observed strengthening.

With aging some rearrangement of dislocations takes place (recovery), but no recrystallisation is observed.

Chapter 5

The Effect of Aging on the Hardness of Chain Links and Cold-worked 430 (No Prior Solution Treatment)

While chapter 4 considered the effects of cold work, recovery and strain aging on the hardness after aging at 475°C, the hardening mechanism which is most strongly associated with this temperature range is the formation of α". Since α" formation is expected to be strongly temperature dependent, a simple test for the presence of this hardening mechanism can be carried out by aging at temperatures other than 475°C. This chapter presents results on the hardness changes of chain links and cold-worked type 430 sheet material after aging at temperatures from 400°C to 500°C. These results support those of chapter 6, in which Mössbauer results are presented which show that the strengthening obtained after relatively long periods of aging at 475°C is indeed due to the Cr-rich α" phase.

5.1. Aging behaviour

In figure 5.1 the aging curves at 475°C of the chain and sheet material (no solution treatment before cold rolling) are presented. The aging behaviour is similar, as the hardness increases only at longer periods of aging (~ 64 hours) in both cases.

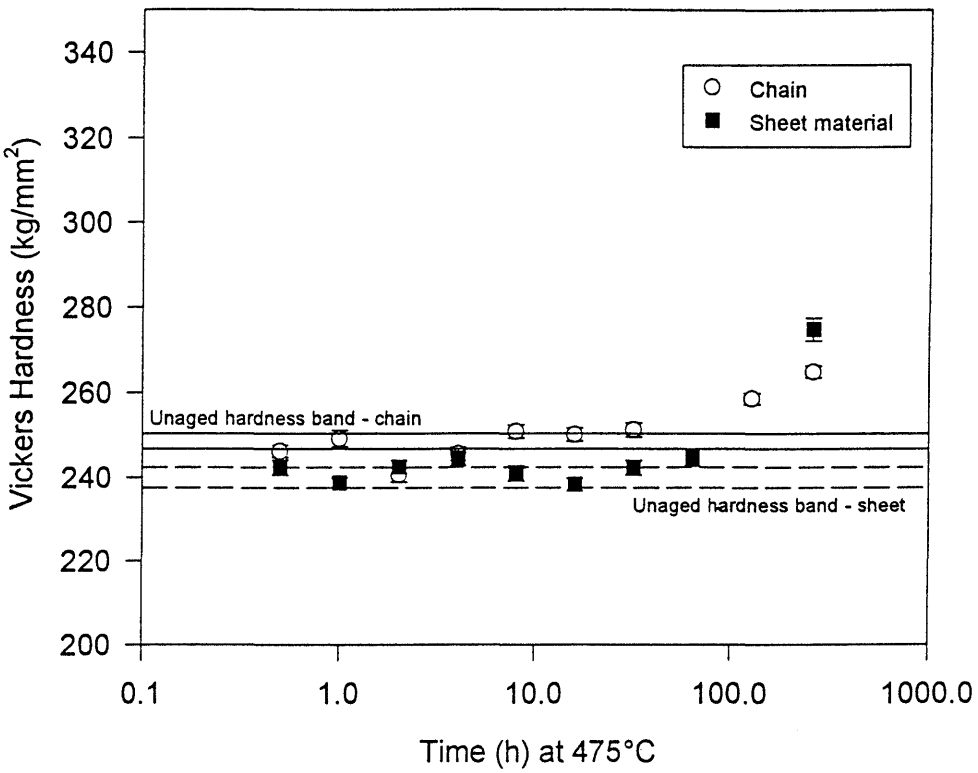

***Figure 5.1**:Hardness of chain links aged at 475 ℃ and of sheet material aged at 475 ℃ (after cold rolling - 38% reduction in area), showing that the aging behaviour of the chain and sheet material are similar*

The initial hardness for the chains is somewhat higher than that of the sheet material, but this is probably due to some martensite in the chain microstructure; investigation of the optical microstructure revealed the presence of two different phases, probably ferrite and some martensite. Martensite may form after annealing above the Ac_1, which - based on the composition as given in table 3.1 - can be estimated to be about 920°C (Pistorius and Coetzee 1996).

The aging behaviour is essentially the same for the curves, both showing an initial "incubation" or plateau region, with a distinct increase in hardness after long aging periods. This increase is most likely due to the precipitation of the Cr-rich α", as supported by Mössbauer results in chapter 6. Although this entails localised Cr depletion, corrosion tests did not reveal any deterioration in general corrosion resistance. It might be that the length scale of the depletion is too small to affect corrosion properties.

To test if the same hardening occurs at temperatures other than 475°C, chain links were also aged at 450°C (figure 5.2); and cold rolled sheet material at 400°C and 500°C (figure 5.3).

The results indicate that the hardening behaviour at 450°C and 475°C is similar, but that no hardening increase is apparent with aging at 500°C. No conclusions can be drawn from the 400°C set as the data points are too limited.

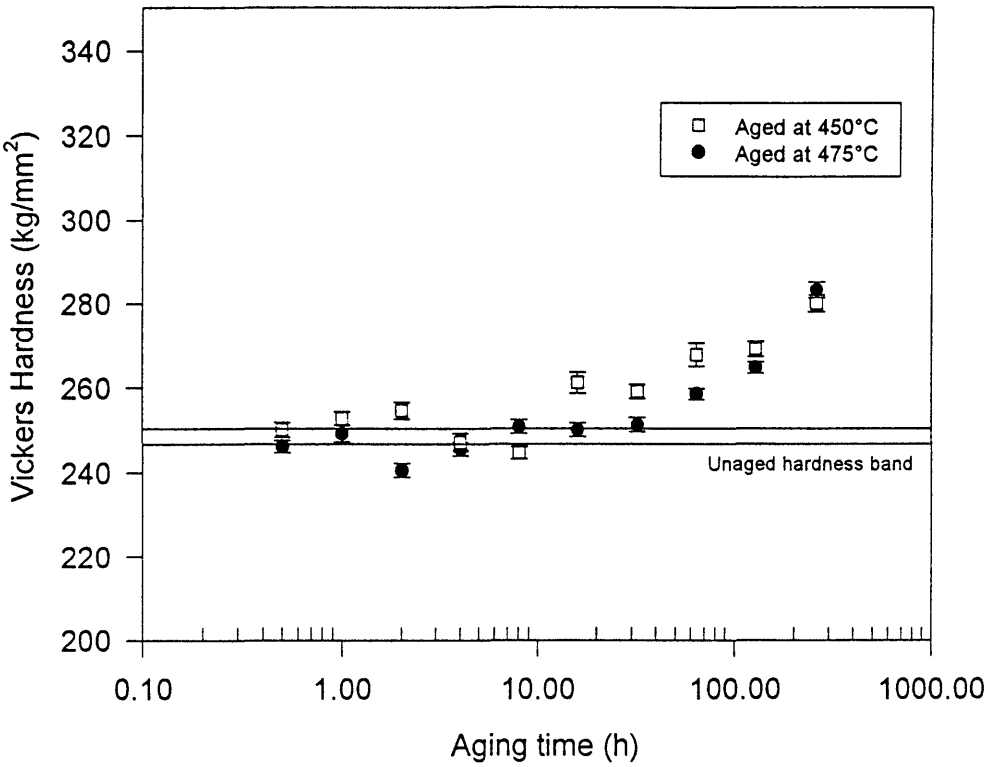

***Figure 5.2**: Hardness of chain links aged at 450℃ and 475℃, indicating that an increase in hardness with long aging periods occur at both temperatures. 95% confidence intervals are shown*

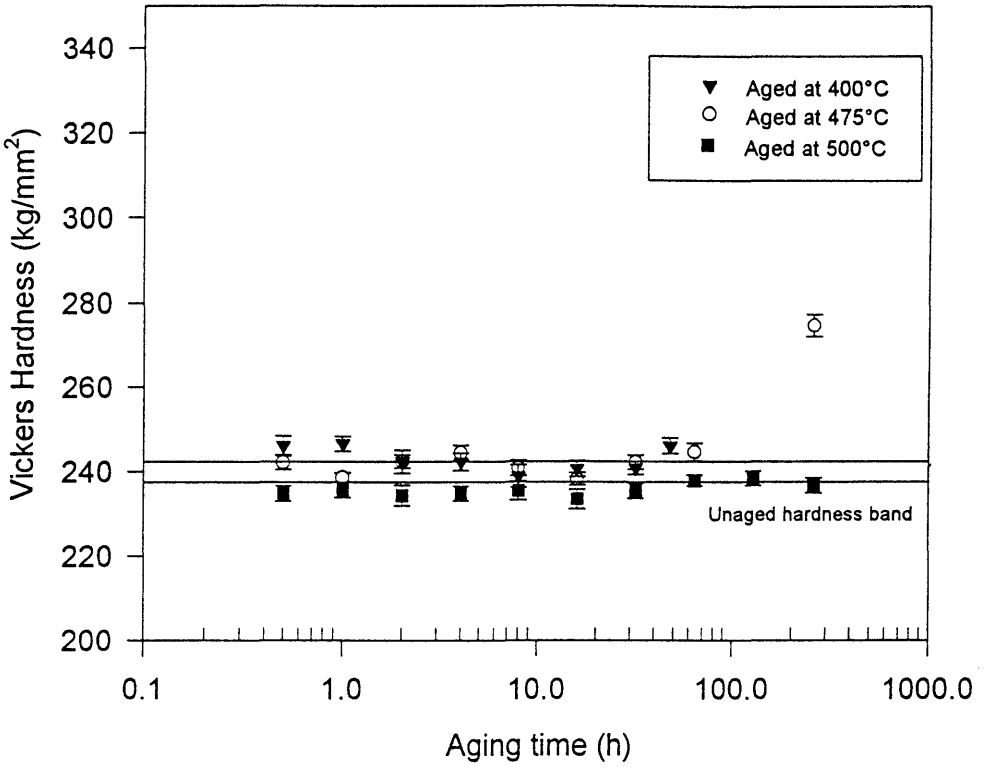

***Figure 5.3**: Hardness of cold rolled sheet material, after aging at 400℃, 475℃ and 500℃, indicating that no hardening occurs after long periods of aging at 500℃. 95% confidence intervals are shown*

The expected equilibrium fractions of α" obtainable at the aging temperatures were determined from the phase diagram (figure 5.4).

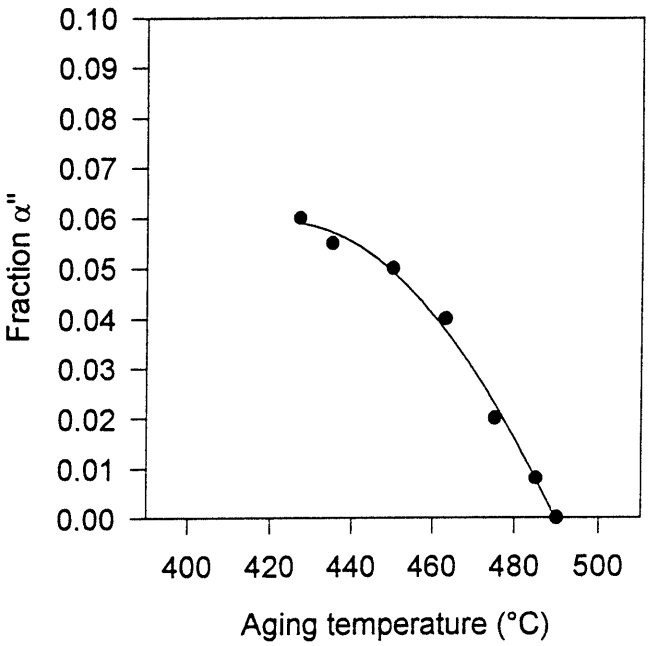

***Figure 5.4**: Expected equilibrium volume fractions of α" in an alloy containing 16.4% Cr at different temperatures as calculated from the thermodynamic assessment of the Fe-Cr-phase diagram by Dubiel and Inden (1987)*

According to the phase diagram the equilibrium fractions of α" at 450°C and 475°C are close enough to expect similar aging behaviour. At this composition (16.4% Cr) aging at 500°C lies outside the miscibility gap and α" is not expected to form - this is confirmed by the fact that the hardness did not increase with aging at that temperature.

The expected two stage behaviour reported by others (chapter 2) was not observed. This is probably due to the low interstitial content of the matrix.

5.2. Conclusions

Aging of the as-received chain (figure 5.1) and cold rolled sheet material (figure 5.2) exhibit the same behaviour - an increase in hardness after approximately 64 hours of aging. This is presumably due to the α" precipitation.

The hardening effect is not present at the higher aging temperature of 500°C, which is consistent with the expected temperature dependence of the equilibrium volume fraction of α".

Chapter 6

The Effect of Solution Treatments on Aging Behaviour

The results of chapter 5 support the suggestion that the hardness increase after aging at 475°C for 64 hours or more results from α" precipitation. If sufficient carbon and nitrogen can be brought in to solid solution, hardening by carbide or nitride precipitation may occur at shorter aging times. The amount of interstitial elements in solution depends on the solution temperature - both because the solubility in ferrite increases with temperature, and because austenite (a carbon and nitrogen sink) forms above the Ac_1 temperature (see figure 2.2). This chapter reports results on experiments which explored the effect of solution treatments on the aging behaviour.

6.1 Determination of Ac_1 temperature

By heating to a sufficiently high temperature, it is possible to enter the three phase ($\alpha+\gamma+M_{23}C_6$) region - as explained in Chapter 2. This boundary ($\alpha+M_{23}C_6 \rightarrow \alpha+\gamma+M_{23}C_6$) is important for subsequent heat treatments; and the temperature at which the transition occurs (the Ac_1 temperature) was determined as follows:

6.1.1. Solution treatments

The start of martensite formation was determined by solution treating 8mm thick samples between 800°C and 1200°C at intervals of 25°C, holding at temperature for 15 minutes, and quenching in water. Additional solution treatment steps were performed with a weld cycle simulator between 900°C and 950°C in steps of 10 degrees (samples held at temperature for 10 minutes). The relatively long holding times ensured that most of the carbon and nitrogen came into solution. The volume fraction of martensite was determined after etching with Ralph's etchant by using a point count method (200 points):

The maximum amount of martensite obtainable with this composition is about 35% at 975°C (figure 6.1). The change in martensite content with temperature reflects how the alloy enters the three phase ($\alpha+\gamma+M_{23}C_6$) and two phase ($\alpha + \gamma$) regions with an increase in temperature, and eventually passes beyond the γ-loop into the single phase (α) region at high temperatures.

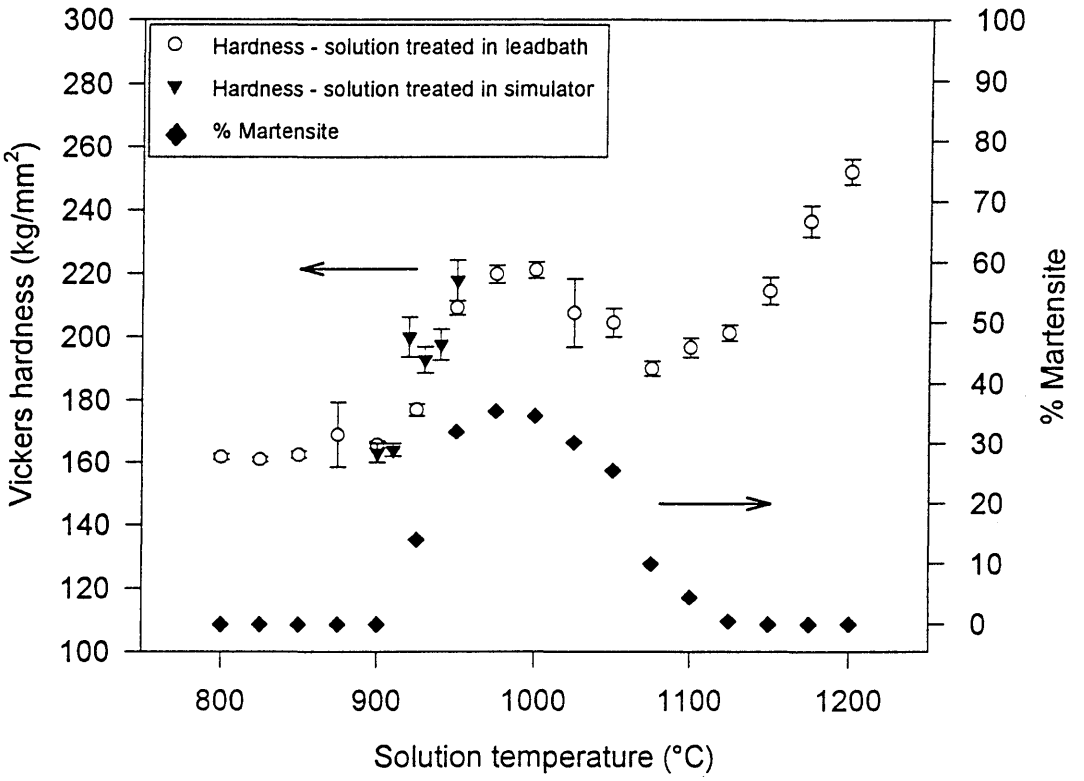

***Figure 6.1**: Vickers Hardness of samples solution treated at different temperatures, followed by quenching in water. A plot of the percentage martensite obtainable at each solution treatment temperature is superimposed on the graph. 95% confidence intervals are shown*

With increasing solution temperatures the distinct increase in hardness coincides with the start of martensite formation. A decrease in hardness can also be seen as the amount of martensite decreases. The second hardness increase (at temperatures higher than 1100°C) is probably due to high temperature embrittlement, in which embrittlement results from a clustering or segregation of carbon atoms in the ferrite matrix, when rapid cooling prevents precipitation of carbon as carbides from solid solution (Demo 1971).

These results indicate that the Ac_1 temperature for this material is approximately 920°C.

6.1.2. The influence of cooling rate after solution treatment

By enhancing the cooling rate through quenching in water (as opposed to air cooling) after solution treatment at 920°C, the hardness could be increased by at least 20 kg/mm^2 over the original hardness (148 kg/mm^2) of the material without damaging the corrosion resistance. This increase in hardness is presumably due to the trapping of carbon and nitrogen in solid solution in the matrix, as the high cooling rate does not allow sufficient diffusion for carbide precipitation to occur. Any effect that the interstitials would have on subsequent aging behaviour would therefore be enhanced by rapid cooling.

Further investigation into the quenching rate revealed that it has a significant effect on mechanical properties. This was established by quenching in water and in brine (2% NaCl) after solution heat treatment at 930°C (annealing). The test sample was 170×70×8 mm in size and the temperature of the specimen was measured by inserting a thermocouple approximately 1 cm into the side of the specimen (figure 6.2).

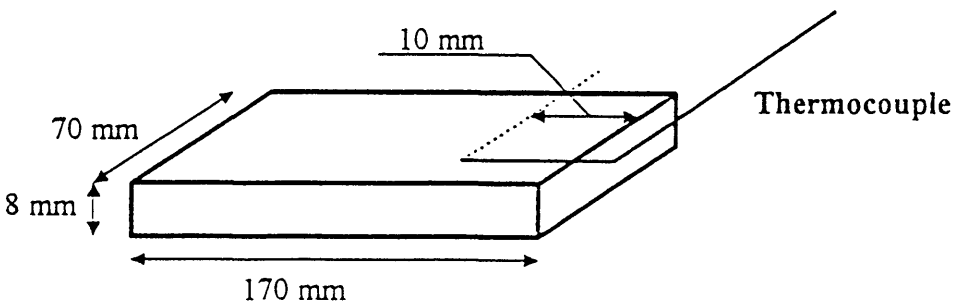

***Figure 6.2**: Configuration of test specimen and thermocouple to determine cooling rates*

Quenching in the brine resulted in a faster cooling rate (650°C/s in a 2% NaCl solution and 160°C/s in water), as the added ions in the brine accelerate boiling of the quenching liquid, thus eliminating any effect a vapour blanket would have on the cooling (Bates *et al.* 1991).

The quenching rate - which is affected by variations in the quenchant temperature and composition - influences the hardness by as much as 23 kg/mm^2 (samples 170×70×8mm in size). This is probably due to the amount of carbon and nitrogen that could be trapped in solution. It was established through aging experiments that the difference in initial hardness does not affect the strengthening *trends*, thus if the strengthening *mechanism* is studied, small variations in quenching conditions are not thought to be of great importance. However, in practical applications (where the absolute hardness, rather than hardness changes, is to be controlled) maintenance of consistent cooling conditions will clearly be crucial.

All solution heat treatments, with the exception of those performed in the weld simulator, were followed by quenching in brine (approximately 2% NaCl)

6.2. Choice of acceptable solution temperatures

Based on the experimentally determined Ac_1 temperature, two solution temperatures were selected for further experiments, one below and one above the Ac_1.

6.2.1. Solution temperature below the Ac_1 temperature

880°C was decided upon as it is within the range of the annealing temperatures used in industry (J. Hewitt, personal communication).

6.2.2. Solution temperature above the Ac_1 temperature

As it had been reported that the addition of martensite to the microstructure increases strength to the extent that the requirements set for conveyor applications could easily be met, the influence of the martensite on aging behaviour was investigated. In order to accomplish that a temperature higher than the Ac_1 had to be selected. As the Ac_1 temperature was established to be approximately 920°C, the selected temperatures were 930°C and 990°C. After the solution treatments the material was cold rolled (38% reduction in area) and subsequently aged at 475°C.

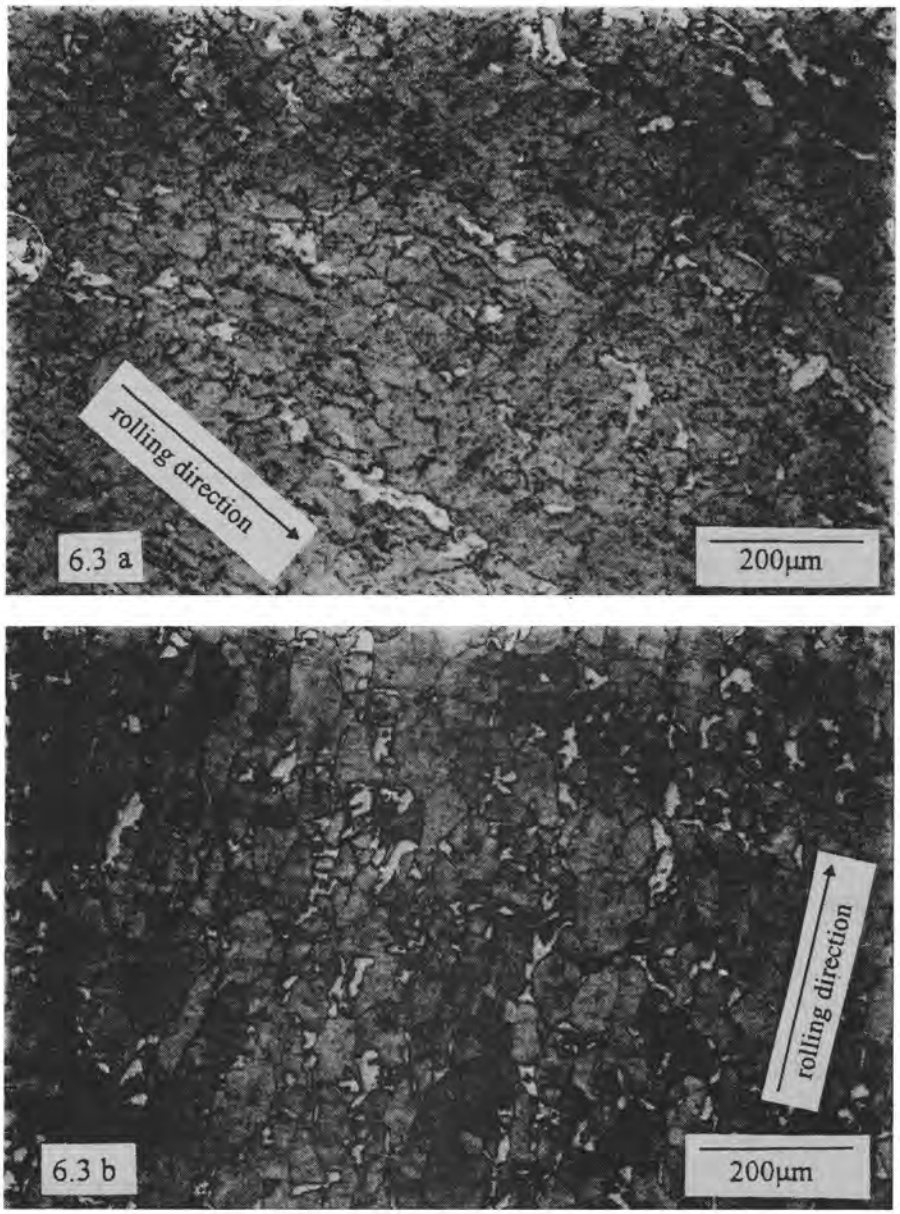

***Figure 6.3**: Microstructures after solution treatment (15 min) at (a) 930℃ (showing ferrite, martensite and carbides) and (b) 990℃ (showing ferrite and martensite)*

The microstructure contains three phases after solution treatment at 930°C; these are ferrite (grey phase), some martensite (white phase) and carbides (black dots). A duplex ferrite-martensite structure results after solution treatment at 990°C.

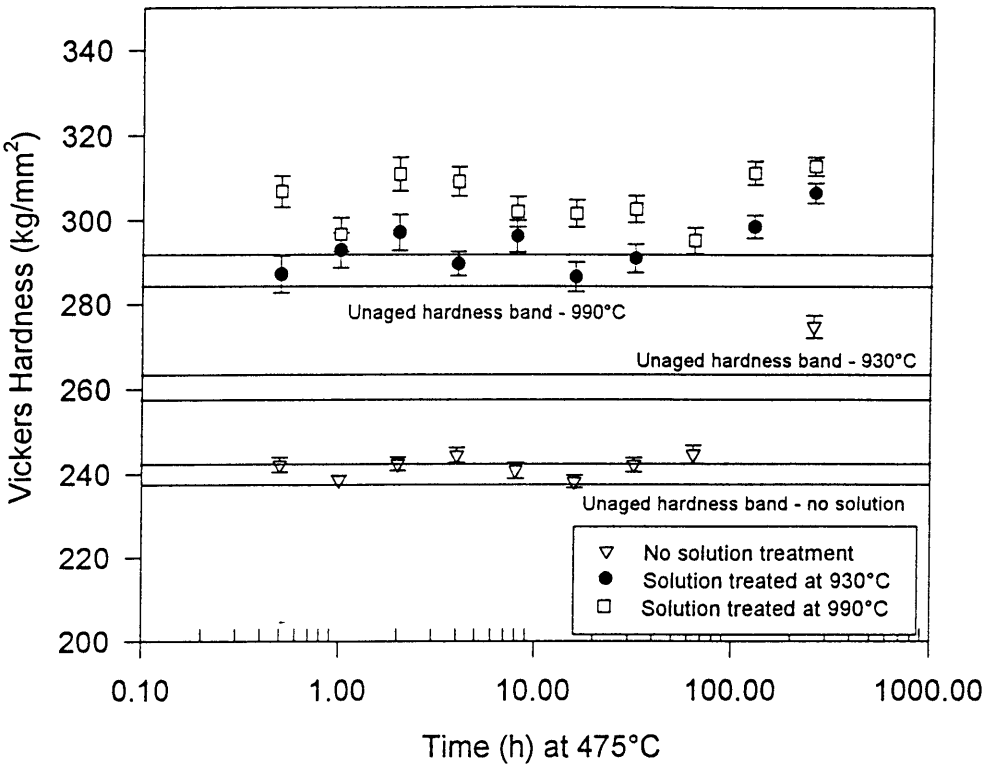

***Figure 6.4**: Hardness after aging at 475℃. Samples were solution treated at 930℃ and 990℃ respectively before cold rolling and aging. For comparison the curve of the material not solution treated is included. 95% confidence intervals are shown*

The hardness curves indicate that the additional solution treatments provide a marked increase in hardness. This is probably due to the increased carbon and nitrogen content as well as the presence of martensite caused by the high solution temperature.

It is also revealed that, although the initial hardness values differ markedly for the two solution treatments, the aging behaviour of the two treatments are similar; in addition, the difference in hardness diminishes at extended periods of aging.

For practical reasons - the temperature being sufficiently close to the present annealing temperature, and thus more easily attainable - the lower solution temperature (930°C) was selected for the subsequent investigation.

6.3. Effect of solution treatments on aging behaviour

6.3.1. Solution treatment at 880°C and 930°C and aging at 475°C

The material (in the form of specimens approximately 170×70×8 mm in size) was solution treated at 880°C and 930°C respectively, in an air furnace for 30 minutes, after which they were quenched in brine (approximately 2% salt) and cold rolled (a 38% reduction in area). Smaller pieces (about 20x20×5mm) were aged in a lead bath at 475°C for 0.5h to 2072 hours, while other samples (15x70×5mm) were aged in the weld cycle simulator where the short holding times could be controlled accurately.

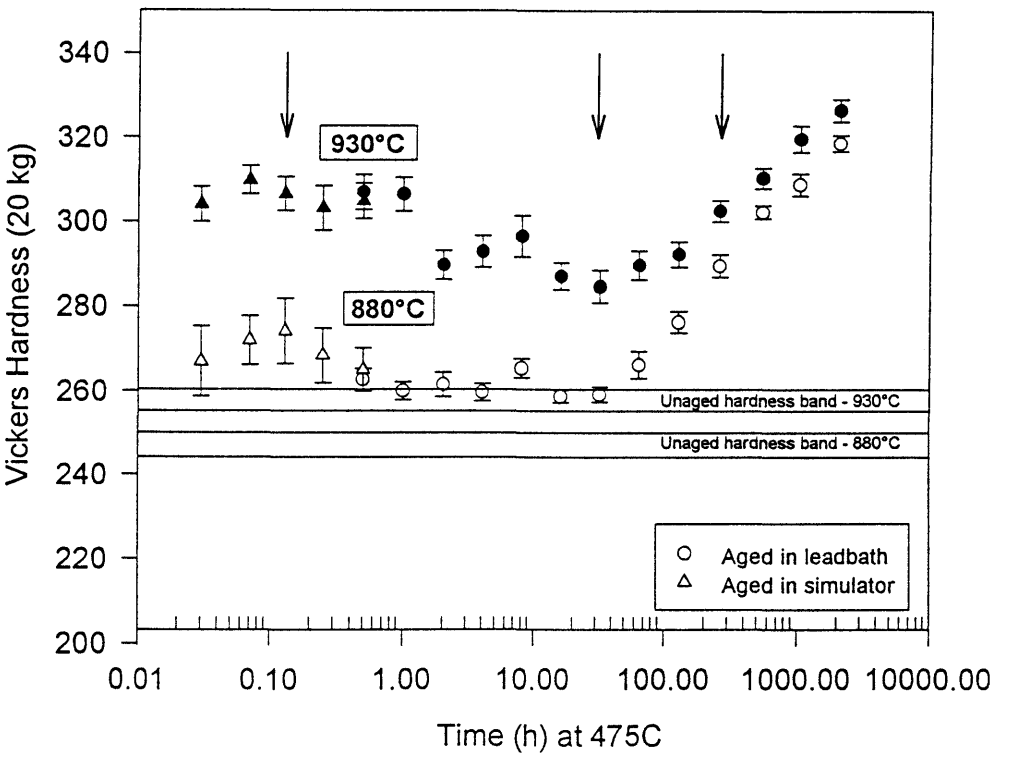

***Figure 6.5**: Hardness of samples solution treated at 880℃ and 930℃, cold rolled and aged at 475℃. 95% confidence intervals are shown. Arrows indicate specimens selected for further examination by TEM and Mössbauer spectroscopy, as well as mechanical testing*

Solution treatment at the higher temperature (930°C) increases the initial Vickers hardness by 10 kg/mm^2 from 247 kg/mm^2 (figure 6.5). However, during the first stages of aging the difference increases beyond this. In both cases a peak can be observed after only 8 minutes of

aging. For the 880°C samples there seems to be an immediate decrease in hardness after this peak, while somewhat of a plateau is present for the 930°C samples. Other authors also noted three stages in hardness with aging in this temperature region. The first stage, however, was not so pronounced (Nichol *et al.* 1980).

This peak in hardness is most likely caused by the precipitation of coherent carbides and nitrides. These seem to be rich in chromium, as Mössbauer studies indicate a Cr depletion of the matrix (section 6.4.2). These precipitates are also expected to be very fine but dispersed throughout the grains and not concentrated at the grain boundaries (Pednekar and Smialowska 1980). The decrease in hardness following this peak is probably associated with overaging, where coherency is lost (Dieter 1988, p. 213) or Ostwald ripening occurs.

For specimens subjected to both solution treatments, the hardness again increases for aging beyond 64 hours. This point possibly indicates the starting of α" formation.

It seems that by aging for only 8 minutes or for more than 22 days the same increase in hardness can be obtained. This has important practical implications for manufacturing and strengthening treatments.

There is no indication of overaging at periods where the α" is the main strengthening mechanism ($t > 64$ hours) in either curve: the material displayed a sustained increase in hardness with aging time. The initial hardness increase is much higher for the 930°C solution treatment, but at very long periods of aging the two curves tend to converge (see 2072 hours). This effect may be explained qualitatively, based on microstructural changes.

The microstructure of the 880°C solution treated sample did not change markedly with aging (figure 6.6(b)) from the initial structure (figure 6.6(a)). The 930°C solution sample, however, show distinct changes in structure: as can be seen in figure 6.7(b), the martensite has the appearance of being tempered. As the martensite is tempered it becomes softer and hence the additional strengthening is lost. Tempering will eventually convert the martensite to ferrite and $(Cr,Fe)_{23}C_7$-carbides (Brooks 1979, p. 186). The softening effect of tempering is also a

plausible explanation for the larger hardness decrease for the martensite containing material, for aging beyond 8 minutes.

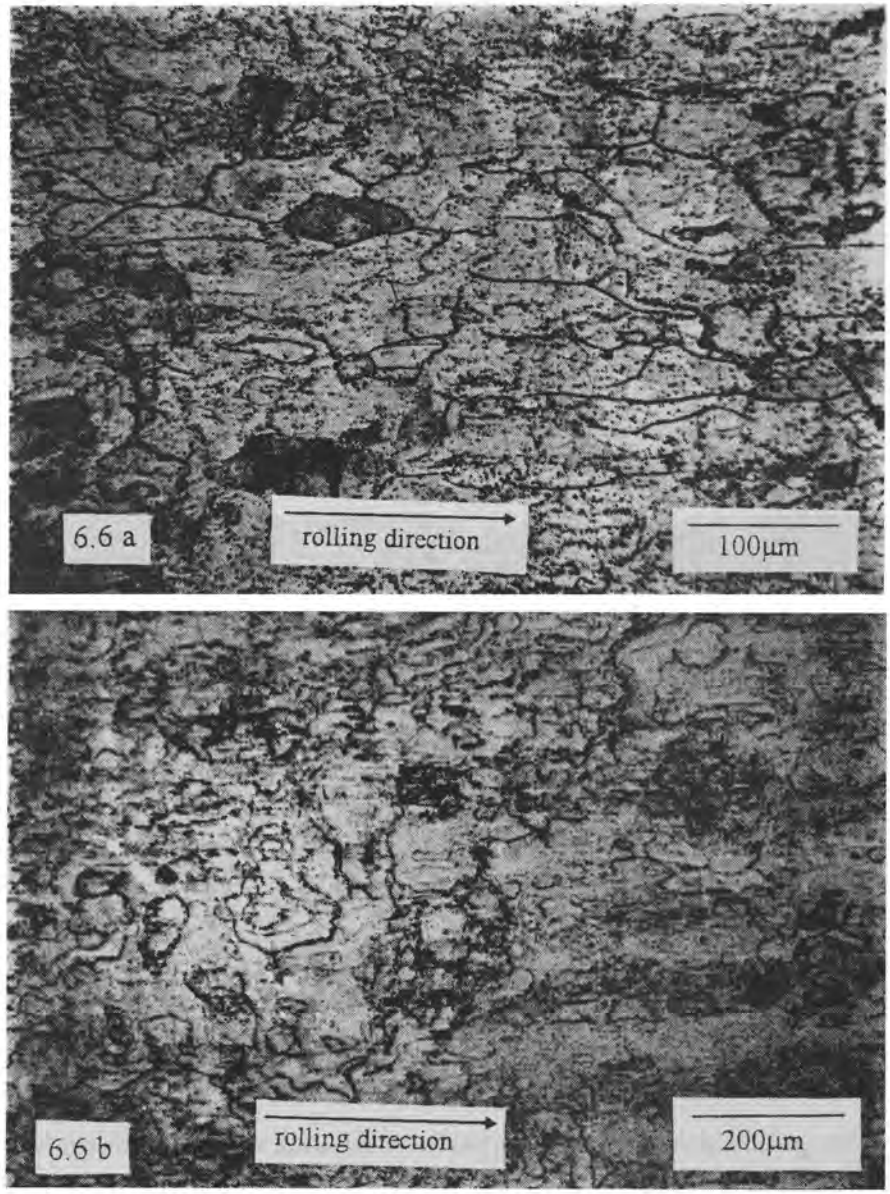

Figure 6.6: *Microstructure after solution treatment at 880℃ and cold rolling (38% reduction), (a) before aging and (b) after aging at 475℃ for 2072 hours*

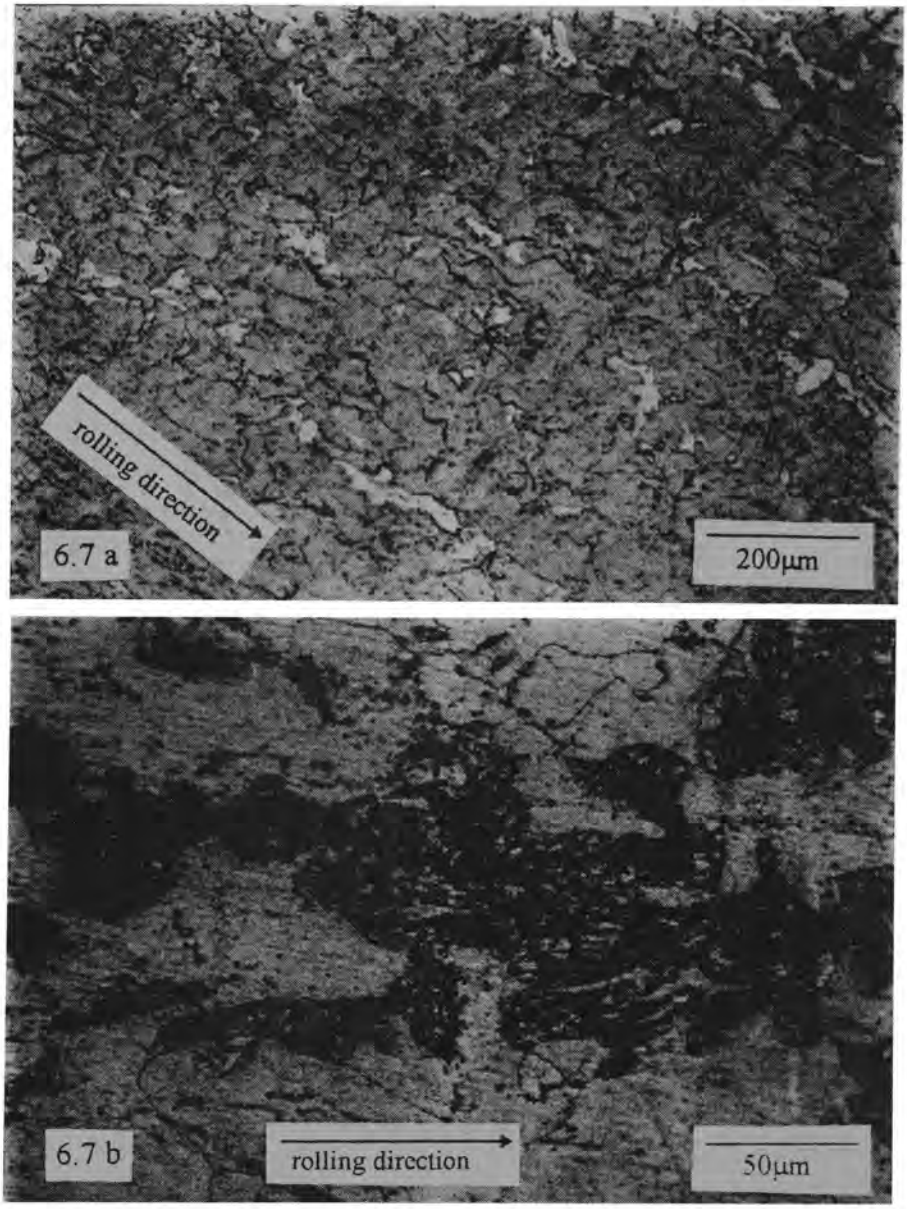

Figure 6.7: *Microstructure after solution treatment at 930 ℃ and cold rolling (a) before aging; and (b)after aging at 475 ℃ for2072 hours*

The effect of α" formation only becomes apparent after aging for approximately 64 hours. This is the case for specimens that had been solution treated before cold rolling and aging (figure 6.5), as well as those that had not been given an additional solution treatment (figure 5.3). The difference between the two solution treatments is only apparent in the short-time aging behaviour (in this case < 64 hours), hence it could be argued that in this case the additional solution treatments only have an influence on strengthening mechanisms based on the effect of carbon and/or nitrogen and that the formation of α" is not affected.

6.3.2. Solution treatment at 880°C and 930°C, and aging at 450°C

Results presented in section 5.1 indicated that hardening also occurs readily with aging at 450°C (figure 5.2). This investigation was therefore extended to the lower temperature to determine whether the aging behaviour would be similar to that at 475°C, with solution treatments prior to cold rolling and aging.

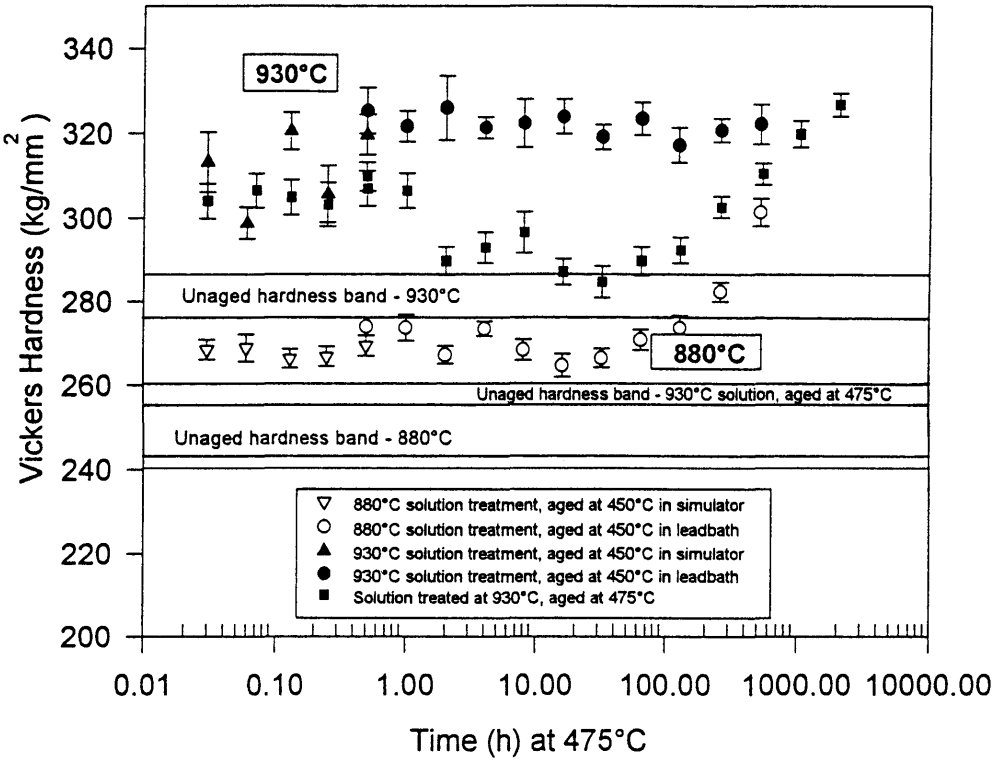

***Figure 6.8**: Hardness after solution treatment at 880 ℃ and 930 ℃, cold rolling and aging at 450 ℃. The curve for aging at 475 ℃ (solution treatment at 930 ℃ and cold rolling) is also plotted, indicating overaging at the higher aging temperature. 95% confidence intervals are shown*

The hardening behaviour is similar for aging at both 450°C and 475°C for the samples solution treated at 880°C. The hardness increase is not the same for the corresponding 930°C solution treated samples, however. When aged at 450°C a hardness increase of about 37 kg/mm^2 is observed, while with aging at 475°C an increase of 46 kg/mm^2 is noticed. This effect might be more pronounced because of the big variance in initial/unaged hardness of the two sets of solution treatments at 930°C, resulting from a difference in quenching conditions.

There does not seem to be the same decrease in hardness as experienced with aging at 475°C, which is associated with overaging. It is thought that overaging of the precipitates does not occur because of the somewhat lower diffusion rates at this lower aging temperature (450°C).

In the 880°C solution treated samples there is again the increase in hardness after longer aging times (>32 hours). No comment can be made about the 930°C results as it is not clear whether hardness would increase with longer aging, although from the phase diagram α" is expected to be present.

6.4. Strengthening mechanisms

The results obtained so far are consistent with observations previously reported for ferritic stainless steels aged around 475°C, namely that short-time strengthening is caused by the precipitation of Cr-rich (cf. section 6.4.2) carbides and/or nitrides, while after some incubation period, α" causes strengthening. It was considered useful to launch a detailed investigation of selected aging periods to elucidate the mechanisms causing strengthening, as well as the influence on mechanical properties (discussed in chapter 7). The periods that were selected are: 8 minutes, which coincides with the point of maximum hardness for short aging periods; 32 hours, which represent the point just before α" seems to have an effect; and 260 hours which should be well within the α" region (indicated by arrows on figure 6.5).

6.4.1. Carbide and nitride precipitates

With the aid of transmission electron microscopy it was possible to identify precipitates of sizes in the order of 1 μm. The precipitates varied from spherical to almost perfect rectangular in form. Through their diffraction patterns they were identified as $M_{23}C_6$ with M = FeCr. The camera constant was determined to be 6.07×10^{-12} through measuring the known diffraction pattern of the α matrix.

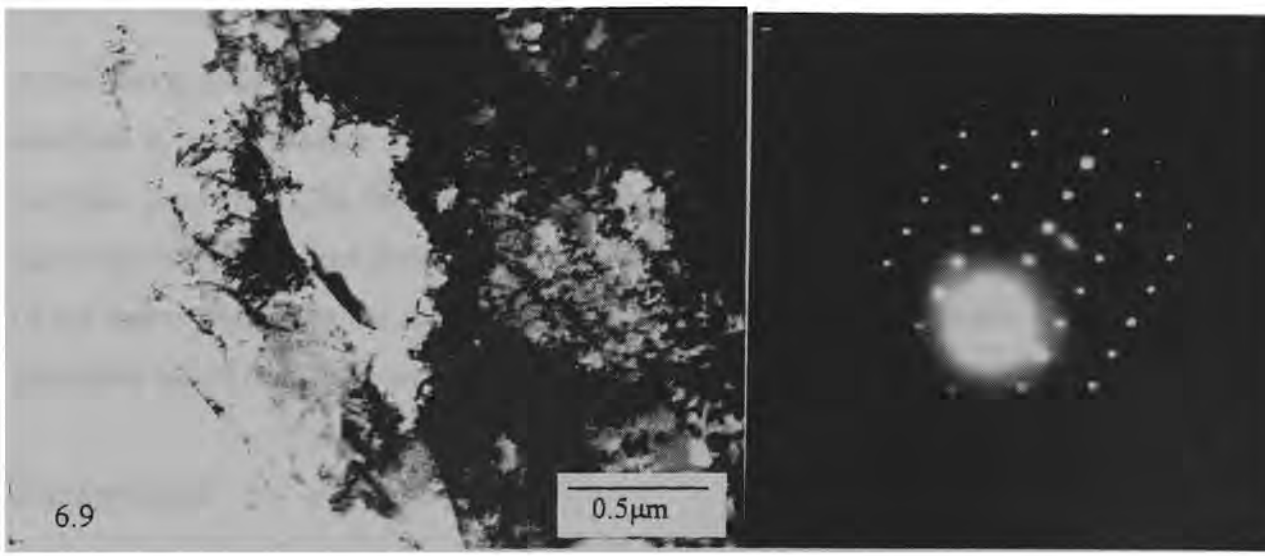

***Figure 6.9**: TEM micrograph of precipitate and selected diffraction pattern (sample solution treated at 930 ℃ and aged for 260 hours at 475 ℃)*

The precipitates were frequently situated on grain boundaries, but sometimes they formed rows in seemingly clear areas. This could indicate that precipitates formed on original grain boundaries or that the grain boundaries were pinned by the precipitates. The relative large sizes of the precipitates, along with the fact that precipitates could be detected in the unaged condition, suggest that these precipitates were present in the original sheet material, and that they are not the precipitates causing strengthening.

It seems very likely, however, that the precipitation of essentially Cr-rich carbides and nitrides are responsible for the initial increase in hardness (figure 6.5), as it has been found that a dramatic decline in toughness and increase in hardness occur before precipitates can be observed. It is suggested that the effects on mechanical properties are due to residual C and N in the matrix, perhaps in the form of extremely small Cr-C or Cr-N clusters (Grobner 1973, Cortie 1995).

No traces of the α" precipitate could be found by transmission electron microscopy. However, Mössbauer spectroscopy was used to detect the α", as described in the following section.

6.4.2. α" precipitate

A tool that is useful for the detection of the α" precipitates is Mössbauer spectroscopy as it is sensitive to small changes in the microstructure and is specifically sensitive to the local magnetic properties. The detection of α" is therefore possible as the α", being Cr-rich, is paramagnetic, whereas the ferrite matrix is ferromagnetic. In addition the magnetic properties of the matrix depend on the amount of Cr in solid solution, hence changes in the magnetic properties can be used to deduce information on the formation of Cr-rich precipitates.

Background

Mössbauer spectroscopy involves bombarding a target with a stream of gamma-rays; small shifts in the energies of the transmitted rays are obtained in the Mössbauer apparatus as a result of the Doppler principle. This is achieved by moving the source and sample relative to one another. The Mössbauer spectra are normally given as plots of absorption against relative velocity (in mm/s). The absorption characteristics are affected by the electronic environment of the nucleus, producing the hyperfine interactions (Czakó-Nagy and Vertés 1988).

The principal hyperfine parameters derived from the Mössbauer spectrum are the hyperfine field, isomer shift and quadrupole splitting.

The splitting of the nuclear energy levels in a magnetic field produces transitions that are each seen as a line in the Mössbauer spectrum. The energy difference between the first and last lines is directly related to the effective magnetic field experienced by the nucleus. This gives rise to the hyperfine field.

The isomer shift arises from the fact that the electron density near the nucleus varies with the chemical state of that nucleus. Thus the position of the resonance absorption peak depends on the chemical environment of the atom.

The charges distributed asymmetrically around the atomic nucleus (electrons, ions and dipoles) result in an electric field gradient that is not equal to zero at the site of the atomic nucleus. The

interaction of this electric field and the quadrupole moment of the atomic nucleus results in the splitting of the energy levels. The energy difference between the quadrupole split levels is known as the quadrupole splitting.

The effect of the principal hyperfine interactions on the 57Fe (the only iron isotope that shows the Mössbauer effect) spectrum can be seen in figure 6.10:

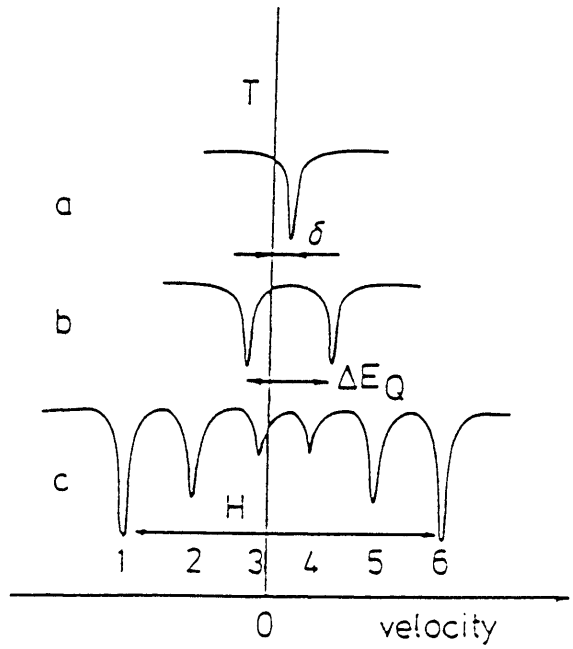

***Figure 6.10**: The effect of the principal hyperfine interactions. (a) isomer shift, (b) quadrupole splitting and (c) hyperfine field (Czakó-Nagy and Vertés 1988)*

Aging

Specimens solution treated at 880°C and 930°C, as well as those without additional solution treatment, were aged at 475°C for different periods. Their Mössbauer spectra and hyperfine parameters were determined.

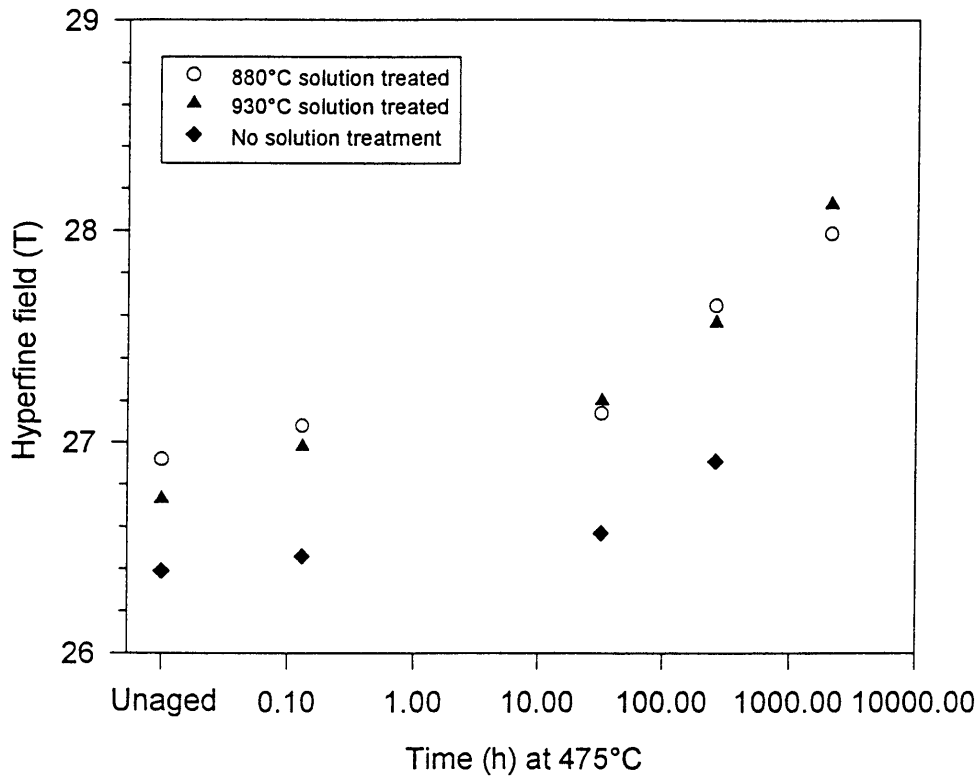

***Figure 6.11**: Distribution of hyperfine field with aging time at 475 ℃, the increase in the field indicates that chromium is removed from the matrix*

The increase of the hyperfine field (figure 6.11) indicates that parts of the matrix become enriched in iron, and by implication, others in chromium. The change in hyperfine field of the solution treated specimens for the period 0 to 8 minutes, is more than double that of the untreated one for the same time period. This increase is most likely caused by the precipitation of Cr-rich carbides and nitrides in the solution treated specimens: the hyperfine field increases as the Cr content of the matrix is lowered. The increase in the field after 32 hours of aging is probably due to α" precipitation. The trend exhibited by the hyperfine field is in good accord with that of the hardness values, namely an initial increase, followed by a second one at longer periods of aging.

That there is some change in composition with aging is verified by the fact that there is a slight increase in magnetic field as aging progresses. This is indicated by a shift to higher velocities of the Fe-sextet (outward expansion), without any paramagnetic effects influencing the profiles. This expansion is characteristic of decomposition via the process of nucleation and growth of a Cr-rich precipitate (Chandra and Schwartz 1971).

It was shown that α" does form at this composition and aging temperature - but this is only clearly evident after very long (approximately 3 months) aging periods (Figure 6.12).

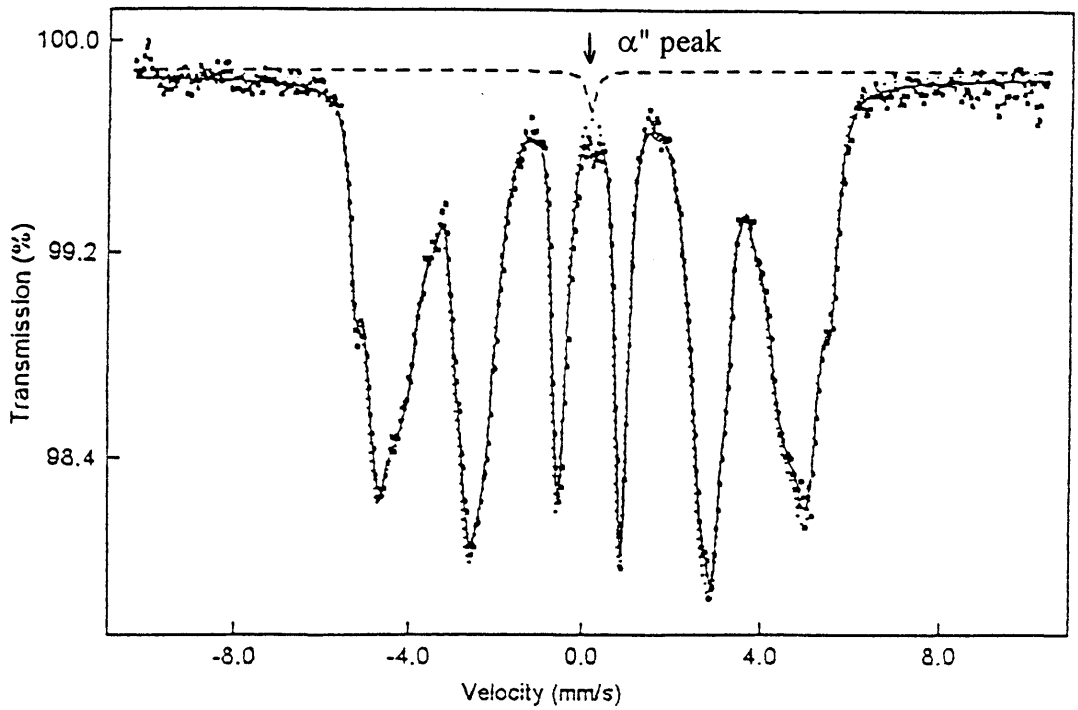

***Figure 6.12**: Mössbauer spectrum of 930 ℃ solution treated sample, cold worked and aged at 475 ℃ for 2072 hours, showing the paramagnetic peak of α" at zero velocity*

The six peaks are characteristic of α-Fe (Chandra and Schwartz 1971, Gonser 1983, Montano 1986) and the presence of the α" is indicated by the peak at 0 velocity, arising from the paramagnetic contribution of the chromium-rich phase.

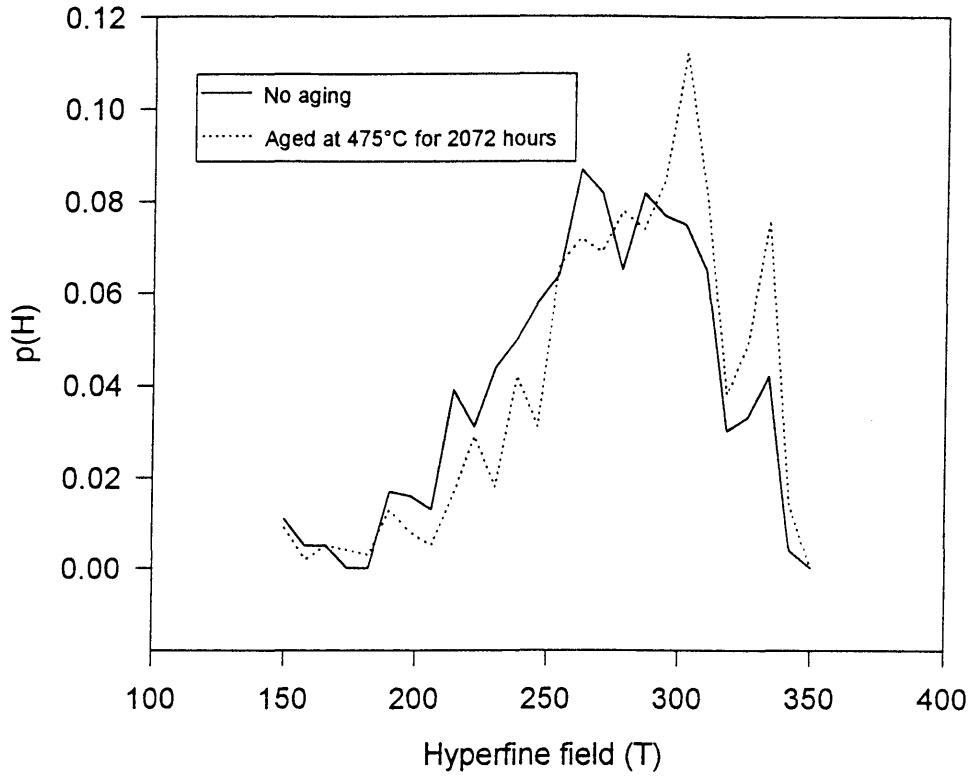

***Figure 6.13**: Field distribution of 880 ℃ solution treated specimens, showing the shift to higher values of the hyperfine field after 2072 hours at 475 ℃*

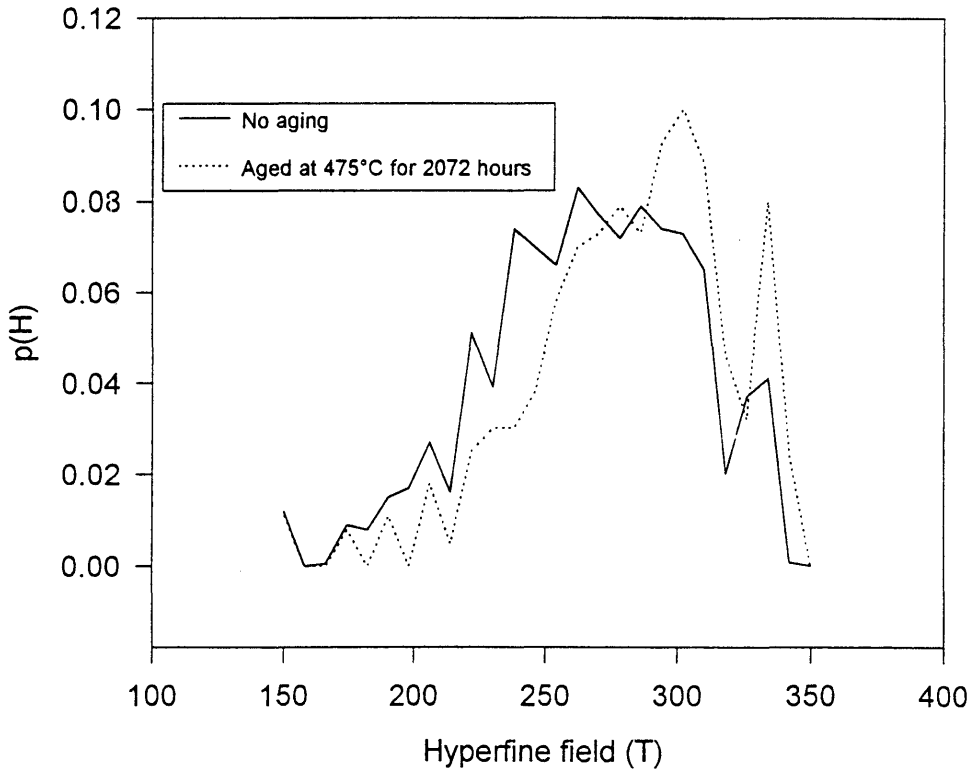

***Figure 6.14**: Field distribution of 930 ℃ solution treated specimens. Before aging and after 2072 hours at 475 ℃, indicating shift to higher hyperfine field values after aging*

The displacement of the p(H) curves to higher values of the hyperfine field without broadening of the distributions (figures 6.13 and 6.14) confirms that the α" is formed through nucleation and growth of particles having the equilibrium composition (Trindade and Vilar 1991), rather than by spinodal decomposition.

It can be concluded that α" precipitation definitely occurs and α" formation is thus assumed to contribute to the strengthening, albeit only at longer aging periods. The precipitates (α") can only be detected after very long periods of aging (for this composition and aging temperature), when the volume fractions of the Cr-rich clusters have become large enough for detection.

6.5. Conclusions

Two stages can be distinguished in the aging behaviour if additional solution treatments are performed before cold rolling and aging. An initial increase in hardness at short aging periods can be observed, which is attributed to the precipitation of Cr-carbides and nitrides, and a second increase at long periods of aging due to the formation of α".

Solution treatments enhance the precipitation of carbides (and nitrides) and cause a subsequent increase in hardness, but do not markedly influence the kinetics of α" formation; the precipitation of α" seems to become appreciable only after 64 hours of aging, regardless of treatment before cold rolling and aging.

Solution treatment at 920°C (higher than the Ac_1) introduces martensite into the structure, which raises the initial, unaged hardness, but does not seem to affect the overall aging behaviour.

With aging at 475°C a decrease in hardness is observed before the formation of α"; this is probably caused by overaging of the carbides and nitrides. No overaging occurred at 450°C, possibly because of the lower diffusion rates.

The α" is formed through the process of nucleation and growth. This is confirmed by the increase in magnetic field as well as the displacement of p(H) curves to higher hyperfine field values.

Chapter 7

Effect of Cold Rolling and Heat Treatments on Mechanical Properties

Chapters four to six presented the hardening that could be obtained by solution heat treatment, cold rolling and aging (primarily at 475°C). Hardness is a convenient way of measuring strength - the reason for its use in the previous chapters - but in actual use the chains are exposed to both tensile and impact loading. Therefore the strength (represented by the yield stress) and the fracture toughness are more applicable mechanical properties. In this chapter the effect of the treatments on properties such as impact strength, fracture toughness, tensile and yield stress and work hardening rate is investigated, while their effect on corrosion resistance is presented in the following chapter.

7.1. Impact strength

Impact tests were performed on specimens solution heat treated at 880°C and 930°C, cold rolled (38% reduction in area) and aged at 475°C for 8 minutes and 32 hours. Unaged samples were also tested. Four sub-size specimens were tested in each condition, having the dimensions given in figure 3.2. Tests were performed at ambient temperature.

The results presented in figure 7.1 indicate that a marked drop in impact strength occurs after only 8 minutes of aging, but that there is not a significant difference in impact strength with aging from 8 minutes to 32 hours.

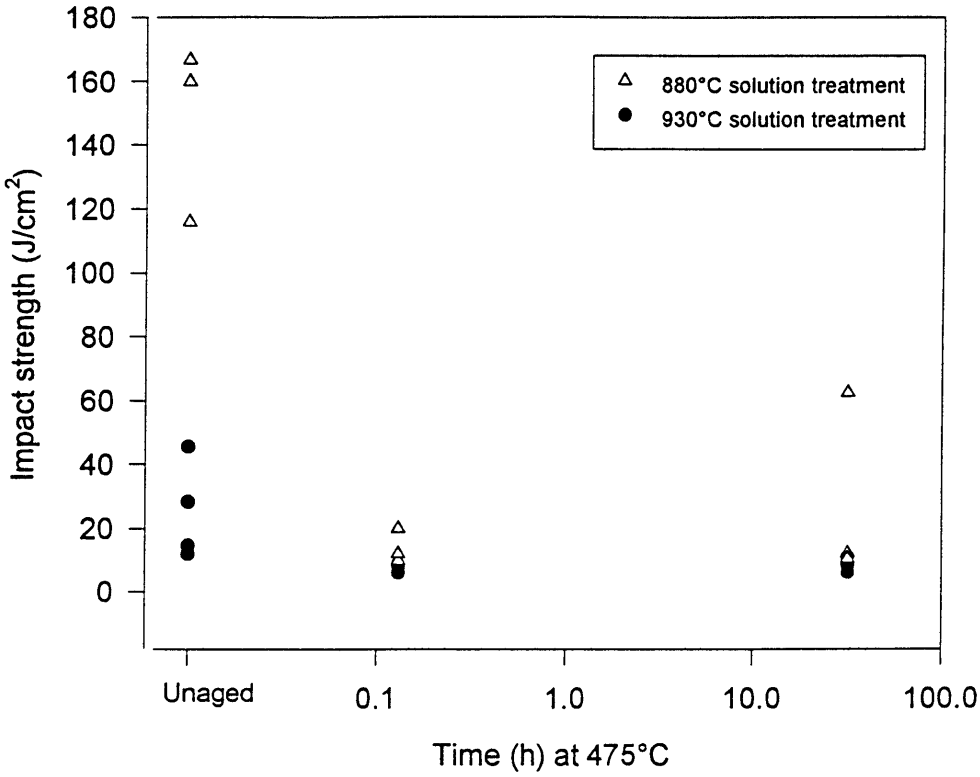

***Figure 7.1**: Impact strength of specimens (55×10×5 mm in size) aged at 475℃, after solution treatment (at 880℃ and 930℃ respectively), and cold rolling. Testing performed at ambient temperature. The results indicate a marked decrease in toughness after 8 minutes of aging*

The lateral expansion of the specimens was determined by measuring the compression side of the impact specimen with a micrometer, and calculating the difference between the initial size (L_i) and expanded size (L_e) as a percentage of the initial size, i.e. $(L_e-L_i)/L_i \times 100$. Like the amount of energy absorbed, the lateral expansion can be used to evaluate the impact resistance - the greater the expansion, the more plastic deformation (and hence energy absorption) before fracture (Rolfe and Barsom 1977, pp. 199-204).

A similar trend, as with the impact strength, is exhibited by the lateral expansion of the specimens (figure 7.2), namely a dramatic decrease in expansion, as aging proceeds.

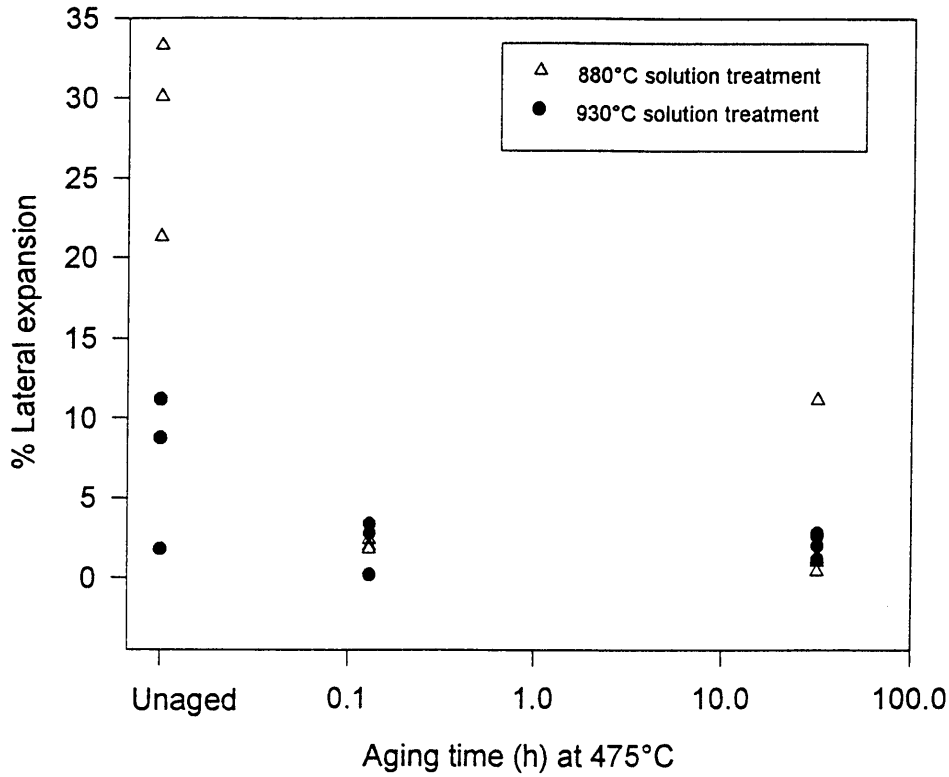

***Figure 7.2**: Lateral expansion of impact specimens, aged at 475℃; after solution treatment at 880℃ and 930℃ and cold rolling. Results show a decrease in % expansion as aging proceeds, indicating a loss in ductility*

Both the impact strength and lateral expansion indicate that embrittlement accompanies the increased hardness obtained by aging. However, these values, as such, do not give an indication of the practical implication of the embrittlement. In this respect the fracture toughness (K_{Ic}) is a more useful property.

Local stresses near a crack depend on the product of the nominal stress and the square root of the half-flaw length. This relationship is quantified by the stress intensity (K). There are several modes of deformation that could be applied to a crack, one of which is known as Mode I, where a tensile stress is applied normal to the faces of the crack. This is the usual mode for fracture-toughness tests and a critical value for stress intensity for this mode would be denoted K_{Ic}. K_{Ic} values are valid material properties, independent of specimen thickness (Dieter 1988 p.351-355).

From the impact strength it is possible to estimate K_{Ic} values. The following equation, linking the CVN values and K_{Ic}, was used:

$$K_{Ic} = 6.79\ (\text{CVN})^{0.75} \qquad (7.1)$$

with K_{Ic} in MPa $(\text{m})^{0.5}$

CVN in J/cm^2

Equation 7.1 can be used for ferritic steels having a yield stress between 270 and 1700 MPa, and an impact range of 14 - 82 J (Hertzberg 1983). The properties of the material investigated here mostly fall into these ranges.

Once the K_{Ic} values are known, it is possible to determine a tolerable flaw-length-before-failure i.e. a maximum crack length that can be tolerated before catastrophic failure at a stress equal to the yield strength. In order to determine this critical crack length (through-thickness) the following equation was used:

$$K_{Ic} = \sigma\ (\pi a)^{0.5} \qquad (7.2)$$

with σ the flow stress in MPa (determined through tensile tests - see section 7.3)

a the critical crack length in m

The critical crack lengths were determined by using the calculated K_{Ic} values and actual, measured yield stress values. The same yield strength value was used for all the specimens of a particular heat treatment. This represents a conservative approach, as the yield stress values are higher than the operational stresses to which the chains are exposed.

The critical crack lengths are shown in figure 7.3. It is indicated by these results that in the worst scenario, the maximum flaw length that can be tolerated is 0.3 mm at a stress equal to the yield strength of 860 MPa (specimen solution treated at 930°C, cold rolled and aged at 475°C for 8 minutes). For the specimens solution treated at 880°C, aging results in a maximum allowable flaw length of 0.8 mm for 8 minutes at 475°C (for a stress of 760 MPa). See also Appendix 14 for the range of values.

It is important to emphasise that these results are for tests at room temperature; the fracture toughness is expected to drop further at lower temperatures - which would be of importance should the chains be used in a refrigeration plant.

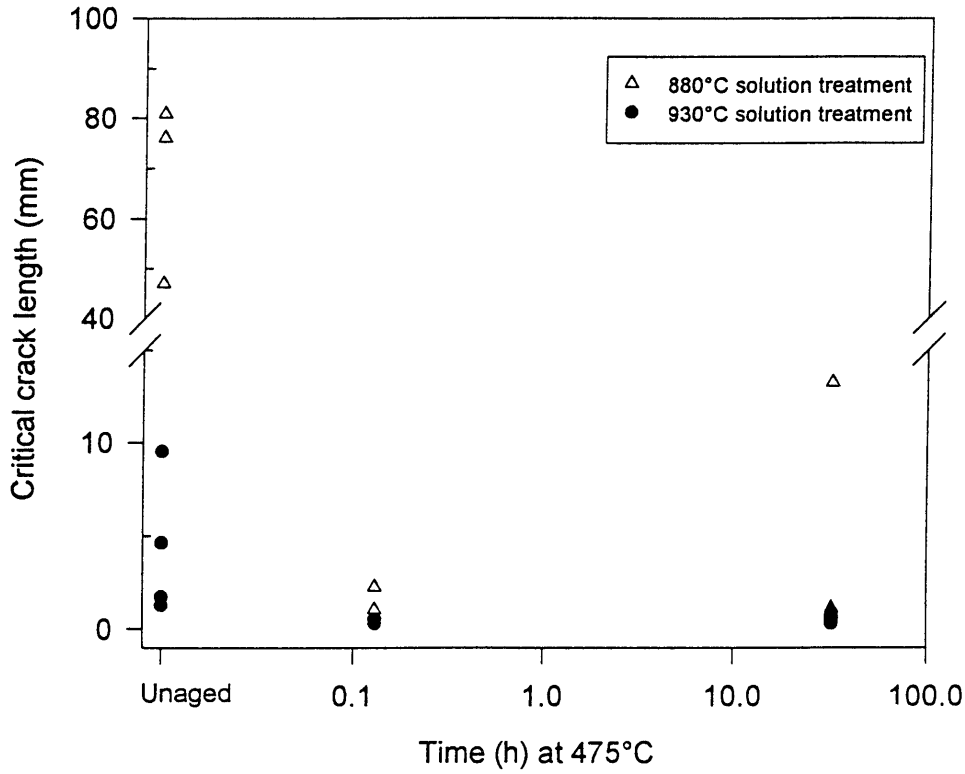

***Figure 7.3**: Calculated critical crack lengths (in mm) of specimens solution treated at 880 ℃ and 930 ℃, cold rolled and aged at 475 ℃, indicating a maximum allowable flaw length of 0.3 mm for 930 ℃ solution treatment, and 0.8 mm for 880 ℃*

The critical crack length (for the 880°C solution treatments) is comparable to the thickness of the chain links (3 mm). It is not expected that there would be flaws of this (calculated) size in the as-manufactured links. Hence, for catastrophic failure to occur, a fatigue crack must first be initiated. Therefore, fatigue is expected to determine the practical lifetime of the chains, although the lower K_{Ic} values indicate that less crack propagation will be tolerated before brittle fracture.

7.2. Fracture surfaces

The fracture surfaces were examined with the aid of a scanning electron microscope.

As expected from the low impact strength, fracture occurred mostly through brittle transgranular cleavage (figure 7.4a), accompanied by some ductile fracture (the fine equi-axed dimple structure) at the grain boundaries (figure 7.4b). In the cold worked condition grain boundaries are no longer the preferred nucleation points for cracks; rather, nucleation occurs at dislocations. This causes the matrix to be brittle, and the grain boundaries to be relatively ductile. The fine dimple structure (figure 7.5a) may well be caused by the carbide particles increasing the number of localised strain centres, initiating microvoids which grow until the ligaments between them fracture (Dieter 1988). Such a condition should also improve the capacity of the alloy to accommodate strain and limit strain concentration at the grain boundaries (Chun and Polonis 1992).

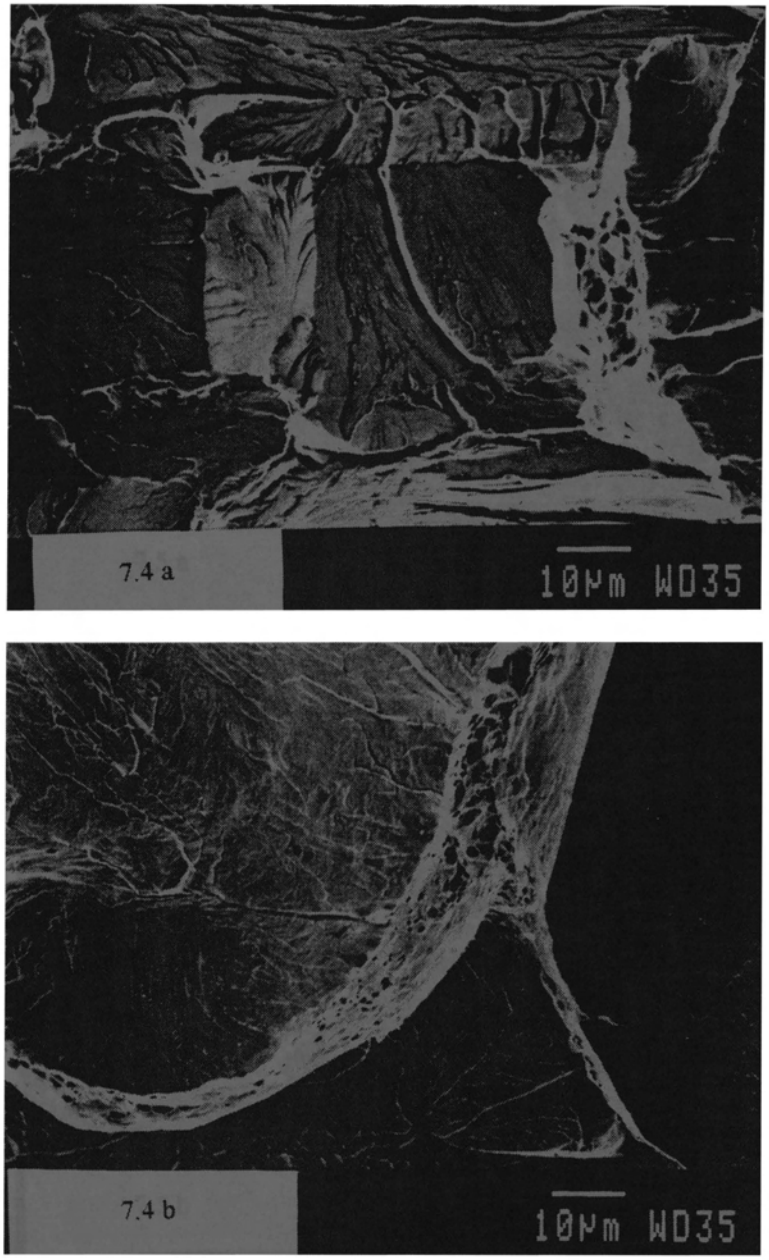

***Figure 7.4**: SEM photos of fracture surfaces (a) Transgranular cleavage fracture (930 ℃ solution treatment, aged at 475 ℃ for 277 hours (b) Ductile fracture at grain boundaries (880 ℃ solution treatment, aged at 475 ℃ for 8 minutes)*

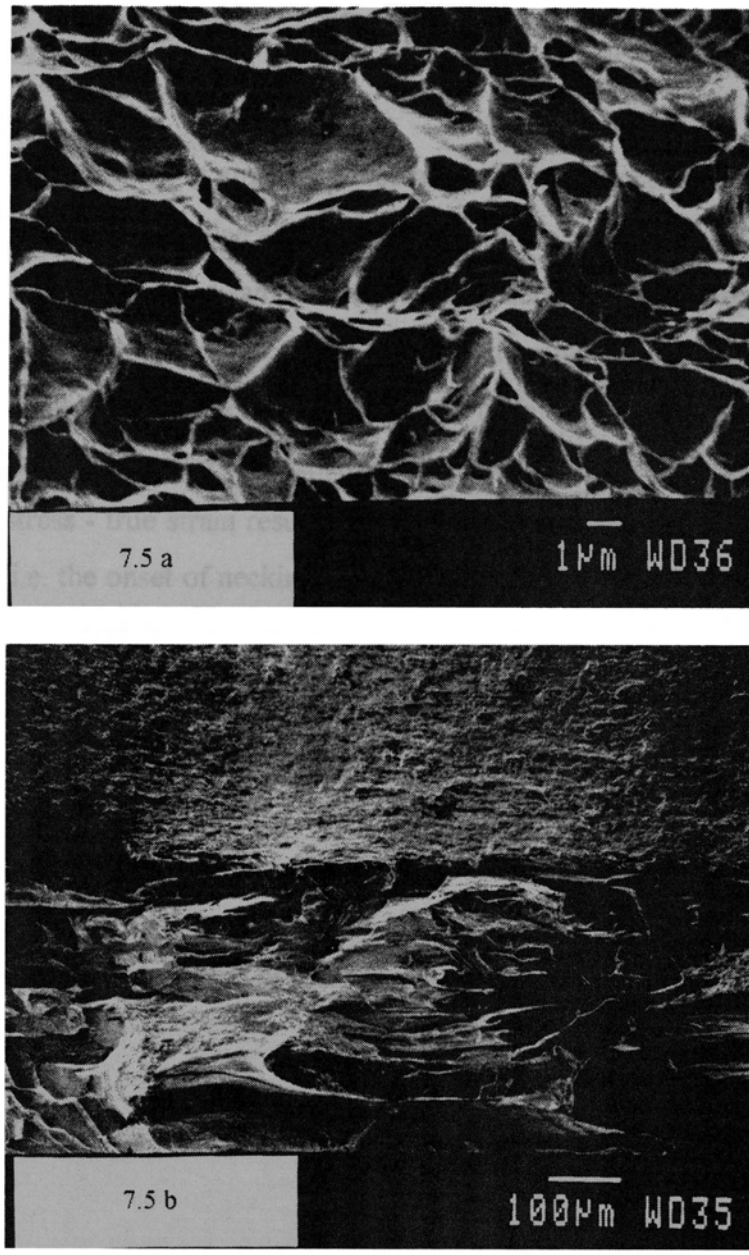

***Figure 7.5**: SEM photos of fracture surfaces (a) Microvoid coalescence (solution treatment at 880 ℃ and aged for 8 minutes at 475 ℃) (b) Transition between shear and cleavage fracture zones of an unaged specimen, solution heat treated at 880 ℃ and cold rolled; having an impact strength of approximately 150 J/cm^2*

In the samples solution treated at 880 °C microvoid coalescence was clearly visible in the regions close to the notch - figure 7.5a. The transition between shear and cleavage fracture zones was also very prominent (figure 7.5b). Crack-dividing delamination effects were prominent, which probably increased the impact strength.

7.3 Tensile tests

Tensile tests were performed at ambient temperature on specimens solution treated at 880°C and 930°C respectively, cold rolled after quenching in brine, and aged at 475°C for 8 minutes, 32 hours and 277 hours. Unaged samples, as well as undeformed and unaged specimens, were also tested. Elongation was measured using a 15 mm gauge length. This is not a standard gauge length for the specific specimen cross-section. However, the tensile behaviour was measured to compare the plastic flow characteristics. These are properly studied by comparing true stress - true strain results, which were only determined for stresses up to the tensile strength (i.e. the onset of necking). For these uniform elongations, the choice of gauge length does not affect the results. It should, however, be borne in mind that the total elongation to failure as measured in this work cannot be compared to that determined using standard gauge lengths. Force and elongation were converted to engineering stress and strain curves; which in turn were converted to true stress and true strain curves for strains up to the onset of necking. For the final graphs the elastic strain component (σ/E, with E = 210 GPa) was subtracted from the total true strain, to give plots of true stress vs. true plastic strain. Figure 7.6 illustrates the calculation process:

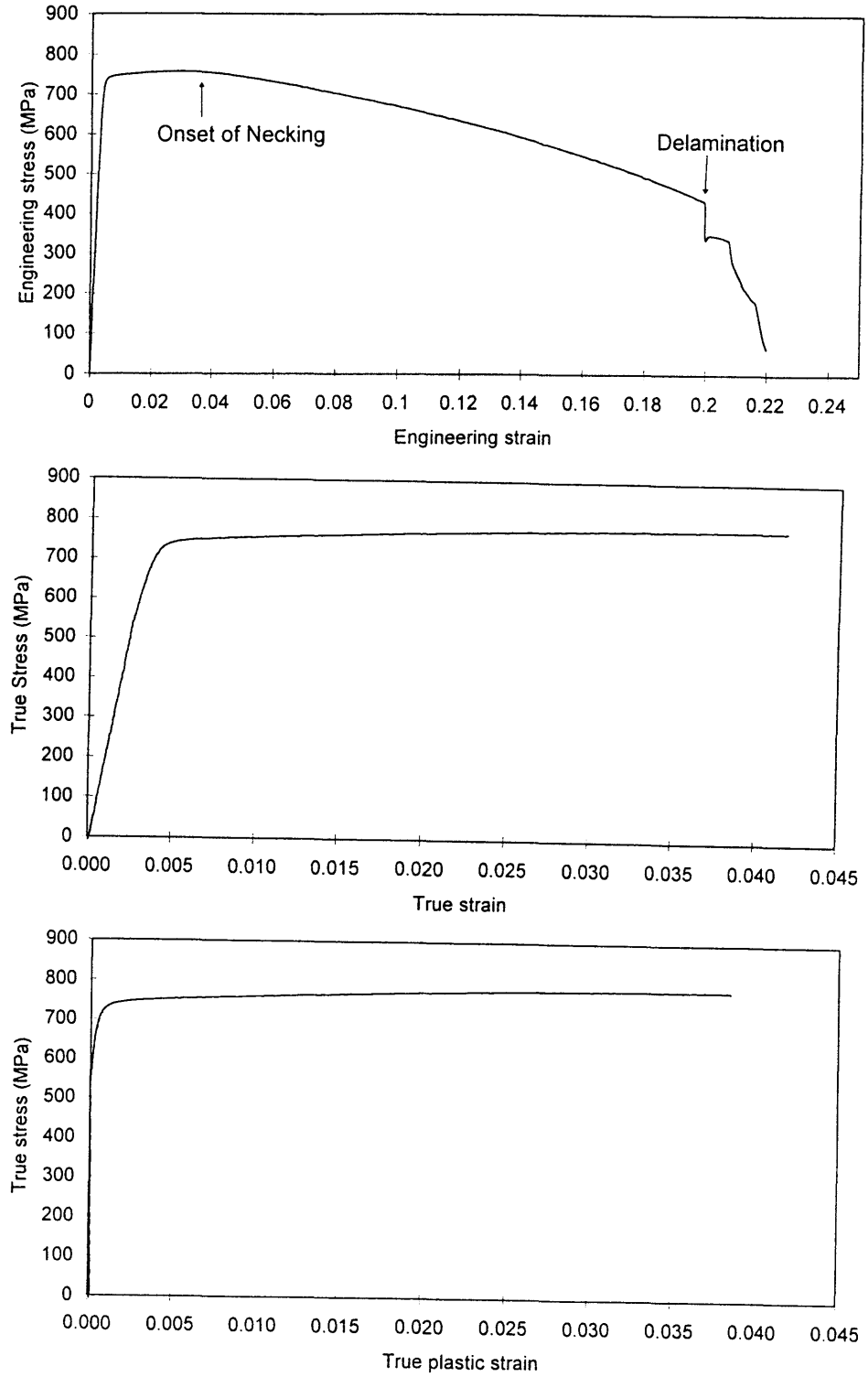

***Figure 7.6**: Results of the calculation of true stress/true plastic strain curves from engineering stress and strain values by subtracting the elastic component of the strain. The arrow in the first graph indicates the onset of delamination, which immediately preceded ductile fracture*

Some typical true stress/true plastic strain curves of the undeformed material are given in figure 7.7, and those of the cold rolled and aged specimens in figure 7.9. Figure 7.8 presents

the engineering stress/strain curves of both the 880°C and 930°C solution treated samples. The results of individual specimens of the same condition varied somewhat (see Appendix 15). This is attributed to the inhomogeneous nature of the original sheet, through factors such as segregation during solidification. It was attempted to minimise bias from just such irregularities by selecting the specimens from different positions in the sheet; and this is probably the reason for the differences in results.

The reduction in area, induced by the cold rolling, can be taken into account in the true strain values by using the following equation:

$$\text{true } \varepsilon = \ln A_0/A \qquad (7.3)$$

and in this case the 38% reduction in area amounts to a true strain of 0.478.

It can be seen from figure 7.7 that this means that the cold rolling deforms the material to well past the maximum uniform tensile elongation (i.e. the onset of necking during tensile testing).

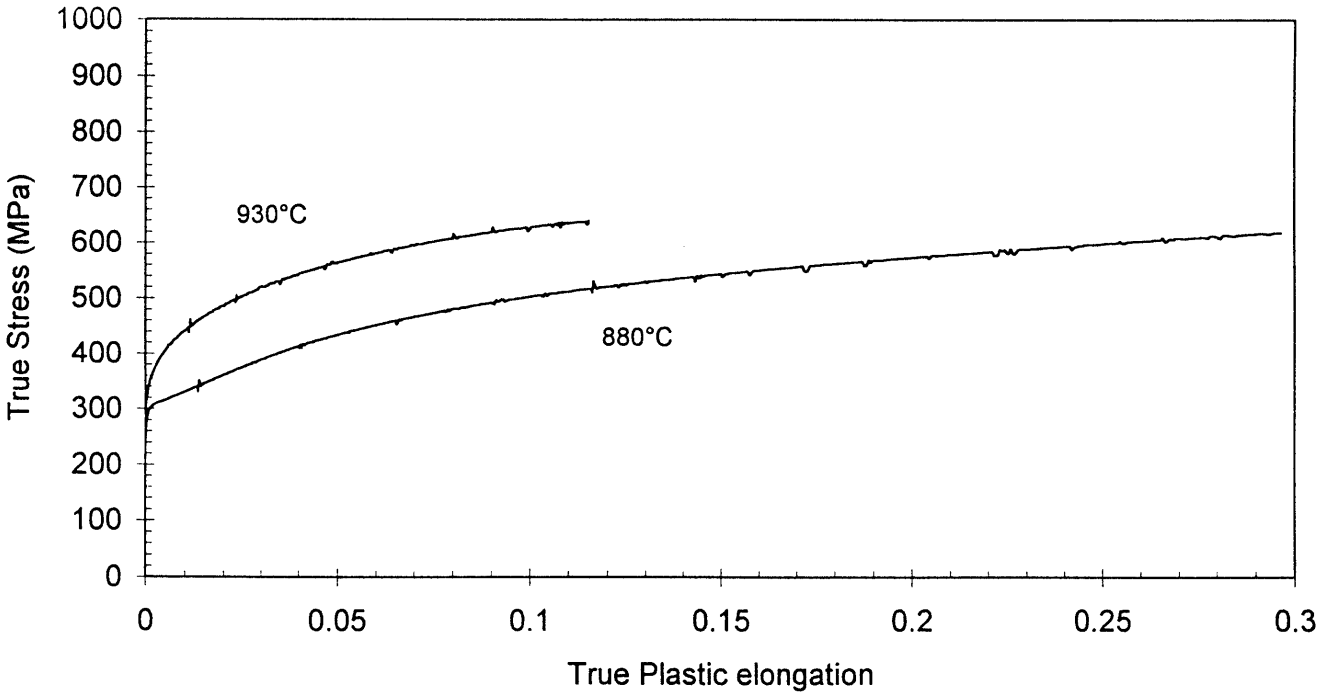

***Figure 7.7**: Typical true stress/true plastic strain curves of undeformed samples (solution heat treated at both 880℃ and 930℃, and quenched in brine). The curves terminate at the maximum uniform elongation. The values indicate that the subsequent 38% reduction in area through cold rolling (true $\varepsilon = 0.478$) is well past the available uniform tensile elongation*

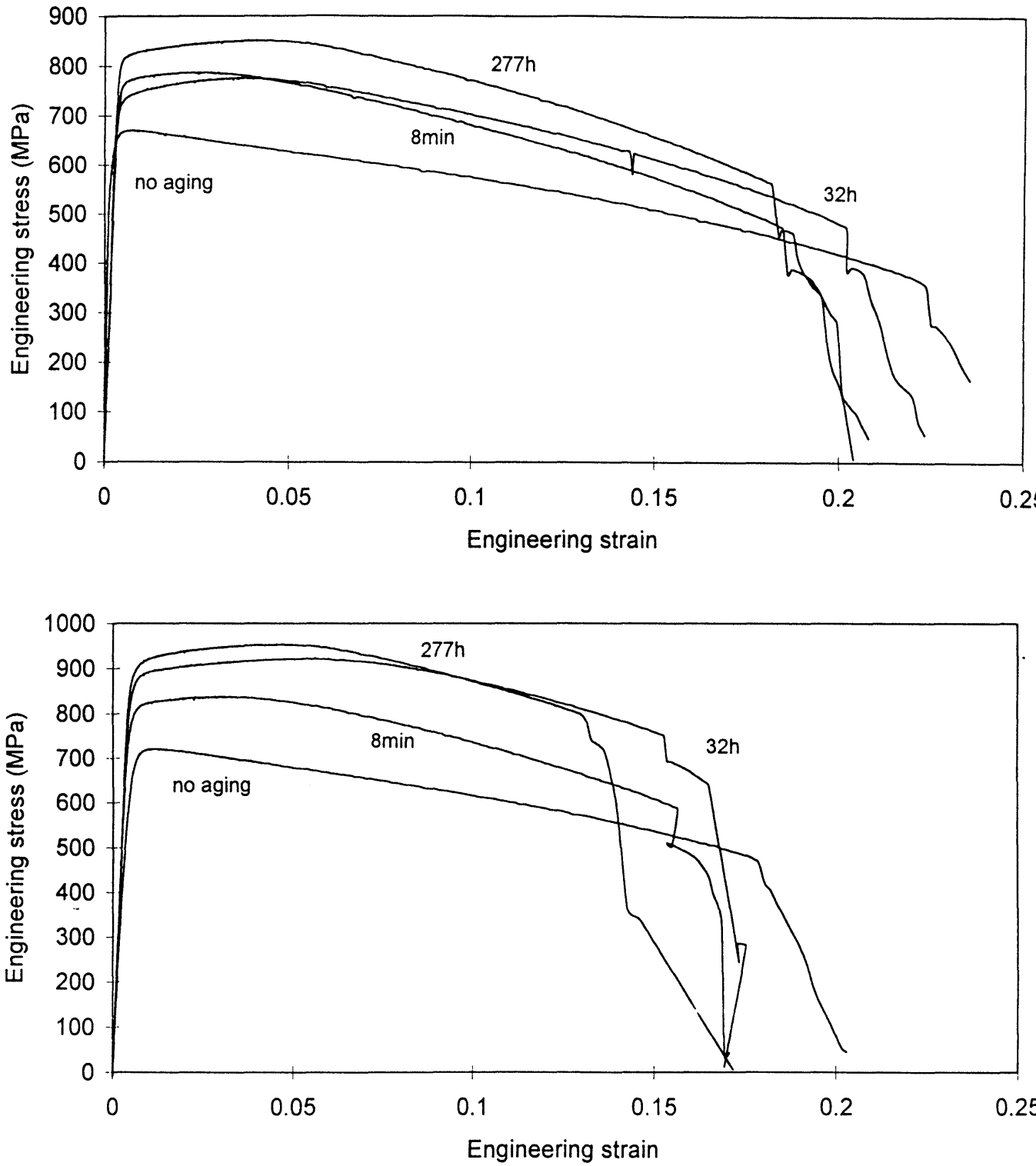

***Figure 7.8**: Typical engineering stress/strain curves of cold rolled samples (solution heat treated at (a) 880℃ and (b) 930℃, quenched in brine); and aged at 475℃ for 8 minutes, 32 hours and 277 hours. Unaged specimens are also shown*

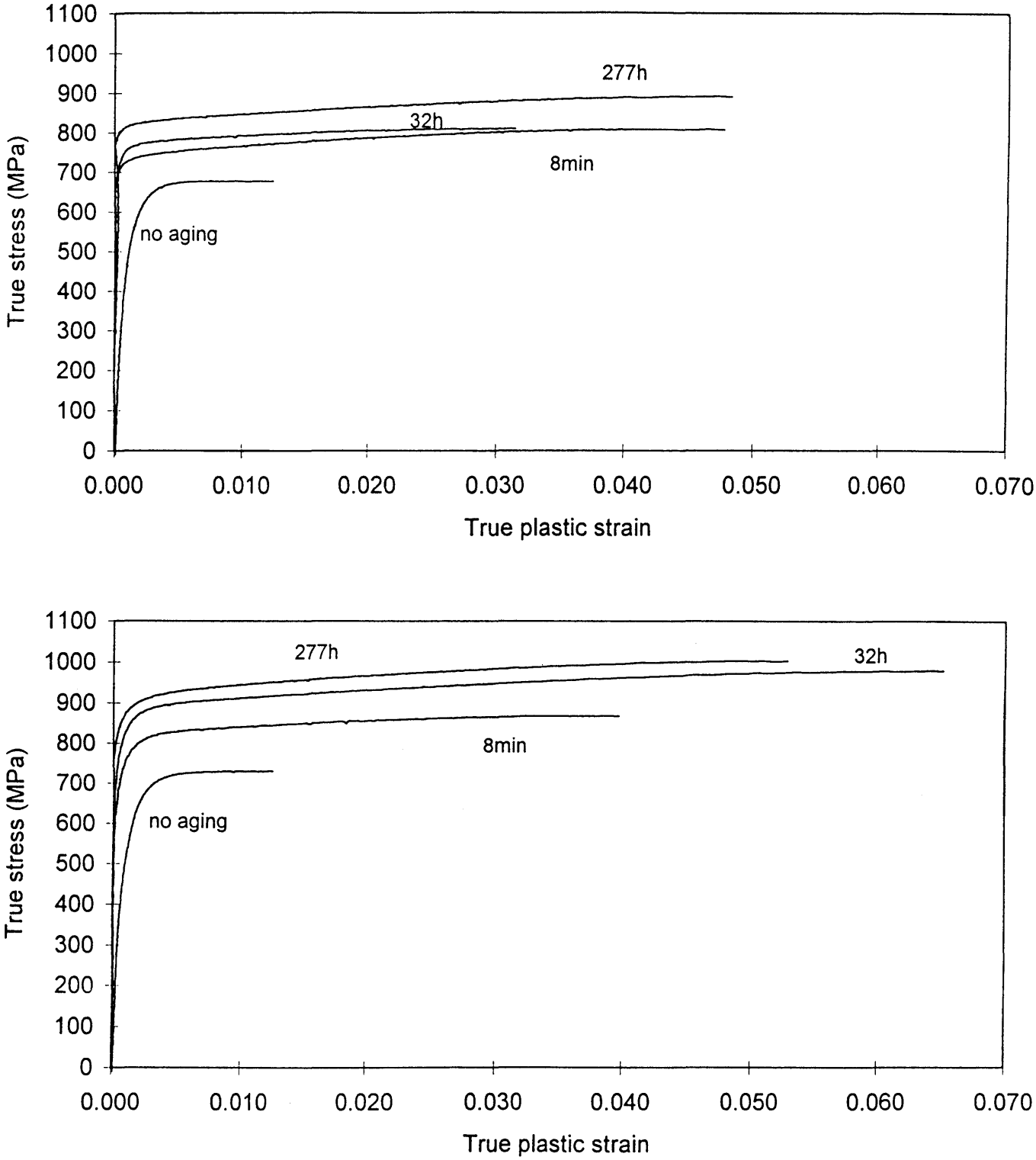

***Figure 7.9**: True stress/true plastic strain of cold rolled samples (solution heat treated at (a) 880℃ and (b) 930℃, quenched in brine); and aged at 475℃ for 8 minutes, 32 hours and 277 hours. Unaged specimens are also shown*

From figures 7.7 and 7.9 it can be seen that an increase in strength is obtained with cold rolling and aging. This increase is probably due to the increase in dislocation density (during cold rolling) and precipitation of carbides and nitrides (during aging); both effects impede dislocation motion. Without aging, little uniform elongation occurs before the onset of necking, in line with the observation that the deformation during cold rolling is larger than the uniform tensile elongation of the undeformed material. The maximum uniform plastic deformation increases in the first aging step (figure 7.10), but is similar for subsequent aging. This is linked to the work hardening rate, which will be discussed later in this section.

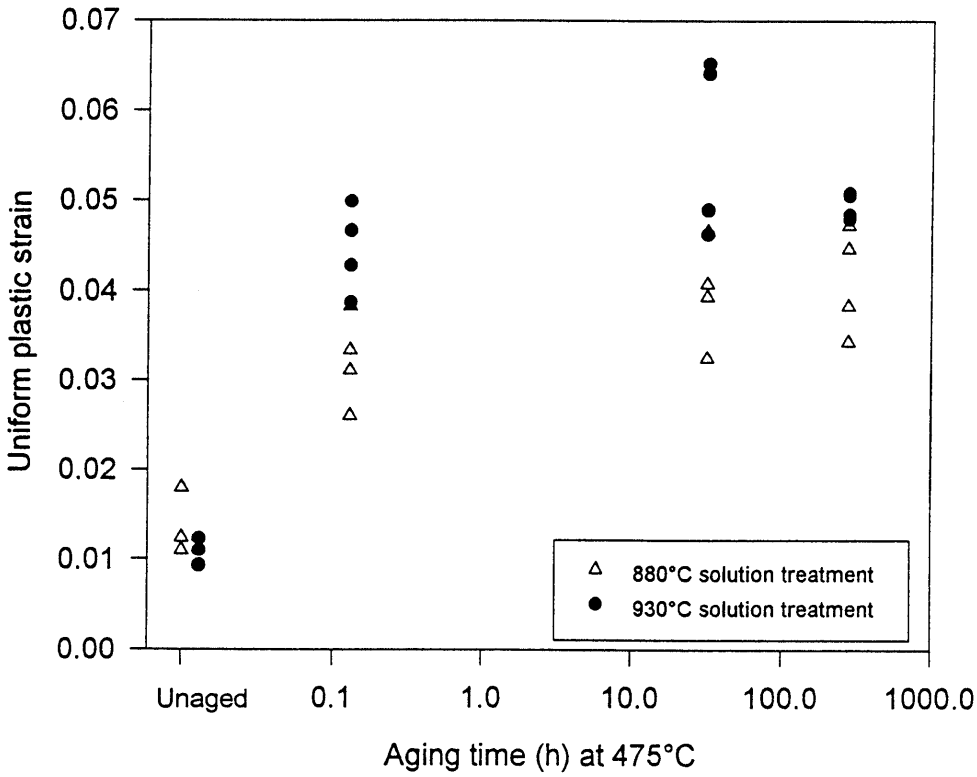

***Figure 7.10**: Uniform plastic strain (true strain at the onset of necking). Results indicate that the uniform plastic strain increases in the first aging step*

Two further aspects arise from the results shown in figures 7.8 and 7.9. The first is that, in the unaged material, plastic flow occurs immediately upon application of an external stress - no elastic region is observed. This is attributed to the residual stresses which arise as a result of cold rolling. During cold rolling deformation is not homogeneous through the thickness of the material. The centre of the material tends to restrain the surface from elongation. The result is a residual stress pattern which consists of a high compressive stress at the surface and a tensile stress at the centre. Because of the residual stresses, parts of the material are at, or

close to, the tensile yield stress, even with no externally applied stress. This causes the material to exhibit macroscopic plastic flow even at low applied stress, as is evident in the tensile behaviour of the as-rolled material (figures 7.8 and 7.9).

Metals containing residual stresses can be stress relieved, by heating to a temperature where the yield stress of the material is the same or less than the value of the residual stresses, thus allowing the material to deform and release the stress (Dieter 1988, p. 557). With aging, even after only 8 minutes at 475°C, these residual stresses are relieved, as is evident from the tensile results. This behaviour was noticed in both the 880°C and 930°C solution treated specimens and is in accordance with the results seen in the TEM micrographs, showing recovery (section 4.3).

The second aspect arising from the curves in figures 7.8 and 7.9, is that, in addition to the relief of residual stresses, the work hardening behaviour is changed by the first aging step. This is evident from the increase in uniform elongation (figure 7.10) and in plots of the work hardening rate (θ). The work hardening rate is defined as the slope of the true stress - true strain curve ($\theta = d\bar{\sigma}/d\bar{\varepsilon}$); the results are shown in figures 7.11 and 7.12.

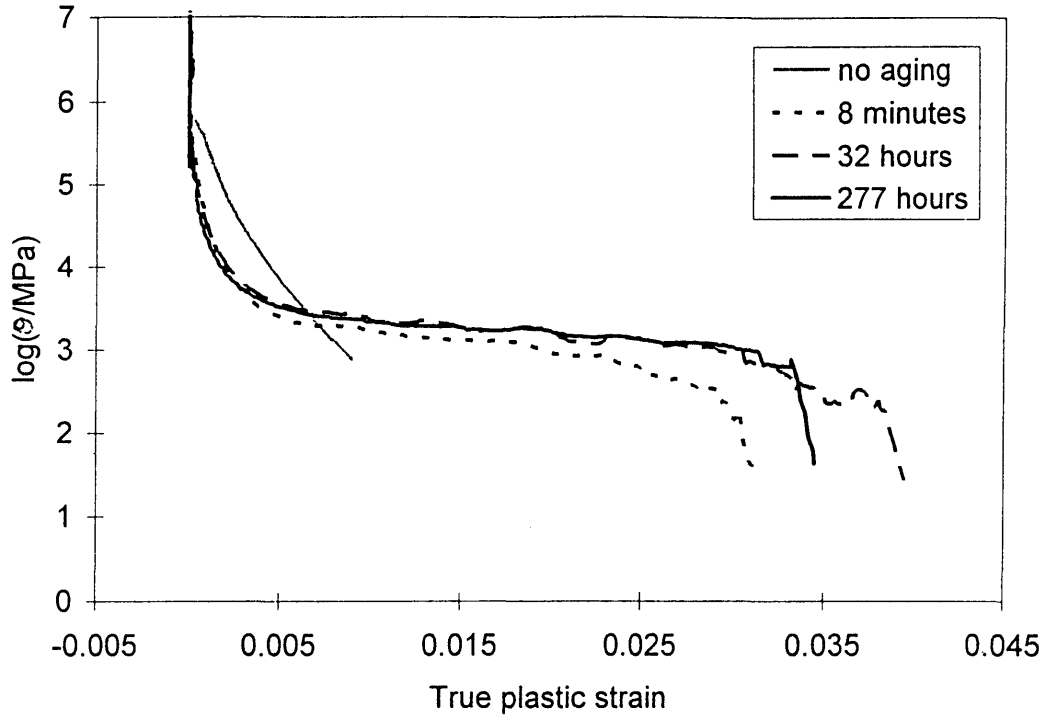

***Figure 7.11**: The effect of plastic strain on the work hardening rate (θ) of samples solution treated at 880℃, cold rolled and aged at 475℃. The results indicate a change in work hardening behaviour after the first aging step, with higher work hardening rates at higher strains for the aged specimens*

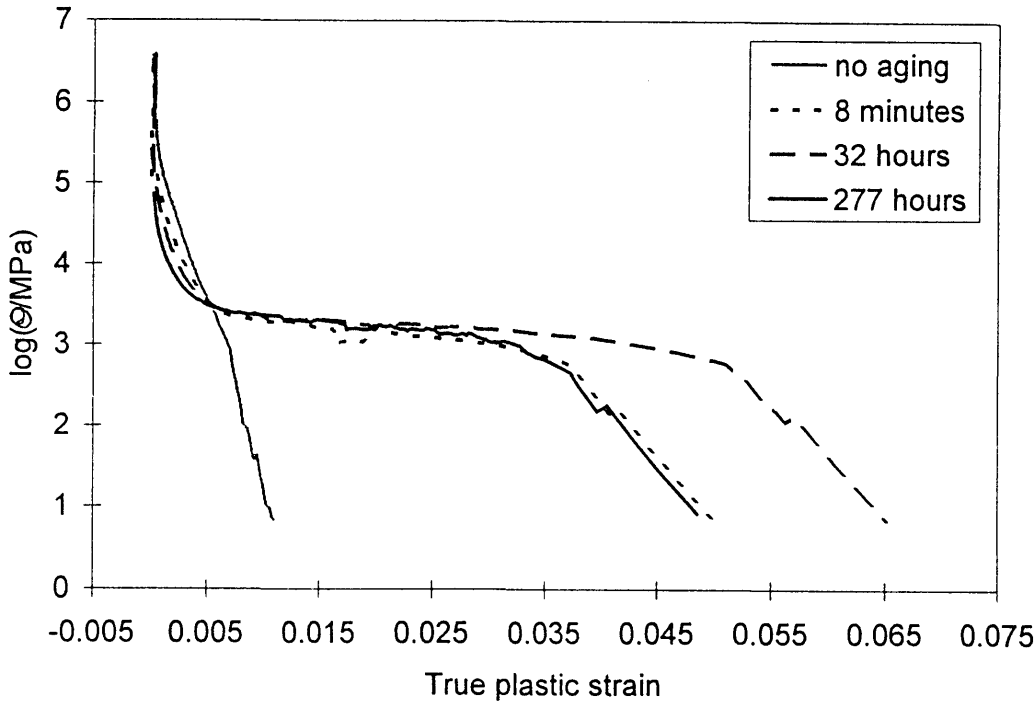

***Figure 7.12**: The effect of plastic strain on the work hardening rate (θ) of samples solution treated at 930℃, cold rolled and aged at 475℃. The results indicate a change in work hardening behaviour after the first aging step, with higher work hardening rates at higher strains for the aged specimens*

In these figures, the apparently higher initial work hardening rate of the unaged specimens results from the occurrence of flow at low applied stress (i.e. the effect of residual stresses), as is evident from figures 7.8 and 7.9. However, the work hardening rate of the unaged specimens drops below that of the aged samples at a true strain of around 0.006, resulting in the lower uniform elongation of the unaged specimens (figures 7.8, 7.9 and 7.10). The work hardening rate of all the aged specimens is similar. The higher work hardening rate of the aged specimens indicates a more rapid increase in dislocation density during deformation; this is presumably the result of the precipitation of nondeforming particles during aging.

While not of importance for the practical use of the chains, interesting effects of cold working and aging on the strain-to-fracture were found. Because of significant plastic anisotropy, the strain-to-failure is not quoted as the reduction in area; but rather as the individual strains in the width and thickness directions (figures 7.13 and 7.14). It is clear that the true strain at ductile fracture is similar for undeformed, deformed and aged material (for each prior solution treatment), with a small decrease in fracture strain after the first aging step. Figure 7.15 gives the ratio of these two strains ($\varepsilon_w/\varepsilon_t$; the R-ratio). Statistically there is little difference between the true strains-to-ductile fracture in the width direction, in the true strain-to-ductile fracture in the thickness direction of the aged specimens, or between the deformed and undeformed samples (no aging involved in either case). There does, however, seem to be small but significant differences between the aged and unaged specimens.

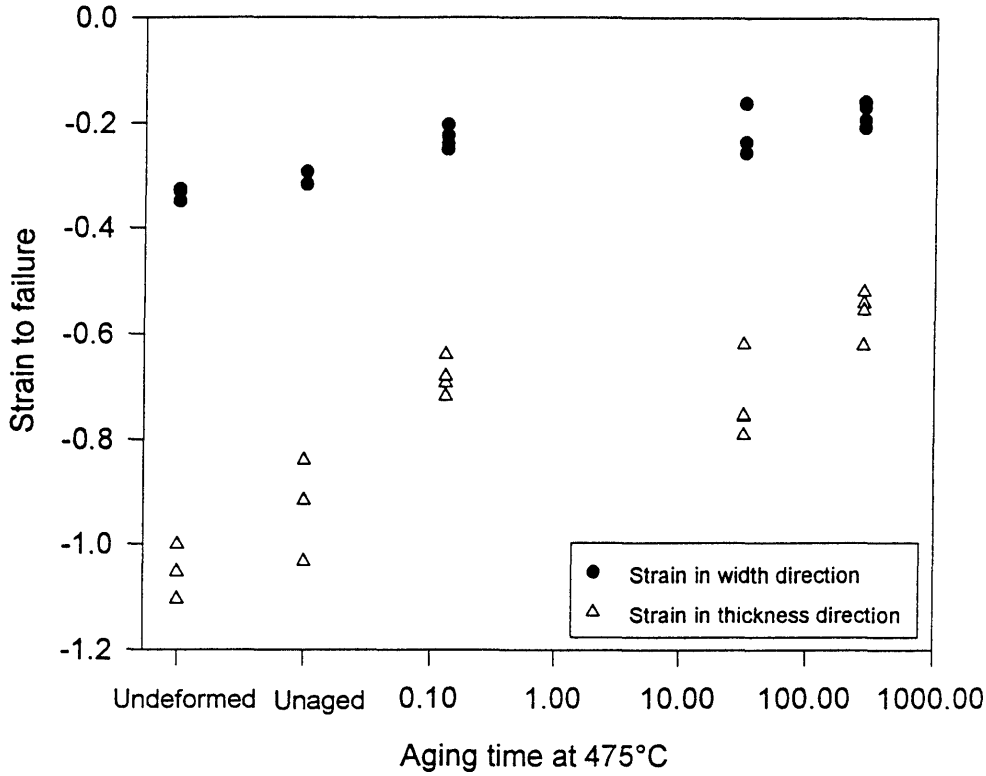

***Figure 7.13**: Strain-to-failure in the width and thickness directions of the specimens solution treated at 880℃. Results indicate that there is little difference in the true strains to ductile fracture*

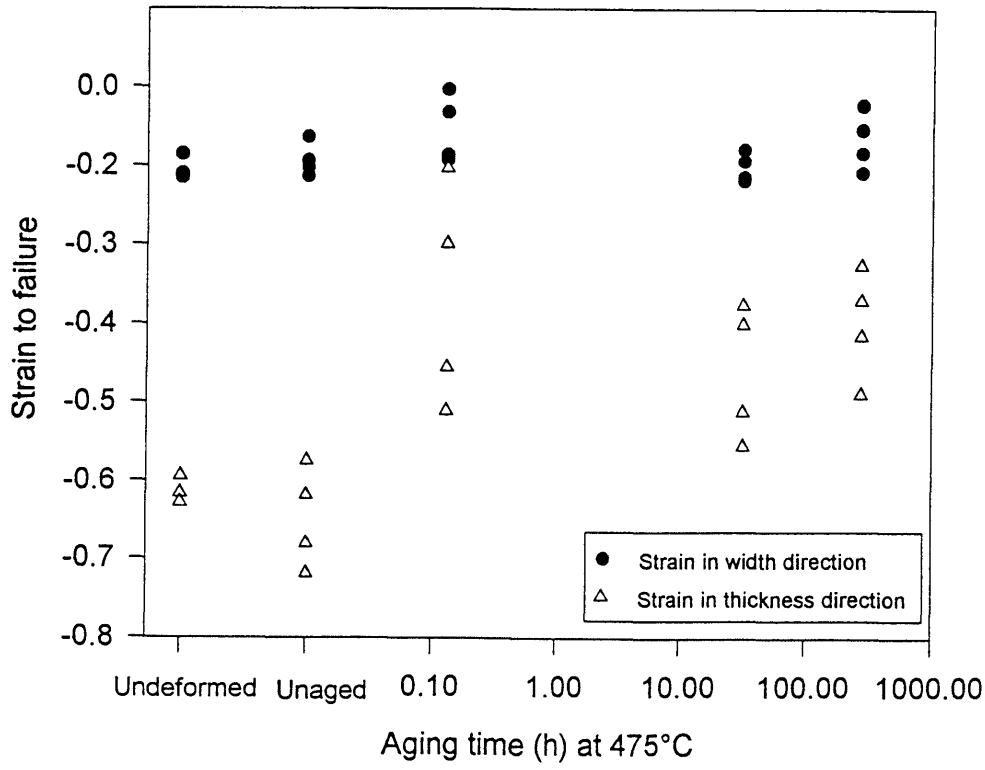

***Figure 7.14**: Strain-to-failure in the width and thickness directions of the specimens solution treated at 930℃. Results indicate that there is little difference in the true strains to ductile fracture*

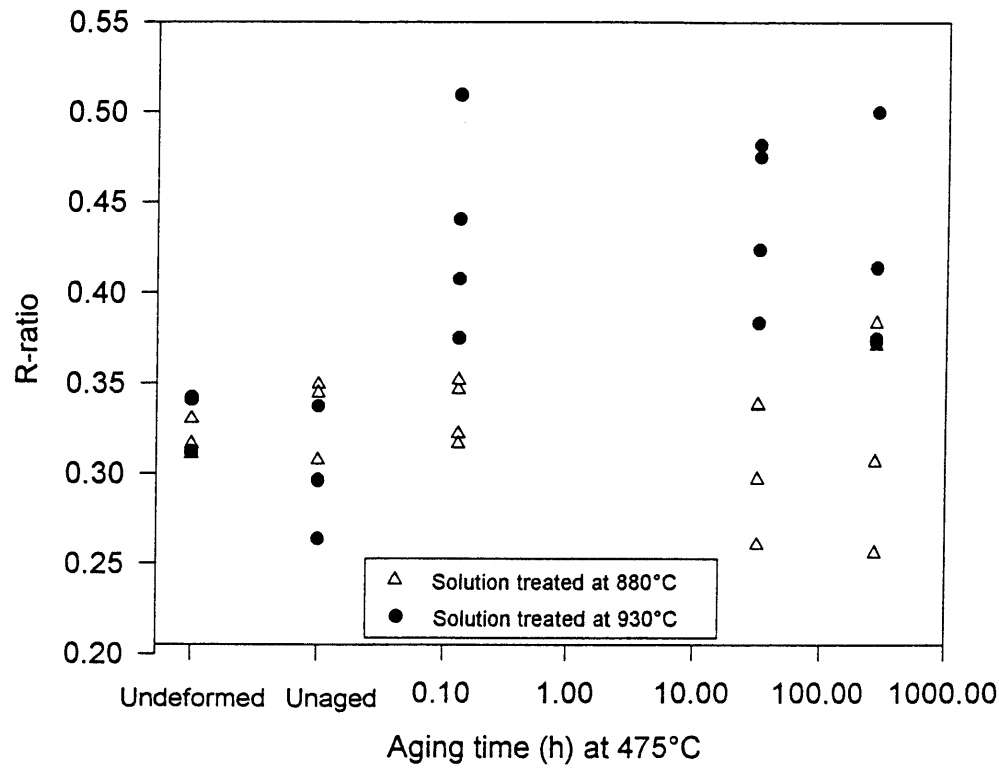

***Figure 7.15**: R-ratio of the true strains ($\bar{\varepsilon}_w/\bar{\varepsilon}_l$). Values do not differ significantly*

The similarity of the strains appear surprising at first, since the cold-rolled material had received a true strain (in the thickness direction) of $\bar{\varepsilon}_t = -0.478$, and hence a smaller true strain to ductile failure might be expected, compared to the undeformed material. However, no such large reduction in fracture strain is observed. Based on the roughly constant R-ratio (figure 7.15), it is also not expected that the crystallographic texture is much changed by the cold rolling.

This effect is explicable with reference to the way in which the final ductile fracture occurs. Figure 7.6 shows that fracture was preceded by an irregular decrease in load. This irregular decrease was not an artefact of the tensile testing machine, but was observed to coincide with delamination (parallel to the rolling direction and in the rolling plane). Delamination occurs as a result of the triaxial stresses which develop in the neck (Dieter 1988, p.292). The magnitude of the triaxial stress depends on the average (applied) stress, and the ratio of the radius of curvature of the neck to specimen linear cross section. This latter ratio correlates with $\Delta\varepsilon_t$ (the difference between the true strain at fracture and the true strain at necking) (ibid.). Figure

7.16 shows this difference for the various heat treatment conditions. $\bar{\varepsilon}_{t,n}$ (true strain at necking) was determined as follows:

$$\bar{\varepsilon}_l + \bar{\varepsilon}_w + \bar{\varepsilon}_t = 0 \qquad \text{(constancy of volume)} \qquad (7.5)$$

with $\bar{\varepsilon}_l$ the true strain in the length direction

$\bar{\varepsilon}_w$ the true strain in the width direction

$\bar{\varepsilon}_t$ the true strain in the thickness direction

and

$$\bar{\varepsilon}_{w,n} = R\bar{\varepsilon}_{t,n} \qquad (7.6)$$

with $\bar{\varepsilon}_{w,n}$ the true strain in the width direction, at necking

$\bar{\varepsilon}_{t,n}$ the true strain in the thickness direction, at necking

$R = \bar{\varepsilon}_{w,f}/\bar{\varepsilon}_{t,f}$ (at fracture), and presumably applicable at the onset of necking too

thus

$$\bar{\varepsilon}_{l,n} + (1+R)\bar{\varepsilon}_{t,n} = 0$$

$$\bar{\varepsilon}_{t,n} = -\bar{\varepsilon}_{l,n}/(1+R) \qquad (7.7)$$

with $\bar{\varepsilon}_{l,n}$ the uniform elongation up to the onset of necking

$\Delta\bar{\varepsilon}_t$ (difference between true strain at fracture and true strain at necking) was determined by subtracting $\bar{\varepsilon}_{t,n}$ from $\bar{\varepsilon}_{t,f}$ (true strain at fracture in the thickness direction).

The figure demonstrates that the neck morphology at fracture is similar for all the specimens. Figure 7.17 gives the traced outlines of the tensile specimens after fracture. It indicates that correlation between the form of the neck and the uniformly elongated region next to the neck is similar for all the tested specimens, the deformed, undeformed and aged.

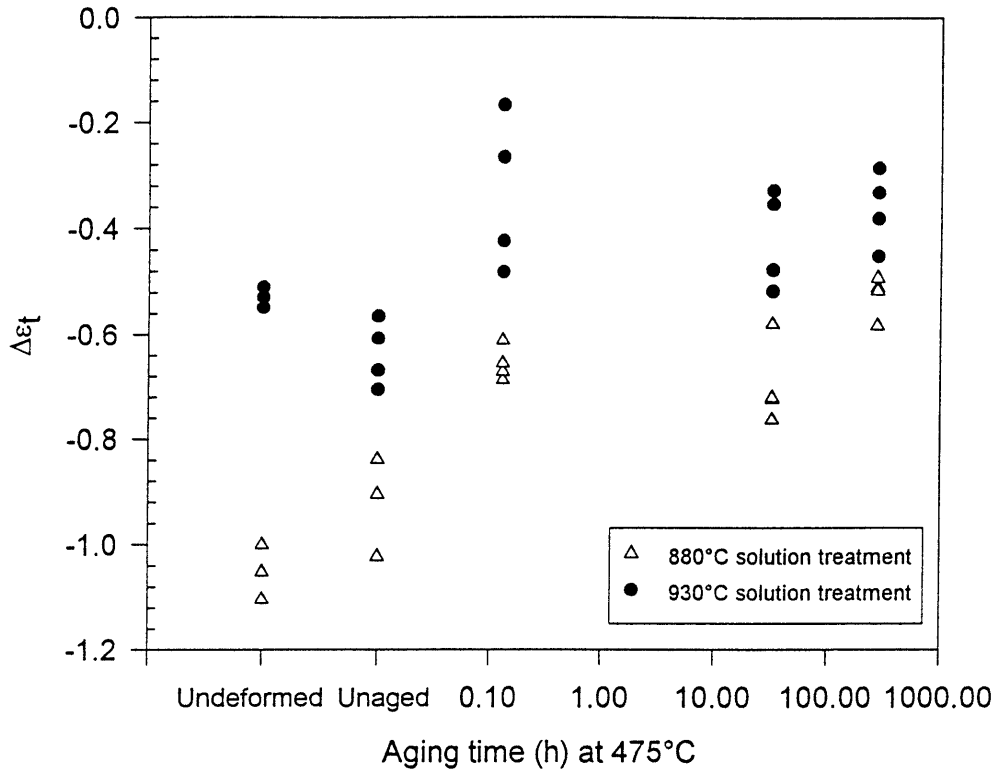

***Figure 7.16**: Difference between the true strain in the neck at fracture and true strain at necking (in the thickness direction) giving an indication of the shape of the neck of the tensile specimen at fracture. Results indicate that the shape of the neck - giving rise to triaxial stress - is similar for all the specimens*

***Figure 7.17a**: Outlines of the necks after fracture of the deformed and undeformed specimens (specimens solution treated at 880 ℃). The neck shapes are similar for all the specimens and delamination cracks can be seen*

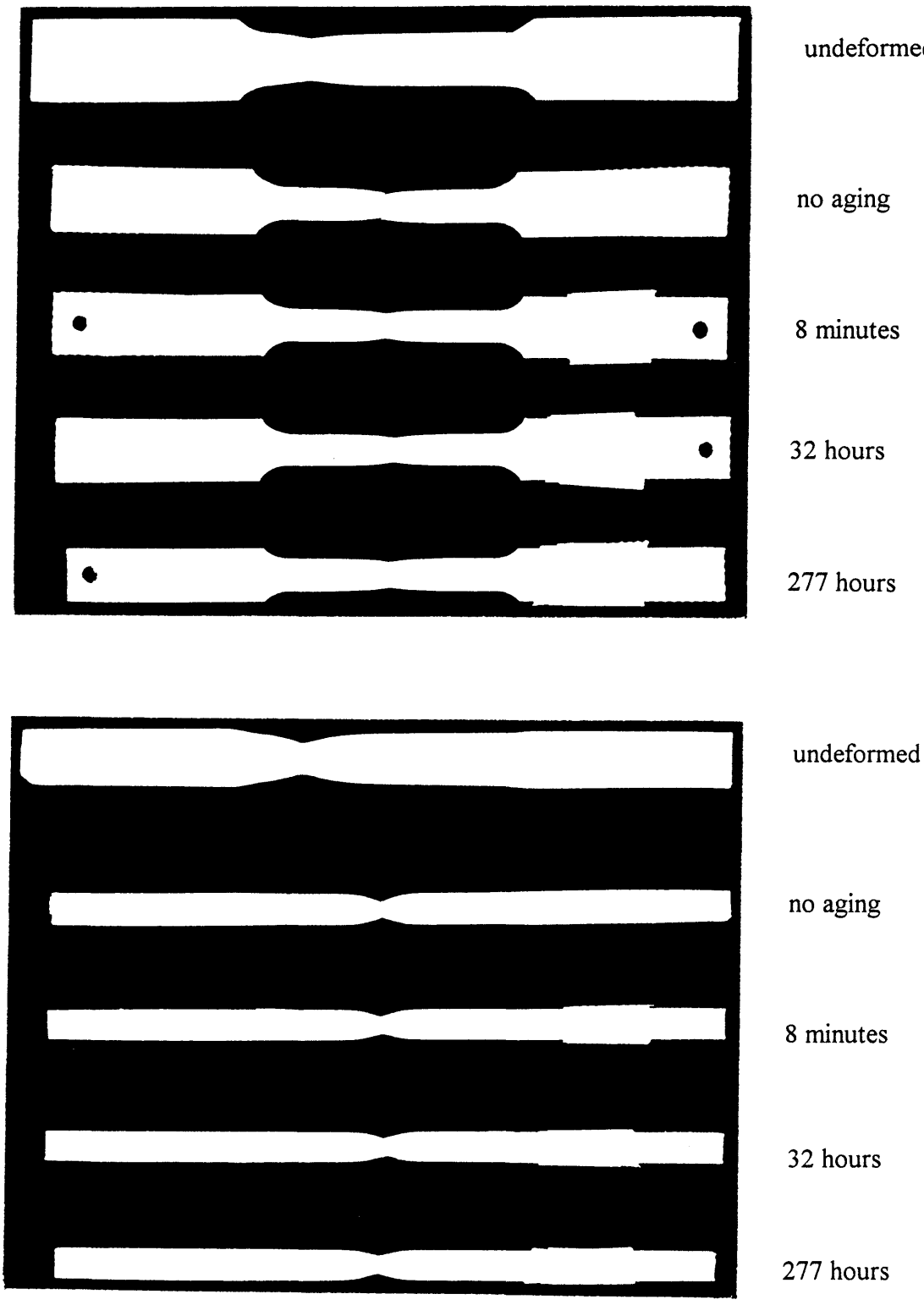

***Figure 7.17b**: Outlines of the necks after fracture of the deformed and undeformed specimens (specimens solution treated at 930 ℃). The neck shapes are similar for all the specimens and delamination cracks can be seen*

In the light of the similar flow stress (figures 7.7 to 7.9) and neck morphology, it is deduced that the triaxial stress assumes a similar value at fracture in all the specimens, in line with the observed role of delamination immediately before ductile fracture.

7.4 Summary of mechanical properties

The mechanical properties (hardness - figure 7.18, tensile strength and yield stress - figure 7.19) exhibit similar trends, namely significant increases in the first aging step (8 minutes), and again at long periods of aging (more than 64 hours). Toughness, however, is sacrificed with the increased strength (figure 7.20), and shows the expected decrease, as embrittlement proceeds. Figure 7.20 was constructed by measuring the hardness of the impact specimens, and converting it into yield strength, with the relationship:

yield strength = 6.291×hardness - 920.07 (7.8)

with yield strength in MPa and Vickers hardness in kg/mm^2

This relationship was obtained by plotting the measured yield strengths (section 7.3) as a function of the hardness of the impact specimens.

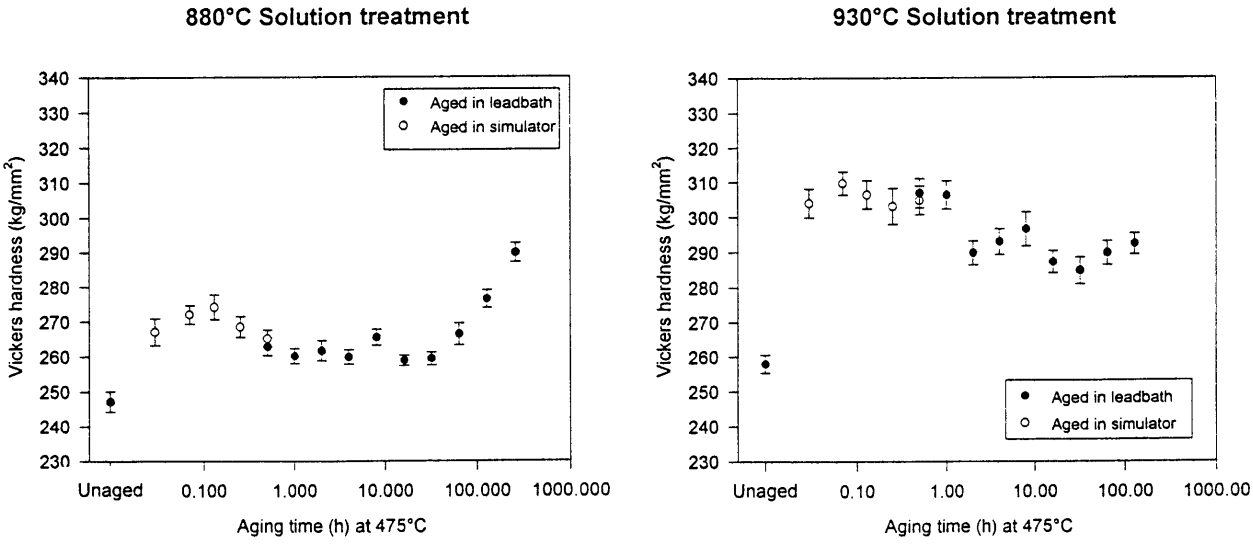

Figure 7.18: Hardness curves of samples solution treated at 880 ℃ and 930 ℃, cold rolled and aged at 475 ℃

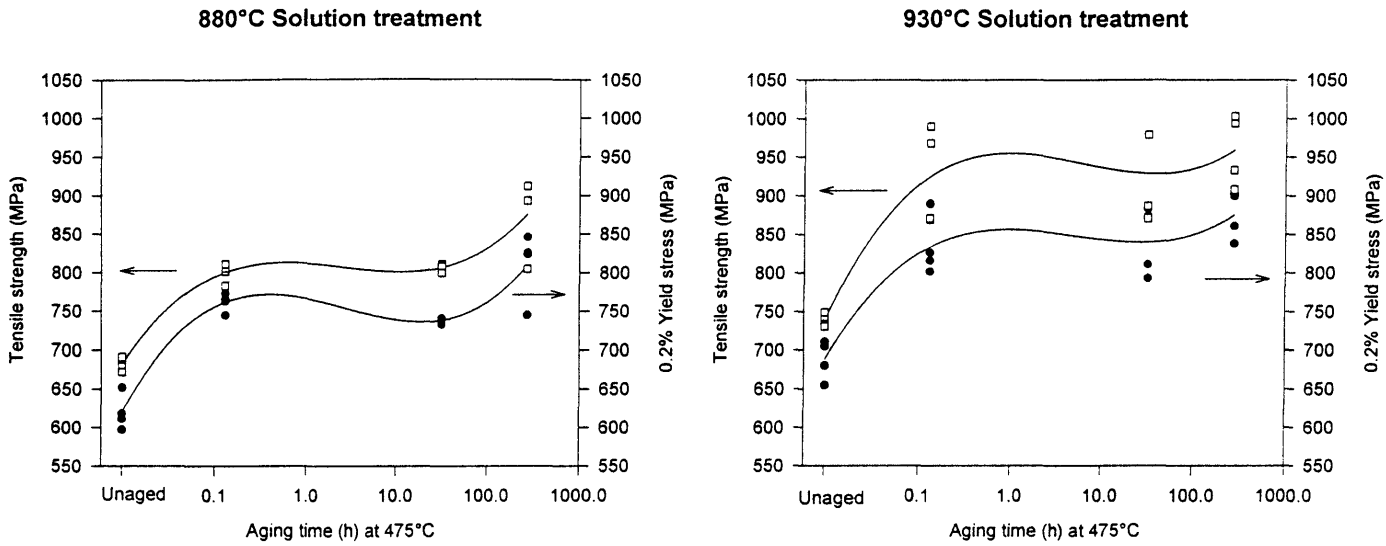

***Figure 7.19**: Tensile strength and 0.2% yield stress of samples solution treated at 880 ℃ and 930 ℃, cold rolled and aged at 475 ℃*

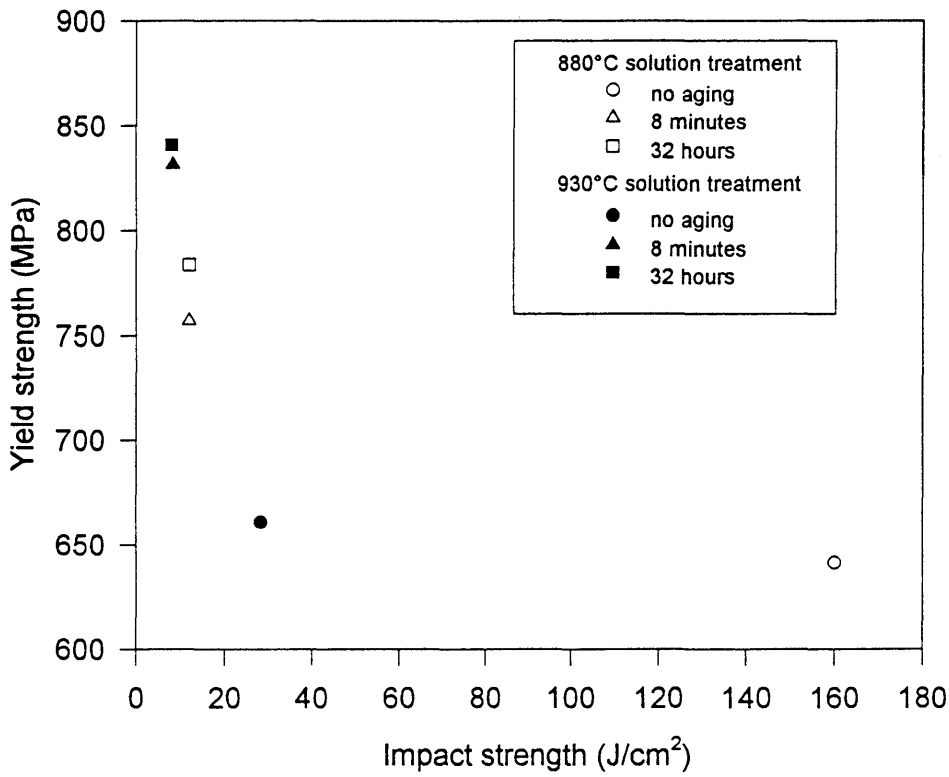

***Figure 7.20**: A plot of the average strength and toughness values which indicated that there is not a significant difference between the relationship, for both the 880 ℃ and 930 ℃ solution treatments*

7.5 Conclusions

Toughness is severely reduced by the aging treatments; fracture occurs mostly through transgranular cleavage fracture.

At worst, a maximum critical crack length of 0.3 mm can be tolerated before catastrophic failure, at a stress corresponding to the yield strength of 860 MPa, for specimens solution treated at 930°C and aged for 8 minutes at 475°C. For solution treatment at 880°C, a maximum crack length of 0.8 mm can be tolerated, but at a lower stress. Fatigue is expected to determine the lifetime of the chains, although the low K_{Ic} values indicate that less crack propagation will be tolerated before brittle fracture.

After the first aging step (8 minutes of aging), increases in the work hardening rate and uniform elongation are observed, and the residual stresses from cold rolling are apparently largely removed. Little change in work hardening behaviour occurs with subsequent aging.
The true strain at ductile fracture is similar in all cases, in line with the observation that delamination occurs (as a result of triaxial stresses in the neck) immediately before ductile fracture.

Tensile strength and 0.2% yield strength exhibit the same behaviour as the hardness, namely an initial increase at short aging times and a second increase at longer periods of aging, in support of the contention that two strengthening mechanisms are involved: the precipitation of carbides and nitrides at short aging periods, and the formation of α" at long periods of aging.

Chapter 8

Effect of Cold Rolling and Heat Treatments on Corrosion Resistance

Due to the surroundings in which the slat band chains are used, general corrosion resistance is a necessity. It is therefore of importance to determine the effect of the strengthening treatments on corrosion properties. To measure the resistance to general corrosion the material was potentiodynamically tested in a 0.5M H_2SO_4 solution, since reducing acids such as sulphuric acid commonly cause general corrosion of stainless steels. A change in polarisation behaviour of the steel in this solution would indicate a change in the general corrosion resistance, even though this solution is more aggressive than the actual environment to which the chains are exposed during use.

8.1. No solution treatment, solution treatment at 880°C and 930°C

No signs of a decrease in general corrosion resistance could be observed after any of the treatments. That is to say, with and without solution treatments, with cold rolling and with aging for up to three months - figure 8.1. This is consistent with results obtained by other authors (Aggen *et al.* 1978, Cortie 1995)

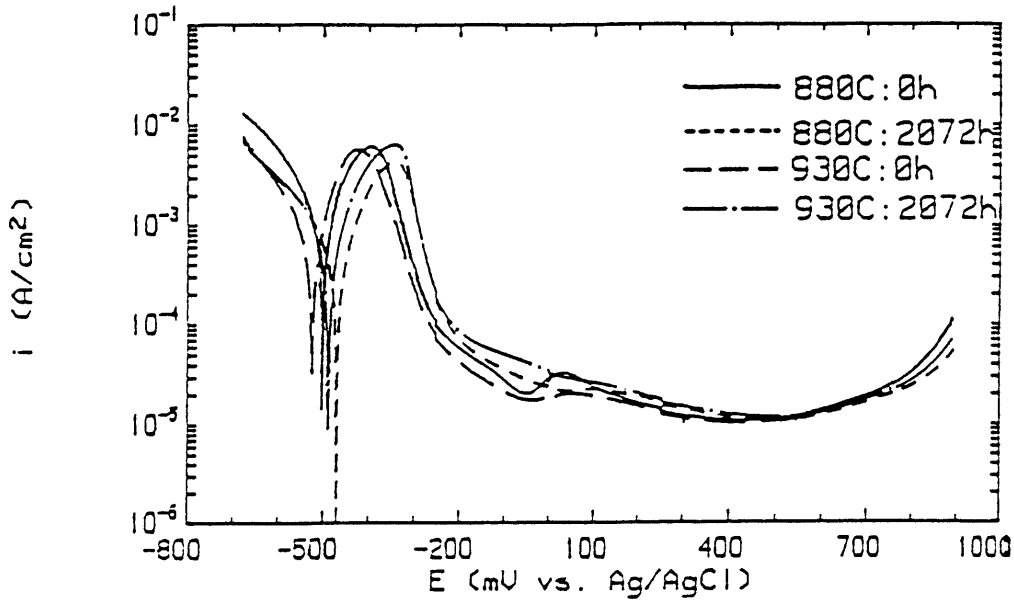

***Figure 8.1**: Polarisation diagrams of (a) solution treatment at 880 ℃, no aging; (b) solution treatment at 880 ℃, aging at 475 ℃ for 2072 hours; (c) solution treatment at 930 ℃, no aging and (d) solution treatment at 930 ℃, aging at 475 ℃ for 2072 hours, indicating that aging has little on no effect on the polarisation behaviour*

Investigation of the pitting corrosion resistance (3.56% NaCl solution) revealed that this property is not affected either, at least not without additional solution treatments before aging at 475°C (figure 8.2).

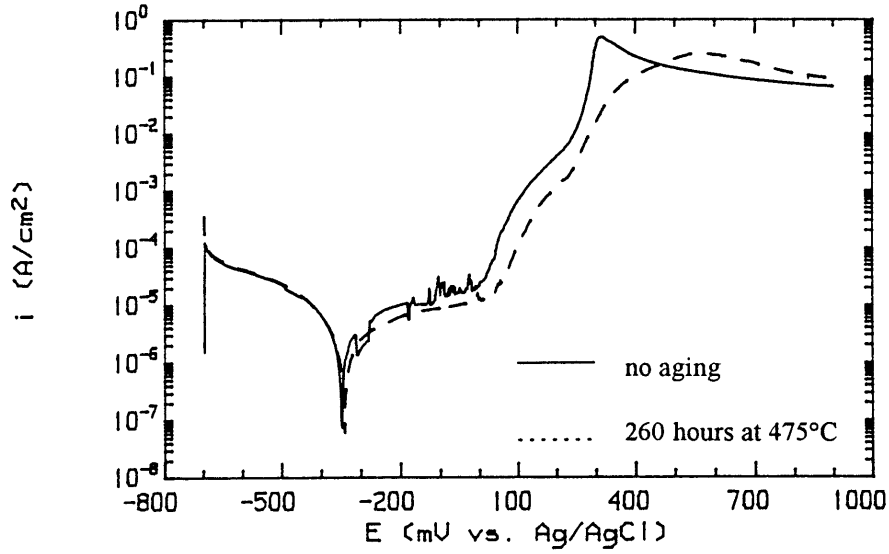

***Figure 8.2**: Pitting corrosion tests of specimens (a) with and (b) without aging (260 hours at 475 ℃) after cold rolling. No additional solution heat teatments. Tested in 3.56% NaCl. Aging does not affect the pitting potential, which is approximately 0.0 $V_{Ag/AgCl}$ in both cases*

The general corrosion properties of the chain links were not affected by any treatments (aging at 100°C, 450°C and 475°C) either.

8.2. Solution treatment at 990°C

With aging at 475°C, after solution treatment at 990°C and cold rolling, pronounced second anodic current peaks appeared after just 2 hours of aging. These peaks disappeared again after about 64 hours at temperature.

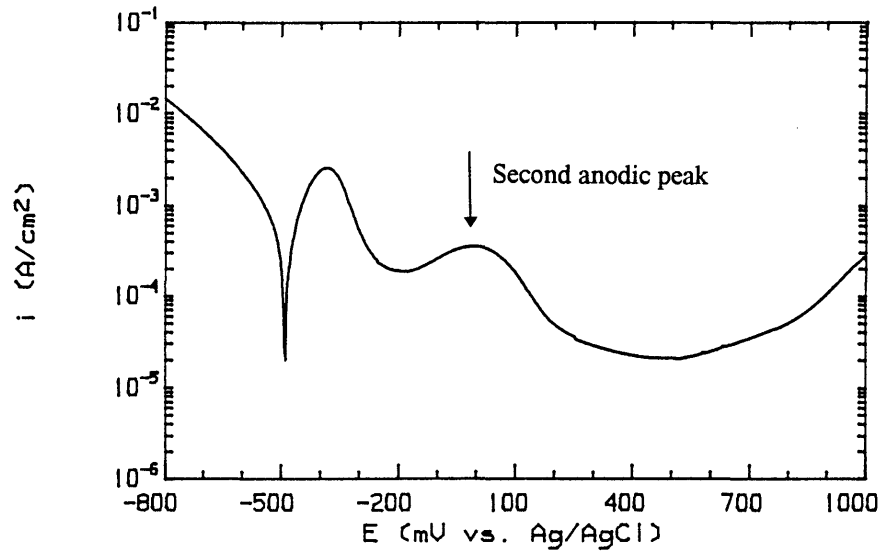

***Figure 8.3**:Second anodic current peak in sample aged at 475℃ for 16 hours (solution treatment at 990℃)*

The fact that corrosion does occur (when these peaks are visible) was confirmed by potentiostatic testing - 5 minutes at 0V - in the 0.5M H_2SO_4 solution. At this potential regions containing less than 12% Cr are active, while more Cr-rich areas are passive (Kirchheim *et al.* 1989). Thus if the measured current density is relatively high, the presence of chromium-depleted regions is inferred. At 0V the second annodic current peaks reached a maximum. The increase of the current density from 1×10^{-4} A/cm^2 to 7×10^{-3} A/cm^2 (figure 8.4) is indicative of active corrosion.

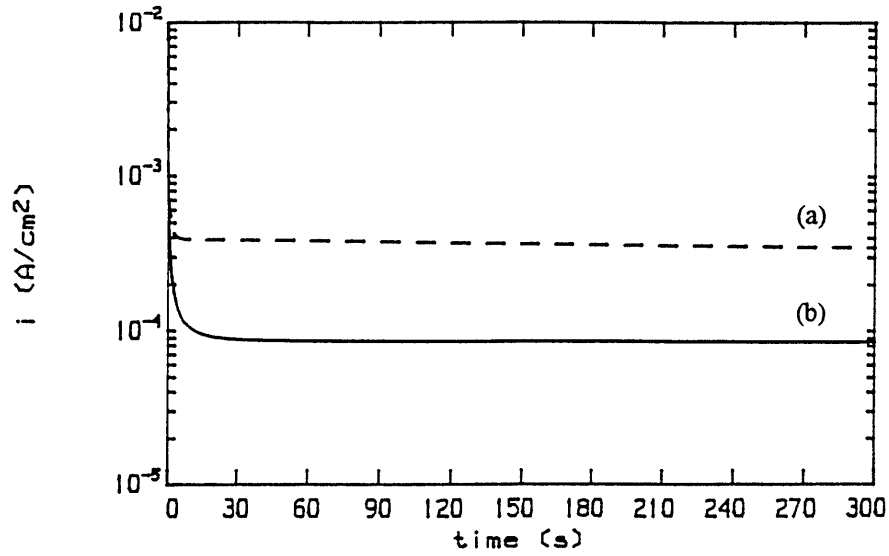

***Figure 8.4**: Potentiostatic tests at 0 V in 0.5M H_2SO_4 of samples (a) aged at 475 ℃ for 16 hours and (b) before aging (solution treatment at 990 ℃). The higher current density in (a) indicates that active corrosion occurs*

The reason for the observed current peak is thought to be sensitisation (Cr depletion of the matrix) associated with precipitation of Cr-rich carbides and nitrides. The disappearence after long periods of aging is probably due to recovery as sufficient chromium diffusion takes place to replenish the impoverised regions.

8.3. Cold work

Cold work does not influence the corrosion resistance as aging proceeds. No change was observed in the polarisation behaviour after cold rolling. These results are discussed in section 4.1.2.

8.4. Solution treatments without cold working

Only after solution treatments at temperatures higher than 1075°C were any signs of deterioration in corrosion properties observed. Second anodic current peaks became evident after solution treatment at these temperatures.

8.5. Conclusions

The heat treatments can be applied to the commercial product, as they do not affect the general corrosion resistance of the material. This is probably because the chromium depletion is not intergranular in nature and hence does not form continuous active regions, and the α" precipitation and its subsequent chromium depletion occur on a short length scale.

Chapter 9

Summary

The previous chapters presented results from the investigation into the possible mechanisms which cause strengthening when a 430 ferritic stainless steel is cold worked and aged in the "475°C-Embrittlement" range.

It was established that cold rolling, by increasing the dislocation density, increases the unaged hardness substantially. It also affects the short-time aging behaviour by enhancing the precipitation of carbides and nitrides. It was found that strain aging does not significantly influence the strength, and that recovery takes place with aging.

It was determined that the short-time aging behaviour is largely governed by the precipitation of carbides and nitrides. The precipitation becomes significant only when the interstitial content is increased by additional solution heat treatments before cold rolling and aging. It was established through Mössbauer studies that the precipitates are most likely chromium-rich. The increased work hardening rate (observed during tensile testing) also testifies to the precipitation of nondeforming particles during aging.

The additional solution heat treatments, if performed above the Ac_1 temperature, introduce martensite into the matrix, which increases the unaged hardness, seemingly without affecting the corrosion resistance.

Only after long periods of aging (more than 64 hours) does the Cr-precipitate (α") - usually associated with "475°C-embrittlement" - influence the hardness.

These treatments do not affect the corrosion resistance and passivation behaviour.

Both impact strength and lateral expansion indicate that embrittlement accompanies the increased strength obtained by aging. Calculated critical crack lengths from the impact data,

however, revealed that the maximum flaw length of 0.8 mm (for specimens solution treated at 880°C) is comparable to the thickness of the chains (3 mm). Since it is not expected that flaws of that size will exist in the as-manufactured links, fatigue will probably determine the lifetime of the chains, although the lower K_{Ic} values indicate that less crack propagation will be tolerated before brittle fracture.

In conclusion it can be said that the cold working and heat treatments seem to be an easy and cost-effective method for increased strength, which would prolong conveyor life.

References

Aggen. G., Deverell, H.E., and Nichol, T.J. (1978). Microstructures versus properties of 29-4 ferritic stainless steel. *Micon* **78**, 334-366.

Anzai, H., Kuniya, J., and Masaoka, I. (1988). Effect of 475°C embrittlement on fracture resistance of cast duplex stainless steel. *Transactions of the Iron and Steel Institute of Japan* **28**, 400-405.

ASM Metals Handbook, ninth edition (1985). American Society for Metals, Metals Park, Ohio. Volume 8, p. 12, volume 9, pp. 692, 693.

Avner, S.H. (1992). *Introduction to Physical Metallurgy.* McGraw-Hill. Singapore.

Bates, C.E., Totten, G.E., and Brennan, R.L. Quenching of steel. In *ASM Handbook vol. 4 Heat Treatment*, pp. 68-69. ASM International. USA.

Binder, W.O., and Spendelow, H.R. (1950). The influence of chromium on the mechanical properties of plain chromium steels. *Transactions of the A.S.M.* **43**, 759-777.

Blackburn, M.J., and Nutting, J. (1964). Metallography of an iron-21% chromium alloy subjected to 475°C embrittlement. *Journal of the Iron and Steel Institute* **July 1964**, 610-613.

Brooks, C.R. (1979). Stainless steels. In *Heat Treatment of Ferrous Alloys*, Hemisphere publishing corporation, Washington.

Chandra, D., and Schwartz, L.H. (1971). Mössbauer effect study of the 475°C decomposition of Fe-Cr. *Metallurgical Transactions* **2**, 511-519.

Charenton, J.C., and Balteneck, S. (1992). Duplex martensitic-ferritic stainless steels with 17% chromium and high yield strength, for conveyor systems in the food processing industry. In *Applications of Stainless Steels '92* **vol.1**. pp.694-704. Jernkontoret, Stockholm, Sweden.

Chun, C.H., and Polonis, D.H. (1992) Metallurgical stability and the fracture behaviour of ferritic stainless steels. *Journal of Materials Engineering and Performance* **13**, 371-382.

Cortie, M.B. (1995). Embrittlement and aging at 475°C in an experimental ferritic stainless steel containing 38% Cr. *Materials Science and Engineering A* **vol. 199**, 153-163.

Czakó-Nagy, I., and Vértes, A. (1988). Mössbauer spectroscopy as an analytical tool. *Trends in Analytical Chemistry* **vol.7 no. 8**, 305-310.

Demo, J.J. (1971). Mechanism of high temperature embrittlement and loss of corrosion resistance in AISI type 446 stainless steel. *Corrosion* **27**, 531-544.

De Nys, T., and Gielen, P.M. (1971). Spinodal decomposition in the Fe-Cr system. *Metallurgical Transactions* **2**, 1423-1428.

Dieter, G.E. (1988). *Mechanical Metallurgy* SI metric edition. McGraw-Hill Book Co. London.

Dubiel, S.M., and Inden, G. (1987). On the miscibility gap in the Fe-Cr system: a Mössbauer study on long term annealed alloys. *Z. Metallkunde*, 544-549.

Dubiel, S.M., Wrzesniewska, T., and Gorczyca, S. (1979). A study of the influence of deformation on a shape of the Mössbauer spectrum of iron-chromium alloys. *Journal of Physic F. Metal. Phys.* **9 no. 5**, 949-954.

Dymek, S., and Blicharski, M. (1985). Microstructure of the ferritic stainless steels after high strains. *Z. Metallkunde* **76**, 777-785.

Fisher, R.M., Dulis, E.J., and Carrol, G.K. (1953). Identification of the precipitate accompanying 885°F embrittlement in chromium steels. *Journal of Metals* **May 1953**, 690-695.

Golovin, I.S., Sarrak, V.I., and Suvorova, S.O. (1992). Influence of carbon and nitrogen on solid solution decay and "475°C embrittlement" of high-chromium ferritic steels. *Metallurgical Transactions* **23A**, 2567-2579.

Gonser, U. (1983). Mössbauer spectrum in physical metallurgy. *Hyperfine Interactions* **13**, 5-23.

Grobner, P.J. (1973). The 885°F (475°C) embrittlement of ferritic stainless steels. *Metallurgical Transactions* **4**, 251-260.

Heger, J.J. (1951). 855°F embrittlement of the ferritic chromium-iron alloys. *Metal Progress* **August 1951**, 55-61.

Hertzberg, R.W. (1983). Deformation and Fracture Mechanics of Engineering Materials. John Wiley and sons, Inc., U.S.A. p.344.

Hillert, M. (1961). A solid solution model for inhomogeneous systems. *Acta Metallurgica* **9**, 525-535.

Kirchheim, R., Heine, B., Fichmeister, H., Hofmann, S.,Knote, H., and Stolz, U. (1989). The passivity of iron-chromium alloys. *Corrosion Science*, vol. **29**, 889-917.

Koutaniemi, P., Heikkinen, V., and Saarinen, A. (1974). Effect of vanadium on the 475°C embrittlement of a chromium steel. *Metal Science* **8**, 94-96.

Krauss, G. (1989). Stainless steels. In *Steels: Heat Treatment and Processing Principles.* ASM International, USA.

Lagneborg, R. (1967). Metallography of the 475°C embrittlement in an iron-30% chromium alloy. *Transactions of the A.S.M.* **60**, 67-78.

Lena, A,J., and Hawkes, M.F. (1954). 475°C (885°F) embrittlement in stainless steels. *Journal of Metals* **May 1954**, 607-615.

Mao, X. and Zhao, W. (1993). Electrochemical polarization method to detect aging embrittlement of 321 stainless steel. *Corrosion* **49**, 335-342.

Marcinkowski, M.J., Fisher, R.M., and Szirmae,A. (1964). Effect of 500°C aging on the deformation behaviour of an iron-chromium alloy. *Transactions of the Metallurgical Society of AIME* **230**, 676-689.

Mashimo, K. (1985). Effect of alloying elements on properties of high chromium-molybdenum ferritic stainless steels. *Transactions of the Iron and Steel Institute of Japan* **25**, B-31.

Miller, M.K. (1987). Morphology of low temperature phase transformations in the iron-chromium system. In *Phase Transformations*, Lorimer,G.W. (ed.), The Institute of Metals, pp. 39-43.

Montano, P.A. (1986). Technological applications of Mössbauer spectra. *Hyperfine Interactions* **1986**, 147-159.

Newell, H.D. (1946). Properties and characteristics of 27% chromium-iron. *Metal Progress* **May 1946**, 977-1006.

Nichol, T.J., Datta, A., and Aggen, G. (1980). Embrittlement of ferritic stainless steels. *Metallurgical Transactions* **11A**, 573-585.

Ning, L., Zhonggang, D. and Menggen, H. (1991). Effect of heat treatment on microstructure and mechanical properties of martensitic-ferritic stainless steel containing 17% Cr and 2% Ni. *Materials Science and Technology* **7**, 1057-1062.

Paxton, H.W., and Kunitake, T. (1960). Diffusion in the iron-chromium system. *Transactions of the Metallurgical Society of AIME* **218**, 1003-1009.

Pickering, F.B. (1979). The metallurgical evolution of stainless steels. In *The Metallurgical Evolution of Stainless Steels*, Pickering,F.B. (ed.) ASM (Ohio) and MS (London) p 17,22.

Pistorius, P.C., and Coetzee, M. (1996). Sensitization of type 430 stainless steel during continuous annealing. *Journal of the South African Institute of Mining and Metallurgy* **96**, 119-125.

Plumtree, A., and Gullberg, R. Embrittlement of a continuously cooled Fe-25Cr alloy. *Metallurgical Transactions* **7A**, 1451-1458

Pollard, B. (1974). Effect of titanium on the ductility of 26% chromium low interstitial ferritic stainless steel. *Metals Technology* **January 1974**, 31-36.

Porter, D.A., and Easterling, K.E. (1992). Diffusion. In *Phase transformations in metals and alloys* (2nd edn), p. 93, p.102. Chapman and Hall, London.

Porter, D.A., and Easterling, K.E. (1992). Diffusional transformations in solids. In *Phase transformations in metals and alloys* (2nd edn), p. 93, p.308-314. Chapman and Hall, London.

Rajkay, L. (1967). Report of subcommittee VI on thermal embrittlement of medium-and high-chromium ferritic steels. *Proceedings of ASTM* **67**, 158-169.

Redmond, J.D., and Miska, K.H. (1982). The basics of stainless steels. *Chemical Engineering* **October 18**, 79-93.

Reed-Hill, R.E., and Abbaschian, R. (1992). Annealing. In *Physical Metallurgy Principles* (3d edn), p.227-233.

Semchyshen, M., Bond, A.P., and Dundas, H.J. (1979). Effects of composition on ductility and toughness of ferritic stainless steels. In *The Metallurgical Evolution of Stainless Steels*, Pickering, F.B. (ed.) ASM (Ohio) and MS (London) p 260-274.

Sheppard, T., and Richards, P. (1987). Structural and substructural observations during thermomechanical processing of two ferritic stainless steels. *Journal of Materials Science* **22**, 1642-1650.

Thielsch, H. (1951). Physical and welding metallurgy of chromium stainles steels. *The Welding Journal* **May 1951**, 209-s - 250-s.

Thielsch, H. (1955). Welding summary. *Welding Research Supplement* **January 1955**, 22-s - 30-s.

Tisinai, G.F., and Samans, C.H. (1957). Some observations on 885°F embrittlement. *Journal of Metals* **October 1957**,1221-1226.

Trindade, B., and Vilar, R. (1991). Influence of nickel on the 475°C embrittlement of Fe0Cr-Ni alloys: Mössbauer effect study. *Hyperfine Interactions* **66**, 351-358.

Truman, J.E. (1992). Stainless steels. In Constitution and Properties of Steels. Pickering,F.B. (ed.). VCH, Weinheim, Germany.

Williams, R.O. (1958). Further studies of the iron-chromium system. *Transactions of the Metallurgical Society of AIME* **August 1958**, 497-502.

Williams, R.O., and Paxton, H.W. (1957). The nature of ageing of binary iron-chromium alloys around 500°C. *Journal of the Iron and Steel Institute* **March 1957**, 358-374.

Appendices

Appendix 1

Effect of cold working. Material solution treated at 920°C and aged at 475°C. With and without cold rolling (fig.4.3)

Aging time (h)	No reduction (8mm)		38% reduction in area (5mm)	
	hardness (HV20kg)	standard deviation	hardness (HV20kg)	standard deviation
0	167.6	4.0	248.7	5.6
0.5	171.1	5.0	274.9	4.4
1	166.3	3.3	270.3	7.2
2	173.4	4.6	275.6	4.2
4	171.1	2.9	271.5	6.3
8	172.2	4.5	277.5	5.9
16	180.6	2.8	267.7	5.5
32	171.0	3.5	271.3	8.0
64	173.7	3.5	274.5	5.6
128	174.1	3.0	280.7	6.6
260	198.0	4.6	294.9	5.7

Appendix 2

Strain aging: Chains aged at 100°C (fig. 4.6)

Aging time (h)	Hardness (HV20kg)	Standard deviation
0	251.1	5.1
0.25	254.2	6.6
0.5	251.6	4.4
1	256.1	5.5
2	254.6	4.6
4	252.6	3.6
8	249.6	3.1
16	252.1	3.4
32	252.7	3.9
64	251.4	4.8

Appendix 3

Strain aging: Sheet material solution treated at 930°C, cold rolled and aged at 100°C (fig.4.7)

Aging time (h)	Hardness (HV20kg)	Standard deviation
0.25	266.7	6.2
0.5	266.7	8.2
1	266.3	6.2
2	264.8	5.4
4	257.7	6.2
14	267.8	8.4

Appendix 4

Hardness of chain and sheet material aged at 475°C (fig.5.1)

Aging time (h)	Chain		Sheet material	
	Hardness (HV20kg)	Standard deviation	Hardness (HV20kg)	Standard deviation
0	248.5	3.9	242.3	3.8
0.5	246.2	3.1	238.7	2.5
1	249.2	4.1	242.5	3.3
2	240.6	3.6	244.5	3.8
4	245.6	3.4	240.9	3.9
8	250.0	3.4	238.3	3.2
16	250.1	3.4	242.2	3.7
32	251.2	3.6		
64	258.6	2.8	244.7	4.5
128	264.9	2.9		
260	283.4	3.9	274.8	5.7

Appendix 5

Chain aged at 450°C and 475°C (fig.5.2)

Aging time (h)	Aging at 450°C		Aging at 475°C	
	Hardness (HV20kg)	Standard deviation	Hardness (HV20kg)	Standard deviation
0	256.4	8.3	248.5	3.9
0.5	250.1	3.8	246.2	3.1
1	252.8	3.3	249.2	4.1
2	254.6	4.2	240.6	3.6
4	247.2	4.4	245.6	3.4
8	244.7	3.1	250.0	3.4
16	261.2	5.4	250.1	3.4
32	259.1	3.6	251.2	3.6
64	267.9	6.0	258.6	2.8
128	269.3	3.9	264.9	2.9
260	280.1	4.2	283.4	3.9

Appendix 6

Sheet material aged at 400°C, 475°C and 500°C (fig.5.3)

Aging time (h)	400°C		475°C		500°C	
	Hardness (HV20kg)	Standard deviation	Hardness (HV20kg)	Standard deviation	Hardness (HV20kg)	Standard deviation
0.5	246.2	5.1	242.3	3.8	234.9	3.8
1	246.7	3.8	238.7	2.5	235.8	4.1
2	242.4	5.9	242.5	3.3	234.3	5.2
4	242.4	4.5	244.5	3.8	234.7	3.7
8	238.9	5.7	240.9	3.9	235.5	4.8
16	240.7	4.1	238.3	3.2	233.5	4.9
32	240.8	3.4	242.2	3.7	235.5	3.8
48	246.1	4.1				
64			244.7	4.5	237.8	2.9
128					238.4	3.7
260			274.8	5.7	236.7	3.9

Appendix 7

Equilibrium volume fractions α" (fig.5.4)

Temperature (°C)	Volume fraction α"
427	0.06
435	0.055
450	0.05
465	0.04
475	0.02
485	0.008

Appendix 8

Hardness after solution treatments at different temperatures. 15 minutes at temperature, water quench, no reduction (fig.6.1)

Solution temperature (°C)	Hardness (HV20kg)	Standard deviation	% Martensite*
800	161.7	2.0	-
825	160.9	1.6	-
850	162.5	2.3	-
875	153.9	2.9	-
900	165.7	2.3	-
925	177.0	4.1	14.0
950	209.1	4.7	32.0
975	219.8	6.0	35.5
1000	221.0	5.5	34.7
1025	211.4	10.0	30.2
1050	204.9	9.6	25.5
1075	190.0	5.1	10.0
1100	196.6	6.4	4.5
1125	201.2	5.3	0.5
1150	214.4	9.1	-
1175	236.4	10.6	-
1200	252.0	8.8	-

* % martensite determined by etching in Ralph's etchant and using a point count method (200 points per specimen)

Appendix 9

Solution treatment at 930°C (45 min) and 990°C (45 min), cold rolling and aging at 475°C (fig.6.4)

Aging time (h)	930°C		990°C	
	Hardness (HV20kg)	Standard deviation	Hardness (HV20kg)	Standard deviation
0	260.5	6.2	288.1	8.1
0.5	287.2	9.4	306.9	7.9
1	293.5	8.8	296.6	8.6
2	297.2	9.2	311.0	8.5
4	289.7	6.1	309.2	7.4
8	296.3	8.2	302.1	7.8
16	286.5	7.5	301.7	7.0
32	290.9	7.2	302.7	6.8
64			304.9	6.8
128	298.1	5.2	311.3	6.0
260	306.6	5.1	312.9	4.7
520	311.8	4.6	320.7	4.5

Appendix 10

Solution treatment at 880°C and 930°C, and aging at 475°C (fig.6.5)

Aging time (h)	880°C		930°C	
	Hardness (HV20kg)	Standard deviation	Hardness (HV20kg)	Standard deviation
0	247.1	6.3	257.9	5.5
0.03*	267.1	8.2	304.1	8.8
0.07*	272.0	5.7	309.8	7.2
0.13*	274.2	7.7	306.6	8.6
0.25*	268.5	6.4	303.2	11.1
0.5*	265.1	5.2	304.9	8.9
0.5	262.8	5.5	306.9	12.9
1	260.1	4.5	306.5	12.6
2	261.6	6.2	289.7	10.5
4	259.8	4.4	293.0	8.0
8	265.5	4.8	296.6	10.5
16	258.8	3.2	287.2	6.8
32	259.3	3.9	284.7	8.2
64	266.3	6.8	289.8	7.3
128	276.3	5.3	292.4	6.5
260	289.7	5.8	302.6	5.3
544	302.4	3.4	310.4	5.3
1040	308.9	5.6	319.8	6.7
2072	318.8	4.2	326.7	5.8

* Aged in weld cycle simulator

Appendix 11

Solution treatment at 880°C and 930°C, and aging at 450°C (fig.6.8)

Aging time (h)	880°C		930°C	
	Hardness (HV20kg)	Standard deviation	Hardness (HV20kg)	Standard deviation
0	241.8	3.0	281.3	11.1
0.03*	268.5	5.1	313.3	15.1
0.07*	268.9	6.9	298.8	8.2
0.13*	266.4	4.9	320.6	9.3
0.25*	266.9	5.1	305.7	14.3
0.5*	269.5	5.2	319.7	10.2
0.5	274.0	4.6	325.4	11.6
1	273.8	6.8	321.7	7.7
2	267.3	4.6	326.0	16.2
4	273.5	3.8	321.3	5.3
8	268.6	5.3	322.3	12.2
16	264.8	5.9	323.9	8.8
32	266.5	4.9	319.1	
64	270.9	5.2	323.4	8.3
128	273.7	6.3	317.2	8.8
260	282.4	5.0	320.7	5.8
520	301.4	7.0	322.1	9.9

* Aged in weld cycle simulator

Appendix 12

Distribution of hyperfine field (T) with aging time (fig. 6.11)

Aging time at 475°C	solution treated at 880°C	solution treated at 930°C
0	26.92	26.73
8 minutes	27.08	26.98
32 hours	27.14	27.20
260 hours	27.65	27.57
2072 hours	27.99	28.13

Appendix 13

Impact strength and % lateral expansion (fig.7.1 and 7.2)

	Aging time at 475°C	Impact strength (J/mm^2)	% Lateral expansion
Solution at 880°C	0	0.84	33.3
	0	-	-
	0	0.80	30.1
	0	0.58	21.3
	8 minutes	0.05	2.4
	8 minutes	0.05	1.8
	8 minutes	0.10	2.0
	8 minutes	0.06	1.8
	32 hours	0.06	1.2
	32 hours	0.06	1.0
	32 hours	0.05	0.4
	32 hours	0.31	11.2
Solution at 930°C	0	0.14	8.8
	0	0.23	11.2
	0	0.06	1.8
	0	0.07	1.8
	8 minutes	0.04	2.8
	8 minutes	0.04	3.4
	8 minutes	0.03	0.2
	8 minutes	0.04	2.8
	32 hours	0.04	2.6
	32 hours	0.05	2.8
	32 hours	0.03	1.2
	32 hours	0.04	2.0

Appendix 14

K_{1c} values and critical crack length (fig.7.3)

	Aging time at 475°C	K_{1c}	Critical crack length (mm)
Solution at 880°C	0	315.0079	80.901
	0	305.4638	760.73
	0	240.0011	46.961
	8 minutes	38.1830	0.804
	8 minutes	38.1830	0.804
	8 minutes	64.2159	2.274
	8 minutes	43.7780	1.057
	32 hours	43.7780	1.115
	32 hours	43.7780	1.115
	32 hours	39.3228	0.899
	32 hours	150.9315	13.248
Solution at 930°C	0	83.3124	4.643
	0	119.3457	9.528
	0	43.7780	1.282
	0	50.7148	1.720
	8 minutes	34.3961	0.509
	8 minutes	33.2031	0.475
	8 minutes	26.0305	0.292
	8 minutes	32.2989	0.449
	32 hours	34.3961	0.534
	32 hours	40.7324	0.749
	32 hours	26.0305	0.306
	32 hours	32.2989	0.471

Appendix 15

Uniform plastic strain (fig.7.10)

Aging time (h)	880°C solution treatment	930°C solution treatment
0	0.0110	0.0094
0	0.0124	0.0093
0	0.0110	0.0110
0	0.0180	0.0123
8 minutes	0.0383	0.0387
8 minutes	0.0260	0.0428
8 minutes	0.0334	0.0466
8 minutes	0.0311	0.0499
32 hours	0.0466	0.0490
32 hours	0.0394	0.0463
32 hours	0.0325	0.0652
32 hours	0.0408	0.0641
277 hours	0.0384	0.0485
277 hours	0.0473	0.0480
277 hours	0.0344	0.0506
277 hours	0.0447	0.0509

Appendix 16

Strain -to-failure in width and thickness directions (880°C and 930°C)

(fig. 7.13 and 7.14)

	Aging time at 475°C	ε_w	ε_t
Solution at 880°C	no deformation, no aging	-0.327	-1.052
	no deformation, no aging	-0.349	-1.104
	no deformation, no aging	-0.330	-1.001
	0	-0.293	-0.839
	0	-0.316	-0.916
	0	-0.317	-1.033
	8 minutes	-0.249	-0.718
	8 minutes	-0.223	-0.693
	8 minutes	-0.202	-0.639
	8 minutes	-0.239	-0.680
	32 hours	-0.161	-0.618
	32 hours	-0.256	-0.756
	32 hours	-0.235	-0.791
	32 hours	-0.255	-0.753
	277 hours	-0.207	-0.539
	277 hours	-0.170	-0.553
	277 hours	-0.192	-0.518
	277 hours	-0.159	-0.620

Appendix 16 (continued)

	Aging time at 475°C	ε_w	ε_t
Solution at 930°C	no deformation, no aging	-0.185	-0.594
	no deformation, no aging	-0.210	-0.616
	no deformation, no aging	-0.215	-0.628
	0	-0.194	-0.574
	0	-0.163	-0.618
	0	-0.202	-0.680
	0	-0.213	-0.718
	8 minutes	-0.192	-0.511
	8 minutes	-0.186	-0.456
	8 minutes	-0.132	-0.299
	8 minutes	-0.103	-0.203
	32 hours	-0.213	-0.554
	32 hours	-0.217	-0.511
	32 hours	-0.178	-0.375
	32 hours	-0.192	-0.399
	277 hours	-0.182	-0.488
	277 hours	-0.207	-0.414
	277 hours	-0.153	-0.369
	277 hours	-0.122	-0.325

Appendix 17

R-ratio of strains ($\varepsilon_w/\varepsilon_t$) (fig. 7.15)

Aging time (h)	880°C solution treatment	930°C solution treatment
no derormation, no aging	0.311	0.312
no derormation, no aging	0.316	0.341
no derormation, no aging	0.330	0.342
0	0.349	0.337
0	-	0.264
0	0.344	0.297
0	0.307	0.296
8 minutes	0.347	0.375
8 minutes	0.322	0.408
8 minutes	0.316	0.441
8 minutes	0.352	0.509
32 hours	0.261	0.384
32 hours	0.338	0.424
32 hours	0.297	0.475
32 hours	0.339	0.481
277 hours	0.384	0.373
277 hours	0.307	0.500
277 hours	0.372	0.414
277 hours	0.256	0.375

Appendix 18

Difference between true strain in the neck and true strain at necking (fig. 7.16)

Aging time (h)	880°C solution treatment	930°C solution treatment
no deformation no aging	-1.052	-0.678
no deformation no aging	-1.104	-0.704
no deformation no aging	-1.001	-0.708
0	-0.839	-0.584
0	-	-0.628
0	-0.926	-0.691
0	-1.043	-0.730
8 minutes	-0.749	-0.542
8 minutes	-0.715	-0.489
8 minutes	-0.667	-0.333
8 minutes	-0.705	-0.239
32 hours	-0.657	-0.592
32 hours	-0.788	-0.546
32 hours	-0.819	-0.442
32 hours	-0.786	-0.445
277 hours	-0.569	-0.526
277 hours	-0.592	-0.448
277 hours	-0.546	-0.408
277 hours	-0.659	-0.365

Appendix 19

Tensile strength and 0.2% yield stress of 880°C and 930°C specimens

(figure 7.19)

	Aging time (h)	Tensile strength (MPa)	0.2% Yield stress (MPa)
Solution at 880°C	0	685	597
	0	679	611
	0	691	652
	0	672	618
	0.13	783	745
	0.13	802	766
	0.13	806	763
	0.13	811	773
	32	810	740
	32	811	741
	32	808	740
	32	800	733
	277	805	745
	277	893	824
	277	893	826
	277	912	846

Appendix 19 (continued)

	Aging time (h)	Tensile strength (MPa)	0.2% Yield stress (MPa)
Solution at 930°C	0	741	705
	0	749	711
	0	734	680
	0	731	655
	0.13	869	802
	0.13	871	826
	0.13	990	816
	0.13	968	890
	32	871	793
	32	887	811
	32	979	883
	32	979	874
	277	933	861
	277	908	838
	277	994	900
	277	1003	903